Effective Curvature Elastic Constants
for Membrane-Polymer Systems

Inaugural-Dissertation

zur

Erlangung des Doktorgrads

der Mathematisch-Naturwissenschaftlichen Fakultät

der Universität zu Köln

vorgelegt von

Thorsten Auth

aus Frankfurt am Main

Jülich 2003

Zusammenfassung

Membranen können durch das Modell einer mathematischen Fläche beschrieben werden, in dem die Krümmungseigenschaften der Membran durch die drei Membrankonstanten 'spontane Krümmung', 'Biegesteifigkeit' und 'Gauß'sches Biegemodul' charakterisiert werden. Experimente zeigen, daß sich durch die Zugabe von Polymeren das Verhalten von Membransystemen deutlich verändern kann. Der kürzlich entdeckte Polymer-Boosting-Effekt in Öl-Wasser-Amphiphil-Mikroemulsionen ist ein Beispiel, bei dem die Daten aus Streuexperimenten mit Hilfe des Membranmodells erfolgreich beschrieben werden konnten. Der Einfluß des Polymers wurde dabei in Form von effektiven Membrankonstanten berücksichtigt.

Das Konzept der effektiven Membrankonstanten wird eingeführt und die Effekte verschiedener Arten von Polymerzugaben zu Membransystemen werden anhand der Literatur diskutiert. Unter Verwendung des Modells frei verbundener Ketten für die Polymere werden mit Monte-Carlo-Simulationen die Effekte von verankerten Polymeren auf die Membrankonstanten für verschiedene Systeme untersucht.

Es wird eine Simulationsmethode beschrieben, mit deren Hilfe die Effekte an der Membran verankerter Polymere mit hoher Genauigkeit im Limes kleiner Membrankrümmungen berechnet werden können. Die Einflüsse von Selbstvermeidung und verschiedenen Polymerarchitekturen werden diskutiert. Es zeigt sich, daß der Effekt der Selbstvermeidung bei linearen Ketten klein ist. Hingegen ergeben die Simulationen, daß sich mit Sternpolymeren die Effizienz des Polymers steigern läßt. Der Polymereffekt auf die Biegesteifigkeit und die spontane Krümmung pro Arm nimmt mit der Funktionalität (d. h. der Anzahl der Arme) des Sternpolymers zu; der Effekt auf das Gauß'sche Biegemodul ist unabhängig von der Funktionalität. Skalenargumente bestätigen das in den Simulationen gefundene Verhalten für Sternpolymere. Der Effekt von Ringpolymeren wird untersucht und der Einfluß von Knoten auf das Verhalten der Ringpolymer-Systeme wird diskutiert.

Es wird ein Algorithmus vorgestellt, mit dessen Hilfe sich, ebenfalls im Limes kleiner Krümmungen, der Einfluß an der Membran adsorbierter Polymere auf die Membrankonstanten simulieren läßt.

Für lineare Polymere in der lamellaren Phase wird im Limes kleiner Membrankrümmungen der Einfluß der eingeschränkten Geometrie untersucht. Die Simulationen zeigen, daß sich der Polymereffekt an der Membran verankerter Polymere auf die Membrankonstanten bei kleinem Membranenabstand qualitativ ändert. Während für große lamellare Abstände das Polymer die Biegesteifigkeit erhöht und den Gauß'schen Biegemodul erniedrigt, werden ab einem Lamellenabstand der ungefähr dem Trägheitsradius des Polymers entspricht, Effekte umgekehrten Vorzeichens beobachtet.

Unter Verwendung eines Modells für verankerte Polymere an einer fluktuierenden Membran wird schließlich der Polymereffekt auf das gesamte Fluktuationsspektrum der Membran simuliert. Das Ergebnis ist eine universelle Skalenfunktion mit einem Maximum bei großen Fluktuationswellenlängen.

Abstract

Membranes can be described by a model of mathematical surfaces where the membrane's properties are characterised by the three membrane curvature elastic constants 'spontaneous curvature', 'bending rigidity' and 'saddle-splay modulus'. Experiments show that the addition of polymers can change the properties of a membrane system considerably. One example is the polymer-boosting effect which has been discovered recently for oil-water-amphiphile mixtures. The scattering data has been described successfully by the membrane model. The effect of the polymers has been taken into account by effective membrane curvature elastic constants.

The concept of effective curvature elastic constants will be introduced, and the effects of different kinds of polymer additions to membrane systems discussed in the literature will be reviewed. Using the model of freely-jointed chains for the polymers, the effects of polymers anchored to membranes will be studied for several systems by means of Monte Carlo simulations.

A simulation technique is described which allows to calculate the polymer effect with high accuracy in the limit of small membrane curvatures. The effects of self-avoidance and of different polymer architectures are investigated. The self-avoidance effect for linear polymer chains is found to be small. However, the simulations show that star polymers increase the efficiency of the polymer. The effects on the bending rigidity and the spontaneous curvature per arm increase with the functionality (i. e. the number of arms) of the star, whereas the effect on the saddle-splay modulus does not depend on the functionality. Scaling arguments confirm the behaviour observed in the simulations. The properties of anchored ring polymers are studied and the effects of knots are discussed.

An algorithm is presented which can be employed to calculate the effect of adsorbed polymers on the curvature elastic constants in the limit of small curvatures.

For linear chains in the lamellar phase, the effect of the confined geometry is investigated, again in the limit of small membrane curvatures. The simulations show that for polymers anchored to membranes, at a small lamellar spacing the effect on the membrane curvature elastic constants changes qualitatively. While for large interlayer spacings the polymer increases the bending rigidity and decreases the saddle-splay modulus, effects of opposite sign are observed for lamellar spacings smaller than the radius of gyration of the free chain.

With a model for polymers anchored to a fluctuating membrane, the polymer effect is simulated for the whole fluctuation spectrum of the membrane. We obtain a universal scaling function with a maximum at large fluctuation lengths.

Contents

CONTENTS

Chapter 1

Introduction

Soft matter physics deals with the behaviour of systems which are characterised by a mesoscopic length scale, between atomic and macroscopic size. These systems are referred to as 'soft' because typically small changes in energies (e. g. adhesion energies) have huge effects on their behaviour. From a theoretical point of view, soft matter physics is a part of classical statistical mechanics. In my thesis, I have investigated properties of polymer-membrane systems by means of computer simulations. Theoretical models for these compound systems have been studied only recently, despite research for systems of each kind is well established. The properties of systems containing only polymers have already been investigated thoroughly and also the properties of pure membrane systems are well known. My work focuses on the description of the effect of polymers anchored to membranes in the so-called mushroom regime by effective membrane curvature elastic constants. The values of the effective constants can be determined using simple polymer-membrane models and they can be employed to study more complex systems within the framework of pure membrane models.

The shapes and fluctuations of membranes are controlled by their curvature elasticity, governed by the membrane Hamiltonian

$$\mathcal{H} = \int dS \left[\frac{\kappa}{2} \left(c_1 + c_2 - c_0 \right)^2 + \bar{\kappa} c_1 c_2 \right] \tag{1.1}$$

where the integral is performed over the whole membrane area and c_1 and c_2 are the principal curvatures at each point of the membrane. The Hamiltonian will be discussed in more detail in chapter 3, but as it defines the membrane's curvature elastic constants, it needs to be introduced as early as possible. κ denotes the bending rigidity, c_0 the spontaneous curvature and $\bar{\kappa}$ the Gaussian saddle-splay modulus.

Polymers can be added to a membrane system as free chains in solution or as chains which are anchored to the membrane, compare figure 1.1. For anchored polymers, different concentration regimes have to be distinguished. In the mushroom regime, polymers do not interact mutually. The polymer chain is not further
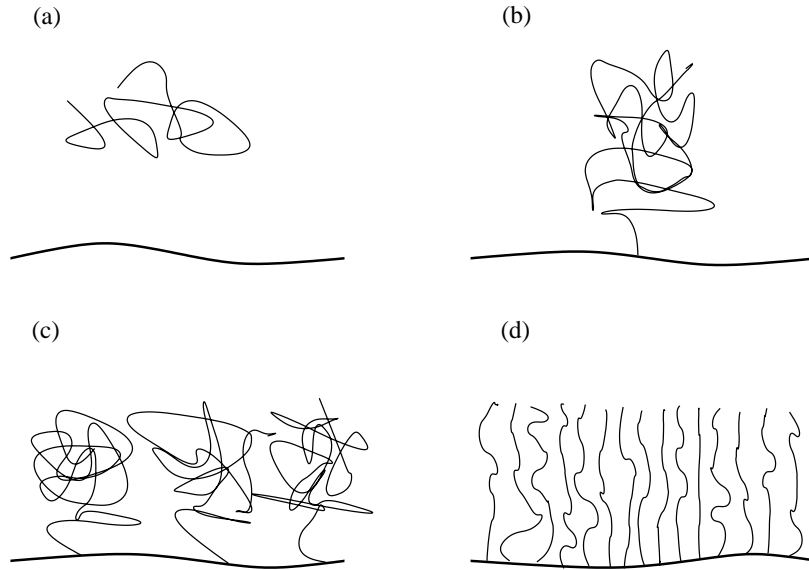
Figure 1.1: A polymer-membrane system for different kinds polymer additions: (a) free chains in solutions, (b) anchored polymers in the mushroom regime, (c) anchored chains at the overlap concentration, (d) polymers in brush regime

constrained and forms a coil (with a monomer density looking somewhat similar to a mushroom). At the overlap concentration, interchain interaction comes into play. The overlap concentration is defined by the distance of roughly the average radius of the polymer coil between the anchor points. In the brush regime, the polymer chains are closely packed, so that they have to stretch away from the membrane. Polymers interact with the membrane either by steric repulsion because of their entropy loss due to confinement, or they influence the membrane's curvature elastic constants. E. g. for asymmetric polymer addition, they affect the spontaneous curvature c_0, i. e. they cause the membrane to bend. In any case, polymers change the bending elasticities κ and $\bar{\kappa}$. In the brush regime, it is most easy to illustrate the effects on the membrane constants. If polymers are anchored only to one side of the membrane, the membrane will bend in order that the chains acquire more space and gain entropy. In case the membrane is decorated with chains on both sides, the polymers will stiffen the membrane. For a curved membrane shape, the inner chains loose entropy by being packed together more tightly. This entropy cost is larger than the entropy gain of the outer chains by their extra space. Thus fluctuations of the membrane are suppressed and κ increases on polymer addition.

In chapter 2, the thesis will be motivated by the discussion of several types of membrane systems with added polymers. The reader will get familiar with the polymer boosting effect, with polymer-decorated vesicles and with polymer-

containing lamellar membrane phases. The discussion will be based mainly on experiments.

An overview over recent achievements in theoretical studies for the mushroom regime will be presented in chapter 3. After a short introduction to the theoretical description of membranes, results of analytical calculations will be reported as well as results obtained by computer simulations. This chapter does not intend to give an introduction to the methodology: chapters 2 and 3 provide the background knowledge on the phenomena observed in compound systems.[1]

Computer simulations are a powerful tool in soft matter physics as the system's behaviour is mainly driven by entropy. The models employed are formulated on a coarse-grained level and can be used to describe a large variety of experimental systems. Universal scaling laws even allow to access several system sizes with the results of one calculation. I will use different techniques for my investigations, but some aspects of modeling and simulation are relevant for all cases and will be discussed in chapter 4. All simulations in this work have been done with the Monte Carlo method. Using Monte Carlo, considerable effort has to be spent to choose an efficient algorithm, because the same code needs to be executed many times. Important qualities of each program are speed (to obtain a proper statistics in reasonable time) and a good random number generator. The question of the execution time of the algorithm is especially crucial for the self-avoidance check of polymers, thus an adequate technique for that task will be described in this chapter.

A simulation and evaluation method has been developed to investigate the influences of polymer self-avoidance and different polymer architectures. The polymers exhibit an excluded-volume interaction with the membrane. Metropolis Monte Carlo and the pivot algorithm have been applied to generate ensembles of system conformations. Information on bending rigidity, saddle splay modulus and spontaneous curvature can be extracted from the simulation data. Details of the method as well as results are presented in chapter 5. The influence of self-avoidance for linear chains has been studied by the simulation of chains with up to 200 bonds. A model-specific correction-to-scaling relation has been established. The corrections describe the data for finite system sizes and allow to extrapolate to the universal values that correspond to an infinite number of bonds. The method is capable to deal with polymers of all architectures provided that they are anchored to the membrane at a single point. I will present and discuss data for self-avoiding star polymers anchored at their center and for ring polymers with and without self-avoidance.

Systems with an additional attractive membrane-polymer interaction require a different sampling algorithm compared to those where interaction is only due to excluded volume. The idea of evaluation is basically the same, but Metropolis

---

[1]If an introduction to the concept of membrane curvature constants is needed, the reader should start with chapter 3.

Monte Carlo is no longer the method of choice. A simulation technique that employs the Pruned Enriched Rosenbluth Method (PERM) will be introduced in chapter 6. As every growth algorithm, PERM delivers values for the partition function of a system which will be needed for further evaluation. The simulations of chains anchored to walls of different curvatures can then provide the data necessary to calculate the polymer effect.

Various experiments are well described by the polymer's influence on membrane fluctuations of a length scale which is large compared to the size of the chains. The studies of self-avoidance, of different architectures and of the polymer adsorption effects only consider this limit. Apart from theoretical interest, for some experimental systems the effects on fluctuations of all length scales are relevant. Simulations of linear chains attached to fluctuating membranes that show the polymer's influence on the fluctuation spectrum are presented in chapter 7.

An intriguing question is the effect of polymers in confined geometries, for example in lamellar membrane stacks. The most naive expectation would be that the absolute value of the polymer effect increases significantly due to the confinement, as the chains will interact with the membrane much more frequently. While this hypothesis seems to be trivial, the consideration of limiting cases reveals a crucial point: Without any additional spacial constraint, the effect of free and anchored polymers on the membrane's bending rigidity and the saddle splay modulus have different signs. A tight compression of the chains in a lamellar phase implies that the anchoring effect of the polymer vanishes, because the anchor no longer affects the polymer conformations. In this case, free and anchored polymers should induce exactly the same changes on the curvature elastic constants. Thus for one of both systems, strong confinement results in a qualitative change of the influence on the membrane fluctuations! Simulation results will be presented in chapter 8.

Finally, the conclusions in chapter 9 summarise the results.

Unless otherwise noted, all values for κ, $\bar{\kappa}$ in this thesis are in units of $k_B T$.

Chapter 2

Experimental background

The flexibility of polymer chains has been discovered in the 1930s [1–6]: Experiments had been done to determine the change in entropy when polymers are solubilised, and to measure the viscosity of polymer solutions. In some solid samples birefringence had been observed if stress had been applied to the materials. Theories that tried to explain the observed effects by rod-like molecules failed. The experimental data led to the conclusion that the polymers had to be flexible molecules in these systems. More recently, several experiments have been done for polymer-membrane systems and will be discussed in the following sections to motivate my theoretical studies.

2.1 Microemulsions

It is common knowledge that under normal conditions oil and water do not mix. Addition of amphiphiles to the system can induce a mixing process. Amphiphiles are molecules that consist of a hydrophobic and a hydrophilic part. Their hydrophilic part likes to be in contact with water whereas their hydrophobic part prefers to be in contact with oil. Thus amphiphiles assemble inbetween both liquids. The properties of the amphiphilic interface are different from those of an interface where oil and water are in direct contact; in particular the amphiphiles lead to a vanishing surface tension.[1] For this reason, amphiphiles are often denoted as 'surface active components' or 'surfactants' in these systems. The effect of vanishing surface tension is used in cleaning processes[2] (figure 2.1) , but can also be employed to mix larger volumes of oil and water or other polar and non-polar liquids (figure 2.2). Under appropriate conditions, addition of amphiphiles will lead to a so-called microemulsion phase.

Recent experiments led to the discovery of the 'polymer boosting effect',

---

[1]Because of the vanishing surface tension, in my terminology the interface formed by the amphiphiles is a membrane, compare [7].

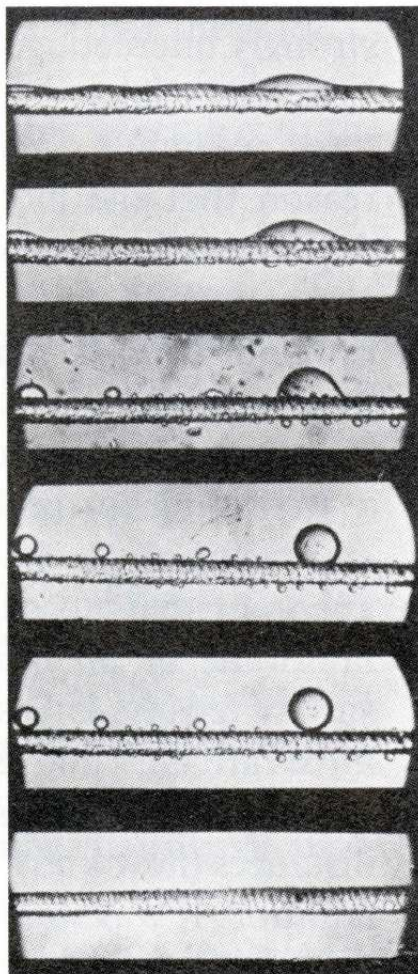[2]In cleaning processes, the amphiphiles are referred to as detergents.

Figure 2.1: Addition of amphiphiles to an oily fiber in water reduces the surface tension between oil and water. This leads to the formation of oil droplets and the oil will be removed from the fiber [8]. The figure shows the system at different times after the addition of the amphiphiles.
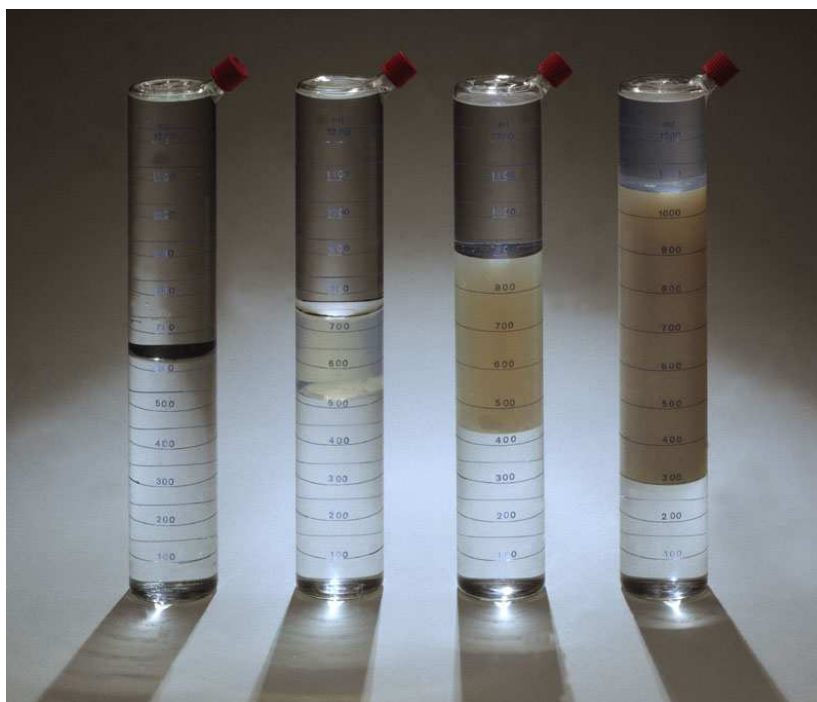
Figure 2.2: Oil and water stay separated under normal conditions (left column). After addition of about 6.5% (per volume) of amphiphile, a certain amount of oil and water is found to be in a microemulsion phase (second column). Further addition of amphiphilic block copolymers (0.5% in the third and 0.9% in the fourth column) dramatically enlarges the microemulsion phase [20].

described in several PhD theses [9–11] and a number of accompanying papers [12–19]: The addition of small amounts of amphiphilic diblock copolymers to an oil-water microemulsion can result in a huge enhancement of the volumes of oil and water which are found in the microemulsion phase.[3] The interfacial area is fixed by the amount of amphiphiles, thus the structural size needs to grow in order to mix larger volumes of both liquids. In the system shown in figure 2.2, the structural size becomes of the order of the wavelength of visible light, which can be recognised because the microemulsion appeares more opaque. The structure of the microemulsion can be revealed on a nanometer scale by freeze-fracture electron microscopy [21] (see figure 2.3). The 3D picture that emerges from this is that oil and water form a bicontinuous sponge-like structure (figure 2.4): From each point in the oil, every other point in the oil can be reached without leaving the oil; the same applies for the water. It has been shown by neutron scattering

---

[3]This implies that the microemulsion phase is shifted in phase diagrams to lower volume fractions of amphiphiles. For a more detailed discussion of this aspect, please refer to the literature.
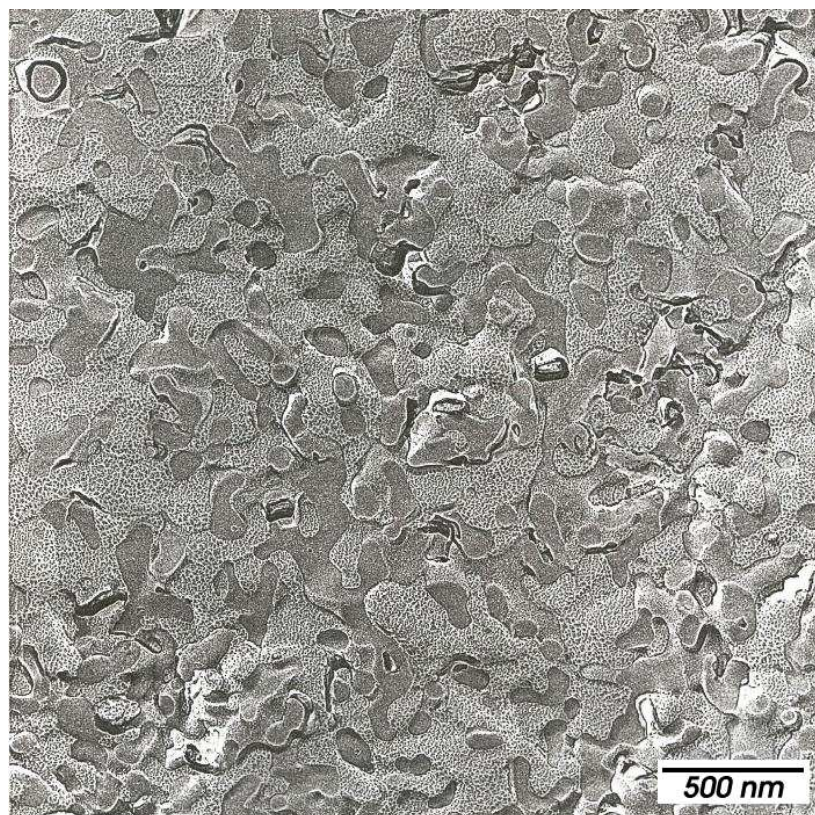
Figure 2.3: A freeze-fracture electron micrograph of the microemulsion phase of an oil-water-amphiphile system [22].
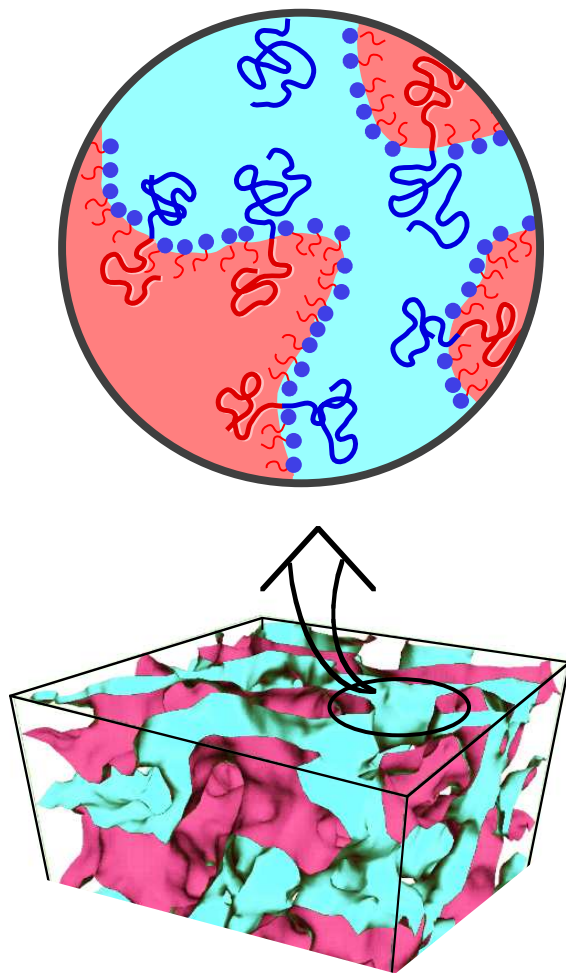
Figure 2.4: The amphiphile separates oil and water within the bicontinuous microemulsion. Experimentally, the polymer is found to assemble at the interface in mushroom conformation [23].

that the polymers assemble — like the amphiphiles — at the oil-water interface. Neutron and light scattering experiments together with modern theories have provided a consistent description of the system's behaviour.

Before continuing the discussion with details of the polymer-membrane system, I will give a short overview on microemulsion research in this paragraph. The theoretical interest in emulsions of two liquids that are formed by addition of an amphiphilic component is rather old [24] and quantitative descriptions of emulsion structure and phase diagrams can be found in articles written in the 1940s [25, 26]. Systematic studies of the solubilisation of different hydrocarbons in aqueous solutions using several kinds of nonionic surfactants have already been reported in the 1960s [27]. The occurrence of bicontinuous structures in fluid-fluid mixtures has first been proposed in the 1970s [28]. Nevertheless, the evaluation of microemulsion scattering data continued to be based on droplet structures for some years, see e.g. Ref. [29]. Only in 1987 Teubner and Strey published a model to interpret the scattering intensity distribution of bicontinuous microemulsions which has been since then applied to investigate different systems [30–34]. In this model, the scattering intensity function is fitted to the functional form

$$I(q) \sim \frac{1}{a_2 + c_1\, q^2 + c_2\, q^4} + b \tag{2.1}$$

with the parameters a_2, c_1, c_2 and b.[4] By Fourier transformation, the correlation function is obtained which contains the two length scales

$$\xi = \left[\frac{1}{2} \left(\frac{a_2}{c_2} \right)^{1/2} + \frac{c_1}{4c_2} \right]^{-1/2} \tag{2.2}$$

and

$$d = 2\pi \left[\frac{1}{2} \left(\frac{a_2}{c_2} \right)^{1/2} - \frac{c_1}{4c_2} \right]^{-1/2} \tag{2.3}$$

where d characterises the domain size while ξ is the correlation length. Roughly at the same time when the first experiments based on the Teubner-Strey model have been done, an active discussion of the scattering properties of bicontinuous microemulsions on a theoretical level took place, which addressed static [35–37] and dynamic [38–41] aspects. Some of the publications of experiments with bicontinuous and droplet microemulsions discuss the elastic constants of the amphiphilic film [34, 42–47].

The polymer-membrane system has been treated theoretically on the basis of a pure membrane system, taking into account for the polymers by effective membrane curvature elastic constants. Calculations employing a Gaussian random

---

[4]The fit parameter b represents an (mainly) incoherent background contribution which can be determined from the scattering intensity at large q values.

field model give an expression for the dimensionless product

$$k\xi = \frac{64}{5\sqrt{3}}\frac{\kappa}{k_B T}\Theta\left(\frac{\kappa}{k_B T}, \delta_m \frac{S}{V}\right) \tag{2.4}$$

with the characteristic wave vector $k = 2\pi/d$ and the algebraic function $\Theta\left(x, y\right)$ which approaches unity for large κ. The parameter S denotes the membrane area, V the sample volume and δ_m the membrane thickness. Membrane fluctuations at smaller length scales lead to a renormalisation of the bending rigidity on the length scale ℓ by

$$\tilde{\kappa}_R\left(\ell\right) = \kappa - \alpha\frac{k_B T}{4\pi}\ln\left(\frac{\ell}{\delta_s}\right) \tag{2.5}$$

where δ_s is the size of the surfactant molecules. The value of α is still under debate, but taken to equal 3 [7, 48–50]. Combining Eqs. (2.4) and (2.5) and assuming κ to be large enough to set $\Theta = 1$ provides an expression to extract the bending rigidity κ from the experimental data[5]:

$$k\xi = \frac{64}{5\sqrt{3}}\frac{\kappa_R\left(\phi_s\right)}{k_B T} \tag{2.6}$$

At the three-phase coexistence, the Gaussian saddle splay modulus $\bar{\kappa}$ can be obtained by exploiting equation

$$\ln\left(\frac{\phi_s}{\phi^*}\right) = -\frac{4\pi}{\bar{\alpha}}\frac{\bar{\kappa}}{k_B T} \qquad , \tag{2.7}$$

where ϕ^* is a constant of order unity [6] and $\bar{\alpha} = -10/3$ [7]. Details of the derivation of these equations can be found in Ref. [16].

The polymers have been shown experimentally not to interact with each other, thus their effects on κ and $\bar{\kappa}$ are proportional to the density σ of chains per membrane area. The polymer effects will certainly also depend on the polymer length which can be characterised by the mean squared end-to-end distances, that the hydrophobic (R_o^2) and the hydrophilic (R_w^2) parts of the polymer would have as a free chains in oil respectively water. The total effect has been found to be proportional to $R_o^2 + R_w^2$.

---

[5] ϕ_s denotes the surfactant volume fraction and is proportional to $1/\ell$.

[6] The constant ϕ^* is determined in order to fulfill

$$\kappa_R\left(\sigma\right) = \left(\kappa_{mem} - \frac{\alpha}{\bar{\alpha}}\bar{\kappa}_{mem}\right) + \frac{k_B T}{12}\left[1 + \frac{\pi}{2} + 2\frac{\alpha}{\bar{\alpha}}\right]\sigma\left(R_w^2 + R_o^2\right) \tag{2.8}$$

where σ, R_o and R_w are determined by the amount of polymer and the polymer chain length; parameters with subscript 'mem' denote bare membrane values, compare chapter 3.

[7] This value is under debate, same as α [7, 48–50]

The theoretical picture describes the experimental results very well. The change of the bending rigidity has been determined experimentally of a system of water, n-decane, $C_{10}E_4$ and PEPx-PEOy [8] to be

$$\Delta\kappa_{exp} = 0.334 \; \sigma \left(R_w^2 + R_o^2 \right) \tag{2.9}$$

in Ref. [16]. The corresponding value of the saddle splay modulus is reported to be

$$\Delta\bar{\kappa}_{exp} = 0.408 \; [\pm 0.014] \; \sigma \left(R_w^2 + R_o^2 \right) \tag{2.10}$$

in Ref. [13]. Both values exceed those found in analytical calculations for ideal chains ($\Delta\kappa_{analytical} = \left(1 + \pi/2 \right)/12 = 0.214$ and $\Delta\bar{\kappa}_{analytical} = 1/6 = 0.167$) by a factor between 1.5 to 2 (compare chapter 3). Note that the evaluation of $\bar{\kappa}$ has been published before the evaluation of κ. In retrospect, the evaluation of $\bar{\kappa}$ seems to be inconsistent: In Eq. (2.8) the theoretical value for the polymer effect of ideal chains has been used to describe the behaviour of κ. As there is a discrepancy found in this value between the experimental data and the analytical theory, it should be more reasonable to use the experimentally determined κ instead of the theoretical value.

For completeness I want to refer the reader to two other recent publications and references therein: The effects of polymers adsorbing at the interfacial layer in microemulsions are discussed in Ref. [51] and the effects of a copolymer with a hydrophobic backbone and hydrophilic side chains added to an oil-continuous microemulsion were published in [52].

2.2 Vesicles

Polymer-dressed vesicles constitute an especially interesting object to study, because the system's architecture is close to the one of biological cells [53].

Of particular interest for my thesis is the micropipet aspiration method for vesicles which allows to measure the effect of anchored polymers on the bending rigidity [54–56] (see figure 2.5). The vesicle diameter in the pioneering experiment by Evans and Rawicz [54] has been $\sim 20\,\mu m$, the glass caliber $\sim 8\,\mu m$. Suction pressures between $\sim 10^{-6}\,atm$ and $\sim 10^{-2}\,atm$ have been applied which led to lateral tensions in the membrane between $\sim 10^{-3}\,mN/m$ and $\sim 10\,mN/m$. The data which is needed to determine the bending rigidity are the suction pressure ΔP, the pipet radius R_p, the mean radius of the exterior vesicle segment R_o and the projection length ΔL inside the pipet. The evaluation takes into account for an (apparent or real) increase in membrane area, which is assumed to be due to damping of fluctuations at low surface tensions and to direct stretching at high surface tensions. The bending rigidity κ (and the bare area dilution module K_α)

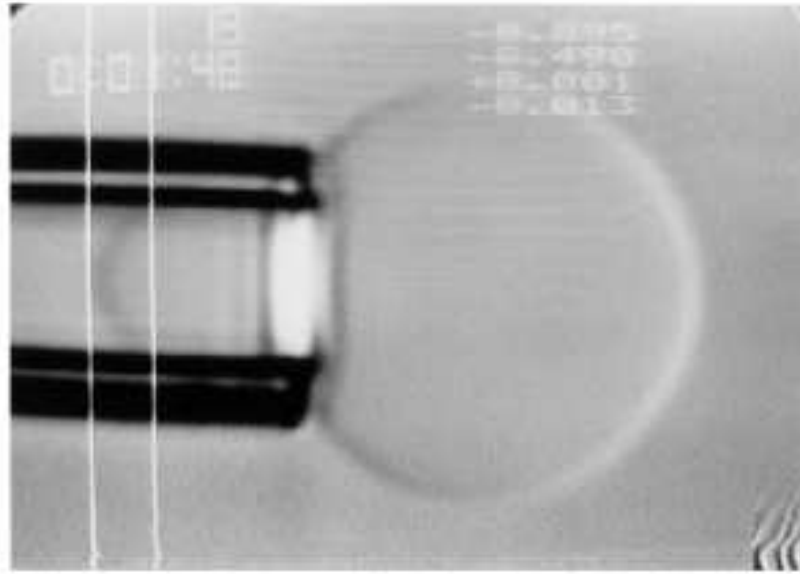[8]polyethylene-propylene/polyethyleneoxid with x PEP and y PEO units

Figure 2.5: Micropipette measurements can be used to determine the bending rigidity of polymer-decorated membranes [54].

of the membrane is then determined using the relations

$$\tau_m \approx \frac{\Delta P R_p}{2}\left(1 - \frac{R_p}{R_o}\right)$$

$$\alpha = \left[\left(\frac{R_p}{R_o}\right)^2 - \left(\frac{R_p}{R_o}\right)^3\right]\frac{\Delta L}{2 R_p}$$

$$\alpha = \left(\frac{k_B T}{8\pi\kappa}\right)\ln\left(1 + c\tau_m A\right) + \frac{\tau_m}{K_\alpha} \tag{2.11}$$

where τ_m is the (uniform) membrane tension, $\alpha = \Delta A/A$ the fractional change in area and $c \approx 0.1$ is used to describe the surface undulations. The third equation is valid for 'high enough' bending moduli (compare Ref. [54]). Note that the polymer effect measured in Ref. [54] is proportional to $\sigma R^2_{polymer}$ as expected for the mushroom regime. However, the experimental values of Evans and Ravicz are measured at the transition to the brush regime, in which a different scaling behaviour is expected theoretically.

Polymer-dressed vesicles have good prospects for application: They are discussed for use in medicine [57–61], e. g. for targeted drug delivery to tumors. Polymer coating enhances the stability of vesicles in biological environments significantly and leads to an increased circulation time in the human blood system. Red blood cells as well as the human vascular system are also coated with a
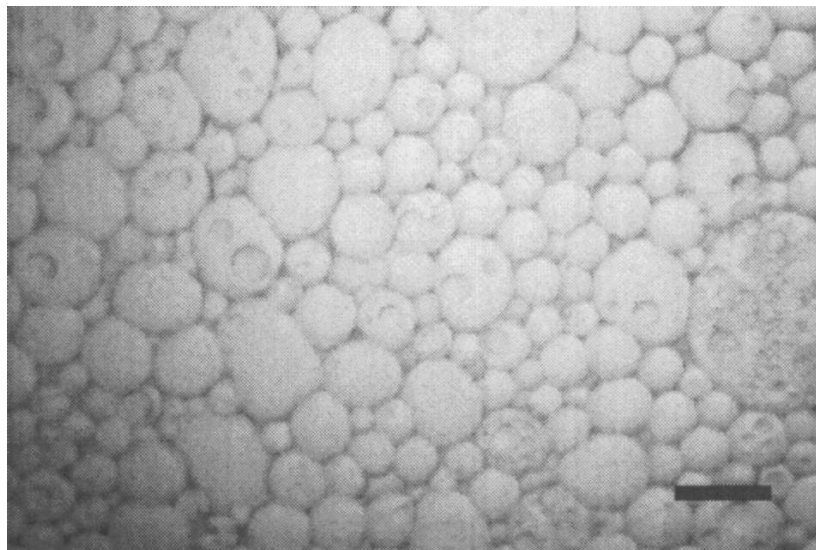
Figure 2.6: A photo-micrograph of an ethylcellulose-stabilised water-in-oil emulsion, taken at 15 °C. The scale bar has a length of $9.23 \, \mu m$. [67]

polymer layer [62]. Because artificially produced dressed vesicles are kind of invisible to the human's immune system, these vesicles are often denoted as 'stealth[9] liposomes'. In other publications they are referred to as 'sterically stabilised liposomes' because their stability is believed to be due to the steric barrier provided by the anchored (or adsorbed) polymers [59,60]. It is interesting to note that red blood cells are best described by the marginal brush regime [10] and this is also the concentration at which stealth liposomes are most efficient [54]. A further increase of the grafting density does not prolong the lifetime of the stealth liposomes in the human body, whereas in vitro experiments have shown an increased repulsion with increased grafting density and chain length [60,63]. Basic research on vesicles with grafted polymers is going on [64–66]. The stabilising effect seems to be not yet fully understood and the rather general statement on the knowledge about stealth liposomes in the review article of Lasic from 1994 is still up to date:

> "Liposomes aggregate and fuse in the presence of hydrophilic polymers but their properties were difficult to explain when block copolymers were adsorbed or surfactants with larger polymeric polar heads were inserted into the liposome membrane, because such systems are inherently ill defined." [60]

After all, I would like to discuss a third subtopic in this section: Emulsion stabilisation. A typical picture of a polymer-stabilised emulsion is shown in figure

---

[9]'Stealth' is a registered trade name by Liposome Technology, Inc.

[10]just above the overlap concentration

2.6. At first glance emulsions seem to be rather different from stealth liposomes. On a second view both systems are very closely related. Emulsions typically consist of oil-in-water or water-in-oil droplets. At least for some systems the interfacial tension between both liquids is considered to be very low [68], which indicates that the membrane picture applies. Polymers that are soluble in the exterior phase are used as emulsion stabilisers. An essential feature of these polymers is the presence of small anchors that graft the chain in the other liquid [67,69–73]. Thus polymer-stabilised emulsions can be discussed in the framework of a theory developed for polymer-dressed vesicles. Authors in both fields also refer to the same publications when they refer to the historic development of their research area (see [60,70,74] and references therein):

- Ink was prepared already in Egypt and China about 2500 BC by mixing lamp black with a solution of a natural polymeric stabilizer.

- Michael Faraday did the first scientific studies on the aggregation of gold particles with and without polymer around 1850.

- Zigmondy coined the term 'protective colloid' and Heller and Pugh introduced the term 'steric stabilisation'.

Anyhow, obviously in emulsion systems as well as for stealth liposomes there is a new aspect compared to the traditional research on colloid stabilisation by polymers: The flexibility of the membrane. The influence of membrane fluctuations on the stabilisation has, to my knowledge, not yet been investigated for stealth liposomes, nor for polymer-stabilised emulsions.

2.3   Lamellar systems

Studies for polymer-membrane systems in the lamellar phase are present in literature for almost 20 years. Helfrich has shown in 1978 that pure lamellar membrane stacks are stabilised by entropic undulations forces [75]. Two years later, the Caille factor of smectic liquid crystal phases has been measured by x-ray scattering [76]. Using this technique, the Helfrich expression for lamellar membrane stacks has been confirmed experimentally [77]. Nevertheless, note that Monte Carlo simulations of lamellar systems show the same qualitative behaviour as reported in the original work by Helfrich, but lead to a different prefactor c_∞ [78–80] for the free energy at mean membrane distance d, per projected surface area and per membrane:

$$f(d) = c_\infty \frac{(k_B T)^2}{\kappa d} \qquad (2.12)$$

Field theoretical calculations for a membrane between walls support the validity of the simulation results compared to the original estimate [81–83].

The first experiments of polymers confined to lamellar phases have been reported, to my knowledge, in 1984. Studies on phase diagrams by NMR and x-ray scattering have been done to investigate the dissolving properties of polymers in a lamellar phase [84]. Reports of the early investigations concentrate on a polymer-induced phase separation [85], measured critical exponents [86] and provide detailed phase diagrams [87, 88]. Especially interesting from my point of view are experiments where the system stays in the lamellar phase because these experiments allow to measure the effect of the polymer on the properties of the lamellar stack quantitatively, exploiting the Helfrich and Caille theories. Two kinds of effects are expected to appear: Polymers directly change the interlamellar interaction and they change the effective curvature elastic constants of each membrane. For non-adsorbing polymers (figure 2.7, B), the interlayer interactions have been found to be attractive in all cases by theoretical arguments.[11] Contributions to the curvature elastic constants have been considered to be negligible in the early publications, based on calculations for the renormalisation of the constants by adsorbed polymers [90, 91].[12] The experiments thus have been considered as ideal systems to study the confinement of polymer chains [89,92,93]. Brooks and Cates have suggested to describe the polymer effect by a modified bilayer thickness adding a term $\Delta d_{BC} = \epsilon_{BC} L_{BC}$ in the energy and pressure expressions of the lamellar system. The variation of ϵ_{BC} allows to describe short-ranged repulsive ($\epsilon_{BC} > 1$) and attractive forces ($\epsilon_{BC} < 1$) between the layers on a phenomenological level while L_{BC}^3 denotes the systems size [92].

More recent experiments report effects that seem to be not compliant with theories which take into account only for the direct interlayer interactions mediated by the polymers. In some studies, even membrane curvature elastic constants are evaluated:

- Warriner et al. [94] investigate a system with linear polymers anchored with one end to the membrane (figure 2.7, A). They observe a phase transition from the lamellar to the gel phase which occurs at increased polymer content as well as for addition of water. This effect might be explained by the same changes of the membrane elastic constants in both cases, see chapter 8. In a consecutive publication, Warriner et al. [95] study the effects of the polymer in a more detailed fashion by the Caille theory.

- The picture of an effective thickness to describe polymer addition, originally introduced by Brooks and Cates, is put forward again in a letter where the thickness is directly related to the geometrical properties of the polymer [96]. Trying to connect this picture with experimental data, it is found that the effective thickness seems to reach a maximum as soon as the

---

[11]The effect is argued to be analogous to the depletion interaction between two plates [89].
[12]The calculations were done for single membranes and unconstrained geometries.
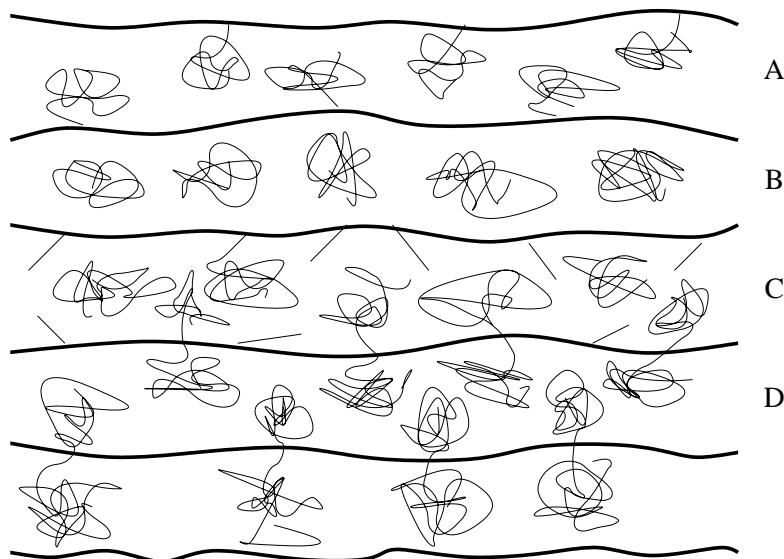
Figure 2.7: A polymer-membrane system in lamellar phase. Systems with different kinds of polymers are visualised. In part A, polymers grafted with one end to the membrane are sketched, part B shows free chains, part C a mixed-polymer system and in part D diblock copolymers assemble at the interface.

polymer mushrooms begin to overlap.[13] At low polymer concentrations the observed effects are stronger than expected in a simple model for the polymer thickness. Both observations can be explained by the assumption that the polymers increase the membrane thickness on areas much larger than those determined by the radius of gyration. Further details of the more elaborate model for the thickness of the polymer layer, including considerations of the stretching of the membrane in the brush regime, are discussed in Ref. [97].

- Yang et al. [98] report a rigidification, i. e. an increased κ when polysoaps are added. Polysoaps have a long backbone which is anchored with sidechains to the membrane (similar to figure 2.7, A). A detailed theory for this situation is not yet available. The interesting point is that the authors explicitly claim that in their case the contribution of the increased layer thickness by the polymer can be neglected.

- Addition of free polymer chains to a lamellar phase was studied in Ref. [99] (figure 2.7, B). The authors find that the bending rigidity κ is insensitive to

---

[13]This observation is consistent with the observations of sterical stabilisation discussed in the vesicles section of this chapter.

the amount of polymer in the lamellar phase while the saddle-splay modulus $\bar{\kappa}$ is strongly decreasing.

- Tsapis et al. [100] have investigated a system with peptides lying on the membrane layers. They have measured a rigidification of the membranes of a high magnitude which could not be explained by the theories for membranes with rigid inclusions [101, 102].

- Taulier et al. [103] have studied a lamellar stack with low molecular-weight polymer inclusions. They explain the observed decrease in lamellar spacing by a thinning of the single layers.

A selection of experiments has been presented in which the effect of polymers added to a lamellar membrane phase is studied. Qualitatively different effects have been observed in the systems. Several variations of the experiments discussed have been investigated: e. g. addition of polymers which assemble within the bilayers itself [104], modification of the lamellar phase by polyelectrolytes [105], investigation of systems with combined electrostatic and polymer effects [106] and coiling of cylindrical membrane stacks with anchored polymers [107]. Among other applications, lamellar systems can be used for the production of amphiphilic polymer networks [108]. There is a huge number of experiments and applications, but as far as I know the number of theoretical studies available is rather limited: Estimates of the smectic compressibility of polymer-containing lyotropic lamellar phases are available [89], investigations of the changes of the bending moduli by rigid inclusions in bilayers of lamellar membrane stacks have been published [101,102,109] and the model of the renormalised membrane thickness [96] is discussed in literature. A new work of Blokhuis et al. [110] investigates the interaction between two planar, polymer-adsorbing surfaces.

I am not aware of a single theoretical study taking into account *direct and indirect* effects of the polymer addition. Such a theory would be valid for the whole range of interlamellar spacings and should be able to combine the data of different experiments in one consistent picture. The theory should also be capable to explain phenomena observed for polymer dressed vesicles in confined geometries, i. e. systems like stealth liposomes and stabilised emulsions. For sure it is necessary that this theory will incorporate, among others, the polymer-effect on the curvature elastic constants as function of the mean interlamellar distance.

Chapter 3

Theoretical background

Several aspects of polymer-membrane systems have been investigated by means of analytical and simulation methods. It is possible to determine effective values of the membrane curvature elastic constants which can be used to model the experimental systems. The results of a one-polymer model apply to systems with low polymer densities where the chains do not interact mutually. For example in the microemulsion experiment, the polymers are found to be in the mushroom regime where the interactions between the chains can be neglected. In this chapter, results and concepts will be presented and I try to avoid to address aspects of modeling and calculational details. The basic techniques which have been employed for my own work will be described in the next chapter.

3.1 The membrane Hamiltonian and curvature elastic constants

The Hamiltonian of a membrane [111–113] (compare also Ref. [114]) is given by

$$\mathcal{H} = \int dS \left[\frac{\kappa}{2} \left(c_1 + c_2 - c_0 \right)^2 + \bar{\kappa} c_1 c_2 \right] \tag{3.1}$$

with the bending rigidity κ, the spontaneous curvature c_0 and the saddle-splay modulus $\bar{\kappa}$. The variables c_1 and c_2 denote the principal curvatures at each point of the membrane (compare figure 3.1) and the integral is performed over the whole membrane area.

The meaning of the membrane curvature elastic constants can be illustrated in simple examples. First consider the integrand at one point of the membrane.

- If $c_1 = -c_2$ and $c_0 = 0$, the first term in the Hamiltonian is zero and the energy to form a saddle-like structure is determined by the saddle-splay modulus $\bar{\kappa}$.
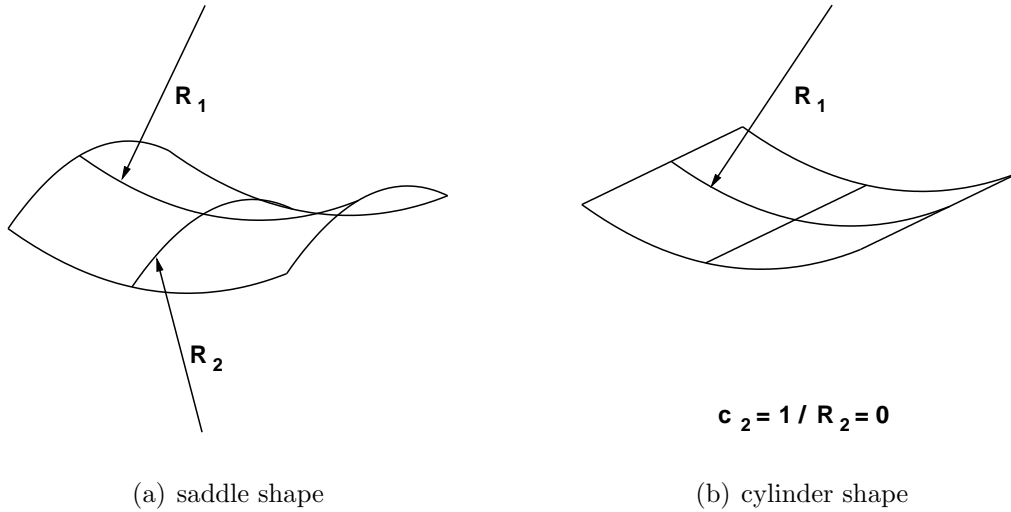
(a) saddle shape   (b) cylinder shape

Figure 3.1: The principal curvature radii at a point of a surface.

- A cylinder-like deformation of the membrane is described by $c_1 = 0$ and $c_2 \neq 0$ or $c_1 \neq 0$ and $c_2 = 0$. For $c_0 = 0$, the energy of the deformation is characterised solely by the bending rigidity κ.

- A finite value for the spontaneous curvature determines a preferred curvature of the membrane which differs from the planar shape. A non-zero spontaneous curvature is expected for asymmetric situations, e. g. a bilayer membrane with two different layers.

Now discuss macroscopic membrane structures.

- For $c_0 = 0$, a high value of the bending rigidity κ will favour a lamellar structure where the single membranes are roughly in a planar shape.

For the evaluation of the saddle-splay part of the integral, the Gauss-Bonnet theorem can be employed [115]. One can show that the topology of an orientable closed surface S with no boundaries is characterised by an integer $g \geq 0$, called the genus of S. The theorem states that

$$2\sqrt{g} \int dS \, c_1 c_2 = 4\pi\chi \tag{3.2}$$

where χ is the Euler characteristic of the surface. For connected surfaces, the result of the integral is characterised by $\chi = 2\,(1 - g)$. The integer g can be interpreted as the number of 'handles' of the surface. A spherical object has no handles and thus $g_{sphere} = 0$ and $\chi_{sphere} = 2$, a torus has one handle and therefore $\chi_{torus} = 0$, an object as sketched in figure 3.2 (c) consists of six handles and therefore has $\chi = -10$.

20

(a) $g = 0, \chi = 2$ (b) $g = 1, \chi = 0$ (c) $g = 6, \chi = -10$
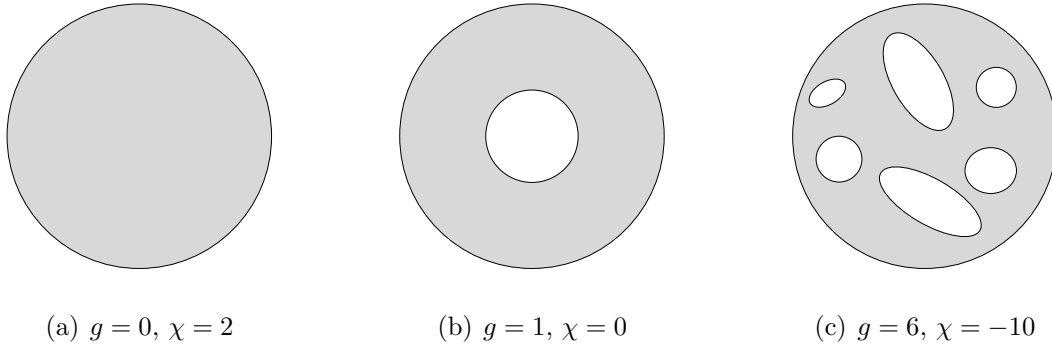
Figure 3.2: The Euler characteristic of different surfaces. A sphere is sketched in (a), (b) represents a torus and (c) is a surface with 6 handles.

- Using the Gauss-Bonnet theorem, it is immediately clear that for vanishing spontaneous curvature a negative value of $\bar{\kappa}$ favours vesicles or droplet emulsions while a positive value would go along with high genus surfaces, as for example bicontinuous microemulsions.

- A non-zero homogeneous spontaneous curvature favours vesicle structures for bilayers, micelles for monolayers.

3.2 Effective membrane curvature elastic constants

General concept

In many cases, the effect of the addition of macromolecules to membrane systems can be described by effective membrane elastic constants.

$$
\begin{aligned}
c_{0,eff} &= c_{0,mem} + \Delta c_0 \\
\kappa_{eff} &= \kappa_{mem} + \Delta \kappa \\
\bar{\kappa}_{eff} &= \bar{\kappa}_{mem} + \Delta \bar{\kappa}
\end{aligned}
\tag{3.3}
$$

where the index "mem" indicates the elastic constants of the bare membrane. The ansatz is very useful to explain the system's properties, especially if the macromolecular size is small compared to the typical system structure size. In this case, direct polymer-mediated effects between 'different' membranes — as for example repulsive forces between layers in lamellar systems (see e.g. [96]) or adhesive forces by polymers that act as anchored stickers [116, 117] — can be neglected.

Different macromolecular additions

It is instructive to compare the effects of the different kinds of added molecules qualitatively. If not stated explicitly, membrane and macromolecules interact via an excluded volume interaction. For macromolecular additions only at one side of the membrane, the dominant effect is a change of the spontaneous curvature c_0, because this term is of linear order in the membrane curvature. All effects are summarised in table 3.1. Addition of spherical colloid [118], rod-like colloid [118, 119, 140, 141] and linear polymer [120] solutions affects the spontaneous curvature in a way that the membrane will bend towards the molecules. The basic effect in these systems is depletion. If the membrane is decorated with end-grafted linear polymer chains, in the mushroom as well as in the dense brush regime the membrane bends away from the polymer [122]. In case the anchored chains experience an additional strong adsorption interaction with the membrane, the membrane is supposed to bend towards the polymer [126] (if the adsorption is not too strong, so that the polymer would completely lie on the membrane [133]). The membrane has been claimed to bend away from the polymer in case of weak adsorption of free chains [121].

Effect of an ideal end-grafted chain

For mushrooms of ideal chains, the effects on the curvature constants read

$$
\begin{aligned}
\kappa_{eff}\,\Delta c_0 &= +\frac{k_B T}{4}\sqrt{\frac{\pi}{6}}\ \sigma\,R_e \\[2mm]
&\approx +0.18\ k_B T\ \sigma\,R_e
\end{aligned}
$$

$$
\begin{aligned}
\Delta\kappa &= +\frac{k_B T}{12}\left(1+\frac{\pi}{2}\right)\sigma R_e^2 \\[2mm]
&\approx +0.21\ k_B T\ \sigma R_e^2
\end{aligned}
$$

$$
\begin{aligned}
\Delta\bar{\kappa} &= -\frac{k_B T}{6}\ \sigma R_e^2 \\[2mm]
&\approx -0.17\ k_B T\ \sigma R_e^2
\end{aligned}
\tag{3.4}
$$

where σ is the number density of chains per membrane area and R_e denotes the root mean squared end-to-end distance of free chains in solution. The values have been obtained by solving the diffusion equation for chains which are anchored to spheres and cylinders of curvature radii much larger than the polymer size [123, 124, 142]. The free energies for the different scenarios are expanded for small curvatures and compared to the membrane Hamiltonian in Eq. (3.1).

type of added molecules	Δc_0	$\Delta \kappa$	$\Delta \bar{\kappa}$	references
spheres	t	$= 0$	> 0	[118]
rods	t	$< 0^{(1)}$	$> 0^{(1)}$	[118, 119]
free chains	t	$< 0^{(2)}$	> 0	[120]
weakly adsorbed free chains	a $^{(3)}$	$< 0^{(4)}$	$> 0^{(4)}$	[90, 91, 121]
strongly adsorbed free chains	t $^{(3)}$	$< 0^{(4)}$	$> 0^{(4)}$	[90, 91, 121]
anchored chains	a $^{(*)}$	$> 0^{(*)}$	$< 0^{(*)}$	[122–125]
weakly adsorbed anchored chains	a $^{(5)}$	> 0	< 0	[126]
strongly adsorbed anchored chains	t $^{(5)}$	< 0	> 0	[126]

Table 3.1: Qualitative effects of low-density macromolecular addition to membrane systems in different cases. The macromolecules are assumed to be small compared with the system's typical length scale. In the column for the spontanuous curvature it is noted, if the membrane bends towards (t) of away (a) from macromolecules which are added only at one side.

(1) There was found a nonanalyticity and an asymmetry for the free energy change by addition of rods with respect to the transition $R \rightarrow -R$ of the membrane's curvature radii. The interpretation of the effects by renormalised membrane constants can only be understood as an approximation. (2) This disagrees with the calculations of Podgornik [127]. (3) The results for the effect on c_0 are taken from Kim and Sung [121], they claim that their results are valid for large curvatures which might lead to different qualitative results. From the results for strongly adsorbed chains and for free chains without adsorption, I would have expected a curvature towards the polymer in both cases for small curvature radii. Unfortunately, I cannot find any proof in literature. (4) κ and $\bar{\kappa}$ are taken from Brooks et al. [90,91]. Podgornik [127] and Clement and Garel [128] agree with Brooks on the signs of $\Delta\bar{\kappa}$ and $\Delta\kappa$ [127], Laradji also finds $\Delta\kappa < 0$ [129]. Note that in the system studied by de Gennes, the membrane gets more rigid [130]. Rigidification is also observed by Garel, Kadar and Orland [131] as well as by Sung and Oh [132] for the adsorption of self-avoiding chains on a membrane. (5) Breidenich, Netz and Lipowsky [133] have found that the presence of a finite length of an anchor segment is crucial for the occurence of the sign change of the spontaneous curvature. Their calculations show that without an anchor segment the membrane will bend away from the polymer in case of weak adsorption and that the induced curvature vanishes for strong adsorption when the polymer lies on the membrane. (*) The same effects as in the mushroom regime of anchored polymers are also observed for brushes [97, 123, 134–139].

The spontaneous curvature enters the membrane Hamiltonian only in form of a product with κ, thus the value for $\kappa_{eff}\Delta c_0$ is specified. As we assume that there is no polymer-polymer interaction, it is obvious that the effect should be proportional to σ. Because κ and $\bar{\kappa}$ have the dimension of an energy, by dimensionality arguments we also need a factor of R_e^2 and a factor of the dimension of an energy. The dependences of the effects on σ and R_e are expected to hold for

all polymer architectures and if the curvature or the amplitudes of the membrane fluctuations are small compared to the polymer size. The ansatz

$$
\begin{aligned}
\kappa_{eff}\,\Delta c_0 &= a_{sp}\;k_B T\,\sigma R_e \\
\Delta\kappa &= a_\kappa\;k_B T\,\sigma R_e^2 \\
\Delta\bar\kappa &= \bar a_\kappa\;k_B T\,\sigma R_e^2
\end{aligned}
\tag{3.5}
$$

can thus be used for all systems studied in this thesis. The determination of the dimensionless prefactors a_{sp}, a_κ and $\bar a_\kappa$ is the crucial point of the calculations.

Results obtained for κ and $\bar\kappa$ should apply for real membrane systems if two chains of equal length are anchored to the same point of the membrane but at different sides (as for example in the microemulsion experiment).[1]

The effect on the spontaneous curvature calculated with the method described seems to be questionable because the model assumes that a single chain, end-grafted to one side of the membrane, induces a sphere-like deformation. Details will be discussed in the next section.

3.3 Membrane shape deformations induced by anchored polymers

A single chain anchored to a membrane has been shown to induce a pinch-like membrane shape. The pinch can be found in simulations [143] and the membrane deformation can be calculated analytically from the pressure distribution of an ideal chain [143–147]. The polymer pulls at the anchor point and exerts a repulsive pressure to the rest of the membrane. The strongest pressure is found next to the anchor point, which corresponds to the density distribution of the polymer (compare figure 4.3). Assuming that the polymer is anchored at $h\,(0) = 0$ above a free membrane, the membrane shape is determined by the radial function [147]

$$
\begin{aligned}
h\,(r) &= -\frac{k_B T}{2\sqrt{6}\pi\kappa}R_e\left[\frac{\sqrt{6}}{4}\frac{r}{R_e}\exp\left(-\frac{3}{2}\frac{r^2}{R_e^2}\right) - \frac{3\sqrt{\pi}}{4}\frac{r^2}{R_e^2}\,\mathrm{erfc}\left(\frac{\sqrt{6}r}{2R_e}\right)\right. \\
&\qquad\left. +\frac{\sqrt{\pi}}{4}\,\mathrm{erf}\left(\frac{\sqrt{6}r}{2R_e}\right) + \frac{\sqrt{\pi}}{2}\int_0^{\frac{\sqrt{6}r}{R_e}}\frac{du}{u}\,\mathrm{erf}\left(\frac{u}{2}\right)\right]
\end{aligned}
\tag{3.6}
$$

The deformation is cone-like

$$
h\,(r) \sim -\frac{k_B T}{\kappa}r
\tag{3.7}
$$

---

[1]If the polymers are only attached to one side of the membrane, a pinch-like deformation is expected (section 3.3) and redistribution effects of the polymers at the membrane will decrease the effect (chapter 7).
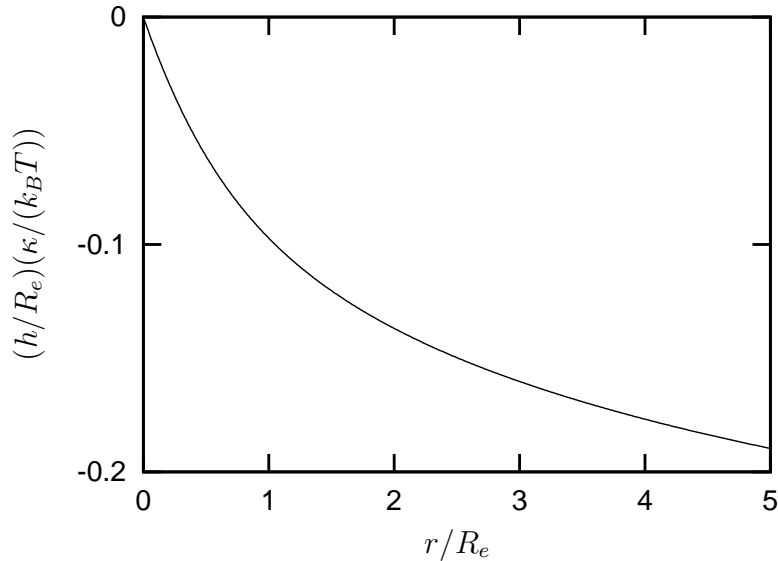
Figure 3.3: The radial shape of a membrane induced by a polymer chain with length R_e, attached above the membrane at $h(0) = 0$ [147].

for $r \ll R_e$, and it has a catenoid shape

$$h(r) \sim -\frac{k_B T}{\kappa} R_e \ln\left(\frac{r}{R_e}\right)$$ (3.8)

for $r \gg R_e$. As shown in figure 3.3, the magnitude of the pinch is already small compared to the length of the chain for $\kappa = 1$, for example in the microemulsion experiment [16]. For higher values of κ like $10-40$ for biological systems [148, 149] and $10-20$ for phospholipid membranes [142, 150], the height scales as $k_B T/\kappa$, compare figure 3.3.

With the pinch shape in mind, the method to calculate a spontaneous curvature by sphere-like deformations seems to be questionable for real systems. However, there is a connection between the pinch and sphere model which supports the validity of the results obtained for the sphere case. In real systems, usually more than one chain is attached to the surface. Each single chain leads to the formation of a pinch, but the average spontaneous curvature of the membrane has been found to be [143]

$$\kappa_{eff}\, \overline{\Delta c_0} = +\frac{k_B T}{4}\sqrt{\frac{\pi}{6}}\, \sigma R_e$$ (3.9)

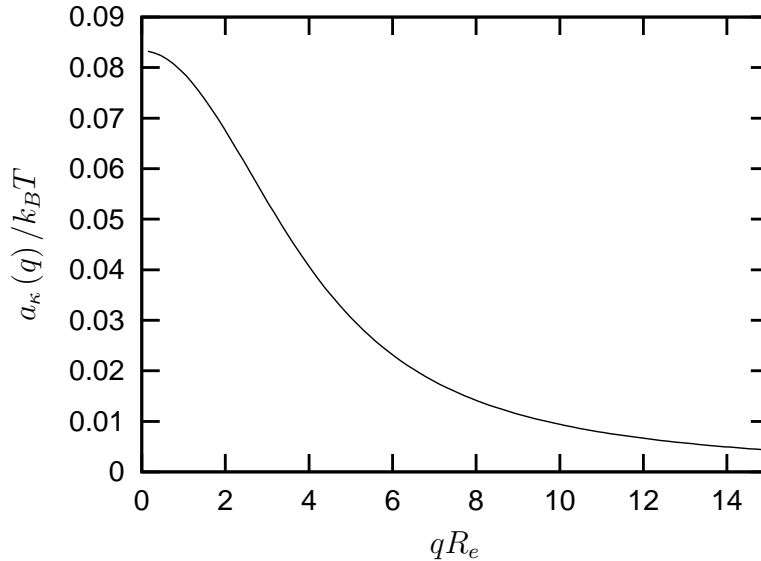which is exactly the same value as obtained in Eq. (3.4).

Figure 3.4: The polymer-contribution to the bending rigidity at different length scales for the model of Bickel and Marques with $q = 2\pi/l_{fluctuation}$ [151].

3.4   Membrane fluctuations

The influence of polymers on the whole fluctuation spectrum of the membrane has been addressed by Bickel and Marques [151] in a recent publication, independently from my studies presented in chapter 7. The authors consider a system of end-grafted linear polymer chains at both sides of the membrane. They find by analytical calculations the relation

$$\kappa\left(q\right) = 6\,k_B T \left(1 + \frac{\pi}{2}\right) \sigma R_e^2 \frac{1}{q^4 R_e^4} \left\{\exp\left(\frac{-q^2 R_e^2}{6}\right) - 1 + \frac{q^2 R_e^2}{6}\right\} \quad . \qquad (3.10)$$

As illustrated in figure 3.4, the influence of the polymer on membrane fluctuations of wavelengths short compared to the polymer size is much lower than for large-scale fluctuations.[2]

3.5   Star polymers

The effect of star polymers on the shape of the pinch has been discussed in Ref. [146, 149], but the effect on κ and $\bar{\kappa}$ is not addressed. Marques and Fournier [152] have studied two Gaussian chains, separated by a wall which prevents both

---

[2]Bickel and Marques specify a value for a_κ in the limit of large fluctuation lengths that exceeds all other values in the literature by a factor of 2. This should not affect the results presented here.

chains to interpenetrate. The authors focus on the anisotropy effects of the inclusion, that have been discussed by Fournier [153] also in a more general fashion. In this context, they obtain $a_{sp} = (7/2)[\sqrt{\pi}/(4\sqrt{6})]\,\sigma R_e$ and calculate the effects on κ and $\bar{\kappa}$. The system can be viewed as an approximation for a two-arm star. Obviously the interchain exclusion effects will be overestimated in this approximation compared to a real star polymer.

Chapter 4

Modeling and simulation
on a mesoscopic length scale

The polymer effect is mainly of entropic nature and details of the chemical structure are not important. As in other soft-matter systems, simple classical models can be employed in theoretical studies [154–157]. Scaling provides the connection with the specific experimental system [158]. Generally, in order to characterise entropy-dominated systems, ensemble averages have to be calculated. For computer simulation studies this implies that a sufficient amount of system conformations needs to be generated. Therefore the models have to be simple enough in order to be able to compute these quantities within a reasonable computation time.

4.1   Simulation techniques

Monte Carlo and Molecular Dynamics

In statistical physics, two main powerful simulation techniques have been developed to sample the phase space: Monte Carlo (MC) and Molecular Dynamics (MD).

- Molecular Dynamics evaluates the equations of motion and is especially useful to determine the system's evolution [159, 160].

- Monte Carlo algorithms traditionally provide information on equilibrium properties of the system [161, 162]. Using a random number generator, different system conformations are generated. An average over the observables provides the desired information. 'Importance sampling' [163] chooses preferably those states of the system which contribute most significantly to the integrals in phase space and makes the method universally applicable to a large number of models and problems.

I have employed the Metropolis Monte Carlo technique [163] for my studies.[1] There is no need to explain details of the algorithm here, because they can be found in many textbooks on Monte Carlo simulations (e. g. Ref. [164]). However, for the discussion of the results, there are two crucial aspects which shall be addressed: the random number generator and error estimation.

The random number generator

The availability of a fast and reliable random number generator is a basic prerequisite for any Monte Carlo simulation. Speed is important, because a huge amount of random numbers is typically generated to determine the conformations. Reliability concerns the question of correlations. The 'random numbers' are never really random, but generated by some algorithm. It is important to assure that the generator does not favour certain regions of the phase space and that there are no correlations between the numbers. In the literature, tests are available to check the quality of the random numbers produced by a generator [165]. Nevertheless, it can never be guaranteed that a generator is suited for a special problem. This should be checked — if possible — for special cases of the system under investigation in which the results are known [166].

It is not difficult to write a short code for a random number generator with the desired properties (e. g. to obtain a uniform or a Gaussian distribution of random numbers) [167, 168]. However, 'ready-made' generators which can be found in literature offer comfort (like the possibility to easily write out the status of the generator and later proceed exactly at this point of the random number sequence) and several tests have already been performed for them. For these reasons, I have decided to use the CPC routine RANLUX [169–171]. Speed-optimized codes are available for this generator [172, 173] and it has been tested in Ref. [174].

Error estimation and binning analysis

Systematic and statistical errors occur in the simulation results. It is difficult to determine the influence of the several sources of systematic errors due to the evaluation steps, but statistical errors of the direct simulation observables can be calculated more rigorously. However, a naive use of the well known expression for the standard deviation of the data might lead to a significant underestimation of the errors due to correlations in the data. Subsequent measurements of an observable might not be completely independent from each other. Let's assume the rather artificial case that exactly the same value is always measured in two subsequent observable snapshots, because the conformation did not change

---

[1]In chapter 6, the PERM algorithm is described. PERM is *not* Metropolis Monte Carlo.

inbetween the two measurements. The standard deviation — given by

$$\sigma = \sqrt{\frac{1}{N\,(N-1)} \sum_{n=1}^{N} \left(f_n - \bar{f}\right)^2} \tag{4.1}$$

for a set of observables f_n with an arithmetic mean value $\bar{f}$ — will in this case lead to an error estimate which is a factor of $1/\sqrt{2}$ too small.

A possibility to get rid of the correlation effects in the error estimation procedure is to perform a so-called binning analysis [175]. Always a certain number of subsequent measurements will be merged in packages of k values

$$f_{B,m} = \frac{1}{k} \sum_{i=(m-1)k+1}^{mk} f_i \qquad m = 1, ..., N/k \tag{4.2}$$

and the standard deviation will be calculated for the $f_{B,m}$. In the case that subsequent measurements do not differ too much due to correlations, the error estimate will grow for $k \to k+1$. If the error estimate stays constant when k is increased, the binned values are considered to be independent from each other and thus the error estimate is reliable. For all simulation errors calculated in my thesis, I have employed binning.

4.2   Membrane systems

The model which describes the membrane by a mathematical surface (Eq. (3.1)) is an established theoretical model, has been successfully applied to experiments [176–180] and confirmed by Molecular Dynamics simulations of amphiphilic bilayers [181, 182]; compare also recent review articles [183, 184].

The Monge representation

If the membrane is 'stiff', i. e. if it's persistence length [7, 185] is long enough that a membrane of the desired size can be described by small fluctuations of a planar shape, the membrane can be represented by a special parametrisation which is called Monge representation in differential geometry. In the Monge representation, the membrane's coordinates are given by a height field $h(x, y)$ as illustrated in the simulation snapshot shown in figure 4.1. In this geometry, topological changes do not take place by definition and the second term in the Hamiltonian turns out to be constant due to the Gauss-Bonnet theorem (Eq. (3.2)). For that reason, the term with $\bar{\kappa}$ is not of interest in the following. In an expansion valid for fluctuations of small amplitudes, this leads to

$$\mathcal{H} = \frac{\kappa}{2} \int d\mathbf{x} \, \sqrt{1 + (\Delta h)^2} \left[\nabla^2 h\,(\mathbf{x}) - c_0\right]^2 \tag{4.3}$$
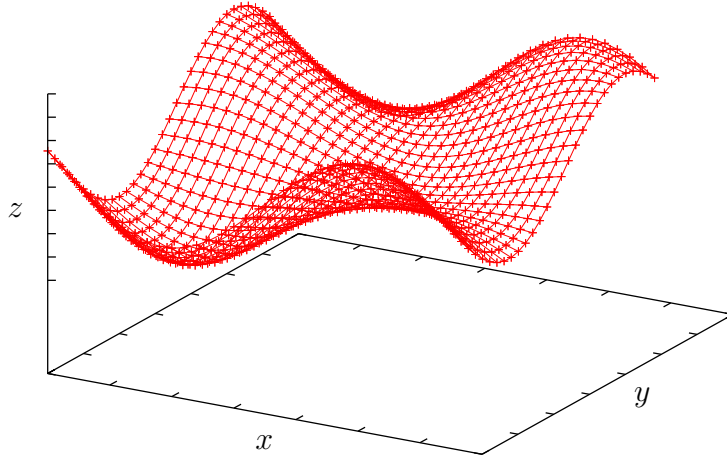
Figure 4.1: The Monge representation. The local membrane position is represented by a height field $z = h(x, y)$.

with $\mathbf{x} = (x, y)$. Often — as in my case — the system is modeled with periodic boundary conditions, the spontaneous curvature is taken to be zero, and the integral simplifies to

$$\mathcal{H} = \frac{\kappa}{2} \int d\mathbf{x} \left[\nabla^2 h(\mathbf{x}) \right]^2 \tag{4.4}$$

in a continuum description. For computer simulations, the continuum model needs to be discretised and the analogous expression is

$$\mathcal{H} = \frac{\kappa}{2} \sum_{\mathbf{x}} a^2 \left[\nabla^2 h(\mathbf{x}) \right]_{\mathbf{x}}^2 \tag{4.5}$$

with the discretised Laplace operator

$$\nabla^2 h(x, y) = \frac{1}{a^2} \{ h(x, y + a) + h(x - a, y) + h(x + a, y)$$

$$+ h(x, y - a) - 4h(x, y) \} \tag{4.6}$$

on a square lattice of grid constant a. Depending on the observables, it can be advantageous to use the Hamiltonian in the Fourier-transformed space

$$\mathcal{H} = \frac{\kappa}{2} \int \frac{d\mathbf{q}}{(2\pi)^2} \, q^4 \, H(\mathbf{q}) \, H(-\mathbf{q}) \tag{4.7}$$

where

$$H(\mathbf{q}) = \int d\mathbf{x} \, h(\mathbf{x}) \exp(-i \, \mathbf{q} \cdot \mathbf{x}) \tag{4.8}$$

and $q = 2\pi/l$ with the fluctuation lengthscale l, see e. g. Ref. [186]. Again, for the use in computer simulation studies, the formula is needed in its discretised version

$$\mathcal{H} = \frac{\kappa}{2} \sum_{\mathbf{q}} \mathbf{q}^4 H_{\mathbf{q}} H_{-\mathbf{q}} \tag{4.9}$$

with $\mathbf{q}$ between $\mathbf{q}_{min} = (2\pi/L, 2\pi/L)$ and $\mathbf{q}_{max} = (2\pi/a, 2\pi/a)$. Note that also for the integral of Eq. (4.7) an upper boundary is determined by the finite size of the molecules forming the membrane and a lower boundary is provided by the system's size.

For the simulations in chapter 7, the Fourier representation of the membrane height field will be used, because the expectation values of interest contain $H(\mathbf{q})$. To change $H(\mathbf{q})$ directly leads to less correlations of consecutive configurations. Nevertheless, the height field data in real space is also needed in order to compare the conformations of membrane and polymer. Therefore a fast routine to switch between $h(\mathbf{x})$ and $H(\mathbf{q})$ is needed. Further remarks on this Fourier transformation and its implementation can be found in appendix A.

4.3   Polymer systems

I have already pointed out in chapter 2 that a polymer can be described by a flexible-chain model, typically a random walk. I have stated that chemical details are not of interest for my systems. The question arises how to connect real polymers to the random walk data and if further requirements for the random walk should be chosen — as different molecules show different properties.

The persistence length and scaling

Comparing a polyethylene chain and a DNA molecule, the polyethylene chain is far more flexible. This 'stiffness' aspect is taken into account by the persistence length, the typical length on which the polymer is well represented by a rod. The persistence length of DNA is approximately $1\,\mu m$, the persistence length of polyethylen is of the order of $1\,nm$. These polymers can be modeled by bonds of the persistence length which are joined by an arbitrary angle. The exact definitions of the persistence length in literature slightly differ [187–190], but this is not important for my further work as my final results are for the limit of persistence lengths which are short compared to the contour length of the chain. In this regime, the properties of the polymer become universal and only scale with the extension of the chain. For example, the end-to-end distance of a rod consisting of segments (each of the same length) scales linearly with the number of segments N, the root-mean-squared end-to-end distance of a random walk scales with $N^{1/2}$ and the radius of gyration of a close-packed polymer chain scales like $N^{1/3}$.

The self-avoiding Pearson walk

The question which kind of random walk to choose is more crucial than the discussion of the persistence length — although for the final results it is also not important. The observables should not differ any more in the limit of large bond numbers. The point is that for the extrapolation to infinite bond numbers, some models might be more suitable, while with others, observables for a given bond number are obtained faster.

- It has to be decided whether to choose a random walk on a lattice or if an off-lattice simulation should be performed. The off-lattice simulation of a polymer is certainly slower than the simulation of a chain with the same bond number on the lattice. The problem of lattice models is, that artefacts of the lattice can occur [191]. This aspect is particularly important in combination with the continuum description of the membrane. Therefore an off-lattice simulation method has been employed in this thesis.

- The bond length can be chosen to be always the same, or to vary with a Gaussian distribution around a mean value. This aspect is for example of considerable interest for hydrodynamic simulations [192], but is not relevant for static properties. Thus a fixed bond length has been chosen.

- The angle between consecutive bonds might be chosen in order to mimic real polymer chains [193, 194]. As my interest does not focus on a certain finite-size system, arbitrary bond angles have been allowed.

An off-lattice model with a fixed bond length, joined by an arbitrary angle at the vertices is called a Pearson walk [195]. Obviously this simple model allows two different parts of the polymer to be in the same location. Self-avoidance can be introduced if beads are attached at the vertices which are not allowed to overlap each other, compare figure 4.2.

The pivot algorithm and more

Once a polymer model has been chosen, the next question concerns the algorithm to generate the conformations. Intuitively the simplest way to generate a random walk is the growth method: choose a random direction, go in this direction a distance a, choose a random direction etc. For a walk without self-avoidance, this method works very well. With self-avoidance, a problem occurs if two spheres happen to overlap. In order not to introduce unwanted bias, these conformations have to be discarded in a simple growth algorithm. This leads to an exponential attrition. If n_0 chains have been started to grow, for large N only

$$n_N = n_0 \exp\left(-\lambda N\right) \tag{4.10}$$

chains with N bonds will be left over.

Considerable effort has been spent and different methods have been developed to investigate self-avoiding polymer chains by means of analytical calculations (see e. g. [196–199]) and simulations (see e. g. [200–209]). Methodologically of special interest is the simulation method of Rosenbluth [210], an extension of which will be discussed in chapter 6. For all other simulations, I have decided for the pivot algorithm to generate the polymer conformations [211, 212]. An arbitrary junction of two bonds of the chain is selected randomly and denoted as a 'pivot point'. It divides the chain in two parts and one part of the chain will be rotated around the pivot point by an randomly selected angle [213,214]. Even for single chains, the acceptance rate of conformational changes calculated by the pivot algorithm is rather low for large bond numbers, but the relaxation time for properties that involve large length scales is extremely short [215]. The algorithm has been successfully applied in several recent simulations and is considered to be very effective [216–220].

Because of the large moves of a long part of the chain, the algorithm is especially suited for not too dense systems. For example in polymer melts, the acceptance fraction would be virtually zero and the pivot algorithm is inadequate for such a problem. Star polymers have been investigated in chapter 5 and certainly there is a threshold value of the arm number for which the pivot algorithm becomes inefficient. Therefore other algorithms have also been implemented: a simple growth algorithm; an algorithm which changes one bond arbitrarily and shifts the rest of the chain; crankshaft algorithms[2] for one and several beads; a 2D pivot algorithm which turns part of the polymer around an axis perpendicular to the anchoring wall. It turned out that the normal pivot algorithm is applicable for 5-arm star polymers, but the crankshaft algorithms have been essential for the simulations of ring polymers (chapter 5) and the 2D pivot algorithm has been employed for the polymers in the lamellar phase (chapter 8). For further details on different polymer changing algorithms, see e. g. Refs. [221,222]. All algorithms have been tested mutually for R_e and for changes in the elastic constants of short chains ($N = 20$) to check for correct coding.

The advanced self-avoidance check

The time needed to check for the overlap of N beads scales like N^2, if it is performed in a naive way. For monomer #1 it has to be checked for overlap with the monomers #2 to #N, for monomer #2 checks have to be done for the monomers #3 to #N etc. Thus in order to handle longer chains, a more elaborate algorithm has to be employed. I have implemented a hierarchical scheme, in which several consecutive monomers are enveloped by one large sphere. Only if large spheres overlap, it will be checked for the overlap of the smaller spheres inside them [223]. In figure 4.2 self-avoidance checks will, for example, be performed

---

[2]The crankshaft algorithm is the off-lattice analogon to the kink-jump algorithm.
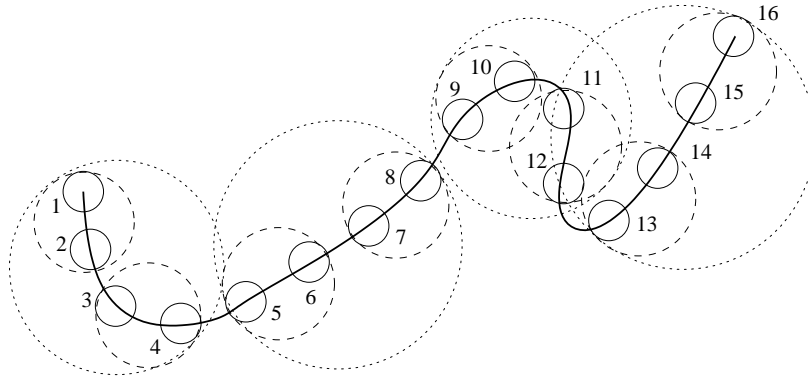
Figure 4.2: This twodimensional sketch demonstrates the hierarchical algorithm used to check for self avoidance of polymer chains. The picture shows three hierarchy levels: 16 discs representing individual monomers, 8 two-monomer discs and 4 four-monomer discs. Self-avoidance between individual monomers will only be checked if the corresponding two-monomer discs overlap or if the monomers are in the same two-monomer disc etc.

for 1 and 2, for 10 and 11, but not for 6 and 7 and not for 10 and 13. Depending on the chain length, several hierarchy levels of 'superbeads' have to be chosen. With the hierarchical algorithm, the time needed for the self-avoidance check of N beads scales only like $N \ln(N)$.

Self-avoidance effects

The most basic property distinguishing self-avoiding polymer chains from ideal chains is their different scaling behaviour. The root mean squared end-to-end distance and the radius of gyration scale like $N^{0.588}$ for a self-avoiding chain in good solvent, instead of $N^{1/2}$ for an ideal chain. Therefore a self-avoiding chain will be much more extended than an ideal chain, if both have the same bond numbers and bond lengths. This 'swelling' behaviour, observed when introducing self-avoidance in the system, is illustrated in figure 4.3.

The most exact estimate for the scaling law of self-avoiding chains is provided by field theory [224, 225]. Rather famous is the Flory estimate, which determines the scaling exponent ν of the scaling relation $R_e \sim N^\nu$ to be

$$\nu = \frac{3}{d+2} \tag{4.11}$$

in d dimensions by simple arguments [226, 227]. The formula is exact for $d = 4$ and a surprisingly good approximation for $d < 4$: the Flory value of 0.6 is very close to the value of 0.588 which is obtained by much more complex calculations.
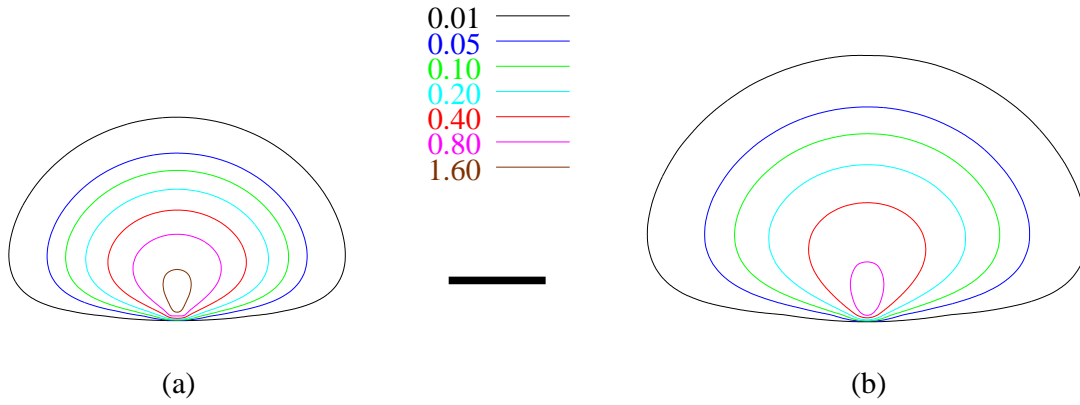
Figure 4.3: Contour plot of monomer densities of (a) an ideal and (b) a self-avoiding chain with 200 bonds and bond length $a_{pol} = 0.1732$. The bead radius for the self-avoiding chain is $0.25\,a_{pol.}$. All density values are given in units of $1/a_{pol}^2$. Bond length and number of bonds correspond to a free ideal chain of $R_g = 1$ and a free self-avoiding chain of $R_g = 1.48$. The length of the scale bar is two.

While the scaling laws can be fulfilled for ideal chains of any bond number, in the case of self-avoiding chains the exponent $\nu = 0.588$ is normally observed only for large N. For smaller numbers of bonds, model dependent correction-to-scaling terms need to be taken into account [228–230]. The self-avoiding Pearson walk can be adjusted to show the 'proper' scaling behaviour already for small chains by choosing an appropriate ratio of the radius r_{bead} for the beads modeling the self-avoidance to the bond length a_{pol}. In figure 4.4, the scaling behaviour for bead radii with $r_{bead}/a_{pol} = 0.1$, 0.25 and 0.5 is plotted. To allow an easy comparison of the slopes, the curves have been shifted. The corrections-to-scaling for a bead radius of $0.25\,a_{pol}$ are very small. If not indicated otherwise, I have used this radius for all further simulations.
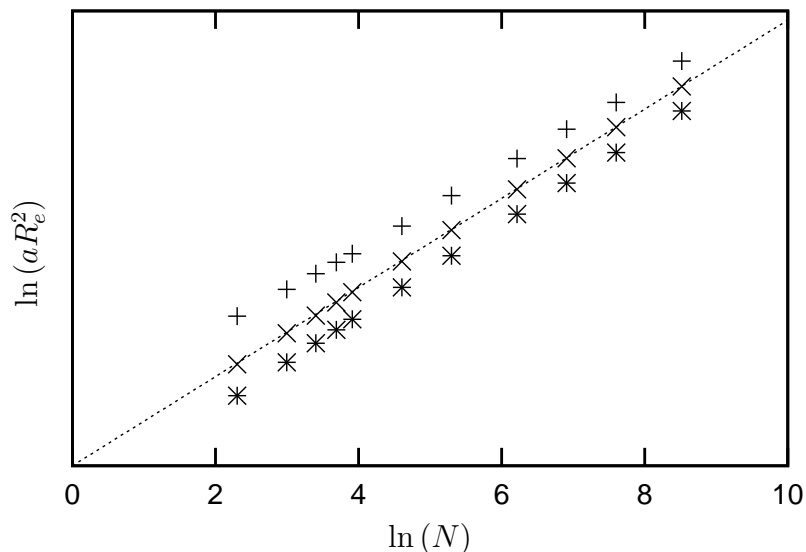
Figure 4.4: The logarithm of the mean squared end-to-end distance of free self-avoiding linear polymer chains is plotted against the logarithm of the bond number. The line has the slope $2\nu = 1.176$ and is used to compare the simulation data with the expected scaling exponent. The factor a is used to shift the simulation data next to each other in order to compare the slope more easily with the the slope of the line. For a bead radius of 0.25 times the bond length ($\times$), the data is shown to obey the scaling relation already for $N = 10$. For a bead radius of 0.10 of the bond length ($+$), the slope of the data for small N is too small, the system's behaviour is similar to the one observed for an ideal walk. In case of touching beads with a radius of 0.50 of the bond length (stars), the slope is slightly larger than 2ν for small bond numbers. For large N — data up to $N = 5000$ is plotted — the slopes for all data sets coincide.

Chapter 5

# Polymer self-avoidance effects and different architectures

In this chapter, the effects of ideal and self-avoiding linear polymer chains, of self-avoiding star polymers, and of ideal and self-avoiding ring polymers on the membrane curvature elastic constants are discussed in the limit of small curvatures.

5.1   Model

The polymers are modeled by a Pearson walk with beads assuring the self-avoidance, as described in the previous chapter. Simulation snapshots that illustrate the systems under investigation are shown in figure 5.1. For the star polymer case, a five-chain star polymer is shown. The chains are coloured differently for clarity, but without any physical significance: All beads — of the same or of different chains — are identical and exhibit excluded volume interactions.

5.2   Simulation and evaluation technique

The investigations focus on systems with high membrane κ values. We study the effect of the polymers by an expansion of the free energy in the limit of small curvatures. We simulate the polymer anchored to a hard wall, thus no explicit variation of the curvature takes place. To connect the simulation with the membrane observables, ratios of the partition functions for spherical or cylindrical shapes of the wall and for a planar wall are evaluated. If a polymer anchored to a planar wall is simulated, the ratios are given by $1 - P_x(R)$ where $P_x(R)$ is the probability for parts of the polymer chain penetrating the region between a virtual sphere $(x = s)$ or cylinder $(x = c)$ that touch the wall at the anchor point and the wall itself. The curvature radius of the virtual sphere/cylinder is given by R. By definition, R is taken to be negative if the membrane curves
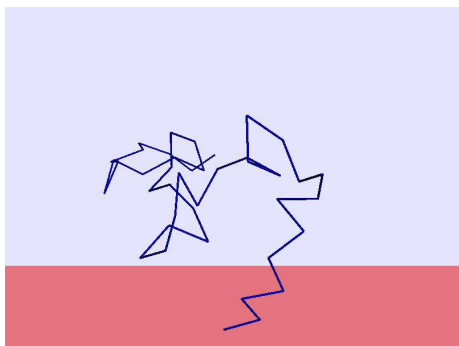
(a) ideal linear chain
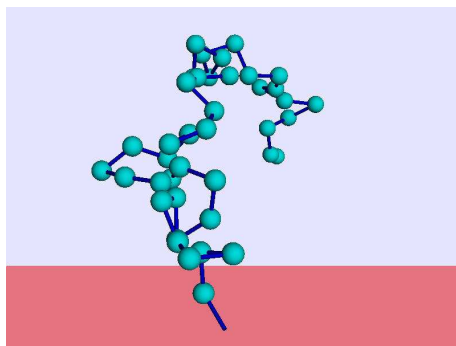
(b) self-avoiding linear chain
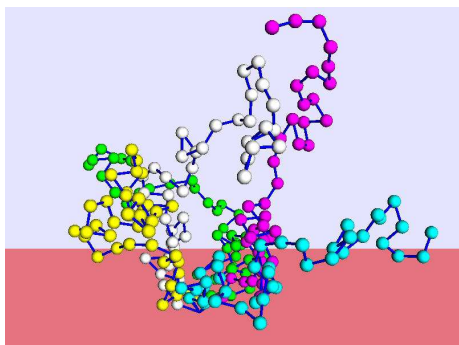
(c) self-avoiding star polymer
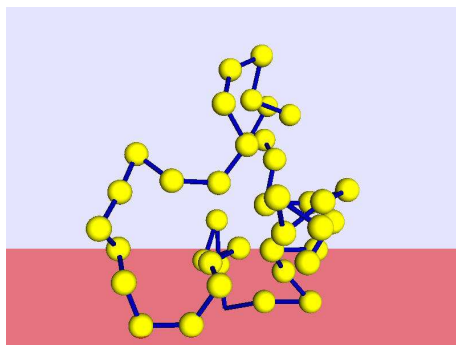
(d) self-avoiding ring polymer

Figure 5.1: Simulation snapshots of polymers anchored to a planar wall. The chains of the star polymer are coloured differently for clarity.

towards the polymer. This is sketched for the more general situation of a polymer anchored to the outside of a sphere — that allows to investigate the polymer effect also for membranes curved away from the polymer.[1] The evaluation of the probabilities is efficient, because the maximum curvature radius R_{max} for which the sphere/cylinder touches the polymer chain can be determined very fast by nested intervals. The contribution of this conformation for all curvatures is then immediately known. We now need to extract the expansion coefficients for small curvatures from the simulation data up to second order. The expansion coefficients are defined by

---

[1]For all architectures, the case of the membrane curving away from the polymer has been evaluated for $N = 20$ by attaching the chain to a sphere, compare figure 5.2.

Figure 5.2: The polymer is anchored to a hard, spherically curved wall. Spheres and cylinders of different curvatures that touch the wall at the anchor point are applied to the conformation. The probability of the polymer entering the red marked region between the wall and the sphere/cylinder is evaluated.
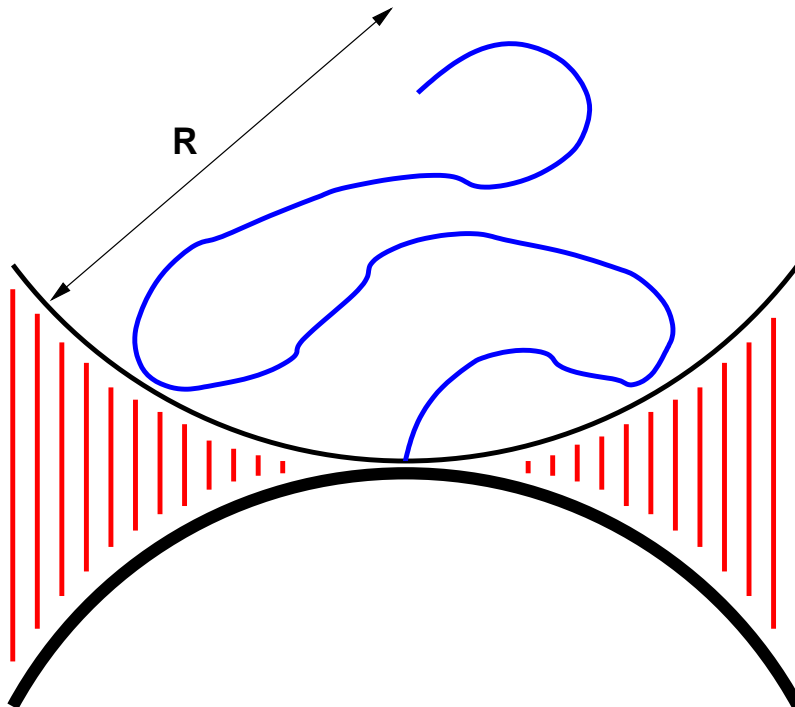
$$
\begin{aligned}
1 - P_c(R) = \frac{Z_c(R,N)}{Z_p(N)} &= 1 - a_1 \frac{R_e}{R} - a_2 \left(\frac{R_e}{R}\right)^2 - O\left[\left(\frac{R_e}{R}\right)^3\right] \\
1 - P_s(R) = \frac{Z_s(R,N)}{Z_p(N)} &= 1 - b_1 \frac{R_e}{R} - b_2 \left(\frac{R_e}{R}\right)^2 - O\left[\left(\frac{R_e}{R}\right)^3\right] \quad . \quad (5.1)
\end{aligned}
$$

$Z_p(N)$, $Z_c(R,N)$ and $Z_s(R,N)$ denote the partition functions of a polymer of N bonds anchored to a plane (index p) resp. to a cylinder / a sphere of curvature radius R. The root-mean-squared end-to-end distance of the free chain in solution scales like $R_e \sim N^\nu$ with $\nu \approx 0.59$ in good solvent (for self-avoiding chains) and with $\nu = 1/2$ in Θ-solvent (for ideal chains). Consistency with the curvature energy requires $b_1 = 2a_1$, compare Eq. (5.5). The simulation data has been fitted to quadratic polynomials in the range from $c_{min} = 0$ to $c_{max} = -1/R_{max}$ for values of c_{max} between 0 and a maximum value C_{max}. Higher order terms also occur in the simulation data, therefore a fit to a quadratic function obviously contains systematic deviations for any finite c_{max}. Fits for very small values of c_{max} should be the best choice in this respect; unfortunately they suffer from

large statistical errors. For ideal chains, the analytical results for the expansion coefficients are given by [231]

$$\frac{Z_c(R, N)}{Z_p(N)} = 1 - \frac{\sqrt{\pi}}{2}\frac{R_g}{R} - \frac{1}{4}\left(\frac{R_g}{R}\right)^2 - \frac{\sqrt{\pi}}{8}\left(\frac{R_g}{R}\right)^3$$
$$- \frac{25}{96}\left(\frac{R_g}{R}\right)^4 - O\left[\left(\frac{R_g}{R}\right)^5\right]$$
$$\frac{Z_s(R, N)}{Z_p(N)} = 1 - \sqrt{\pi}\frac{R_g}{R} \tag{5.2}$$

with the well-known relationship $R_g^2 = R_e^2/6$ [224]. Using the analytical expansions for ideal chains, a least-squares fit procedure[2] can be shown to be very accurate to extract the first and second order coefficients from the data:

- Fit the data simultaneously with the constraint $b_1 = 2a_1$ to the quadratic expressions (5.1) to get sets of expansion coefficients a_1, a_2, b_1 and b_2. Perform the fit several times in a range $[c_{min}, c_{max}]$ for different c_{max}.

- Fit the values of a_1, a_2, b_1 and b_2 to a quadratic polynomial in c_{max}.[3] The constant term of the polynomial is the corresponding expansion coefficient of the partition function ratio.

In figure 5.3, the simulation data, the linear as well as the linear plus the quadratic term are plotted. This figure demonstrates nicely that the expansions hold for positive and negative values of R, which is a necessary prerequisite to describe the polymer effect by effective membrane curvature elastic constants. To calculate the polymer contribution to the curvature energy, expansion of free energy differences instead of the partition function ratios are required. They can easily be obtained by

$$F = -k_B T \ln Z \tag{5.3}$$

and the expansion $\ln\left(1 - ax - bx^2\right) = -ax - \left(b + a^2/2\right)x^2 - O\left(x^3\right)$, valid for small x:

$$\frac{F_c(R, N) - F_p(N)}{k_B T} = a_1\frac{R_e}{R} + \left(a_2 + \frac{a_1^2}{2}\right)\left(\frac{R_e}{R}\right)^2 + O\left[\left(\frac{R_e}{R}\right)^3\right]$$
$$\frac{F_s(R, N) - F_p(N)}{k_B T} = b_1\frac{R_e}{R} + \left(b_2 + \frac{b_1^2}{2}\right)\left(\frac{R_e}{R}\right)^2 + O\left[\left(\frac{R_e}{R}\right)^3\right] \tag{5.4}$$

---

[2]For all fits in this thesis, the nonlinear least-squares Marquardt-Levenberg algorithm which is implemented in `gnuplot` has been employed.

[3]I have only applied the quadratic polynomial to ideal and self-avoiding linear chains. For the other architectures, fits where performed up to linear order and 'by eye' because of larger statistical errors. I expect that therefore systematic errors occur for these systems due to the crude approximations in this step.
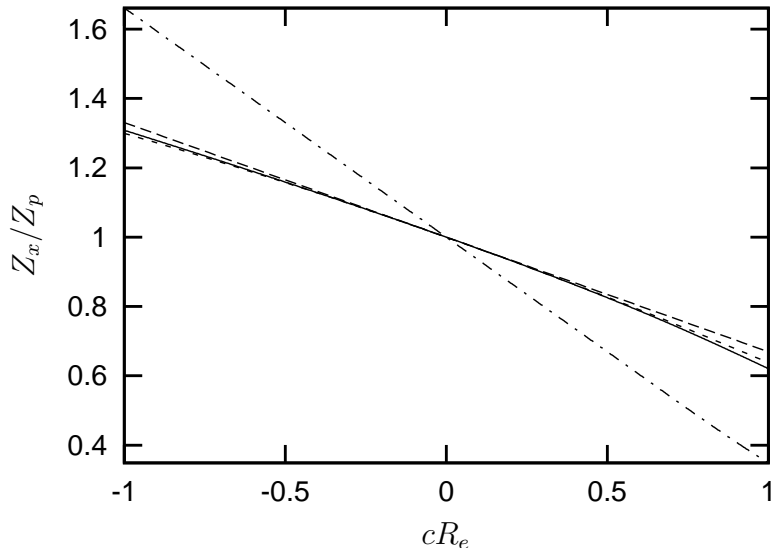
Figure 5.3: Simulation results for the partition function ratios $Z_x(R, N)/Z_p(N)$ of an ideal linear chain with 20 bonds. In addition, linear and quadratic terms of the fit are shown. In the sphere case, all terms of higher order than linear vanish and the fit exactly matches the simulation data. Cylinder: simulation data (solid), linear (long dashes) and linear plus quadratic (short dashes) contribution. Sphere: simulation data (dashed-dotted).

The curvature Hamiltonian (compare Eq. 3.1) of the membrane for spherical and cylindrical membrane shapes reads

$$\mathcal{H}_c = \int dS \left[\frac{\kappa}{2} \frac{1}{R_c^2} - 2\kappa c_0 \frac{1}{R_c} + 2\kappa c_0 \right]$$

$$\mathcal{H}_s = \int dS \left[2\kappa \frac{1}{R_s^2} - 4\kappa c_0 \frac{1}{R_s} + 2\kappa c_0 + \bar{\kappa} \frac{1}{R_s^2} \right] \quad . \tag{5.5}$$

The polymer free energies in Eqs. (5.4) and the curvature energies in Eqs. (5.5) relate the simulation data to the membrane curvature constants: [4]

$$a_{sp} = -\frac{a_1}{2}$$

$$a_\kappa = (2a_2 + a_1^2)$$

$$\bar{a}_\kappa = (b_2 - 4a_2) \tag{5.6}$$

---

[4]The terms that do not depend on the curvature are obviously not of interest for this question.

An error estimate is obtained by the fit errors of a_1, a_2 and b_2, which propagate like $\Delta a_{sp} = \Delta a_1/2$, $\Delta a_\kappa = 2\Delta a_2 + 2\,|a_1|\,\Delta a_1$, $\Delta \bar{a}_\kappa = \Delta b_2 + 4\Delta a_2$. If systematic errors are present, i. e. if a linear function has been used for the fits to the data in figure 5.4, the values for the expansion coefficients will be too small.[5] Thus the value of the error estimate is especially uncertain in the cases with linear fits for the functions $a_1(c_{max})$, $a_2(c_{max})$ and $b_2(c_{max})$.

The method described so far supplies values of the polymer effect for chains of finite bond numbers. To obtain the universal curvature elastic constants, the results have to be extrapolated to infinite N. The data is well described by a linear function in $N^{-1/2}$. This allows to extrapolate to $N^{-1/2} = 0$ by a least-squares fit, compare figure 5.5. Note that the finite-size corrections are supposed to depend on the discretisation length a_{pol} and the total length of the polymer chain R_e. Thus a function $\alpha_0 + \alpha_1(a_{pol}/N^\nu)^\mu + \alpha_2(a_{pol}/N^\nu)^{2\mu} + O[(a_{pol}/N^\nu)^{3\mu}]$ for the corrections-to-scaling relations is expected. Similar corrections have been observed for example for the hydrodynamic radius of polymer chains in solution [232] and for a self-consistent field theory calculation of the effect of long block copolymers on the interfacial curvature elasticity in a ternary mixture of two homopolymers and a short block-copolymer [125].

5.3   Ideal linear chains: validation of the method

Ideal, freely hinged chains may serve as a test for the method developed. The limit of vanishing persistence length can be calculated analytically by solving the diffusion equation, as discussed in chapter 3 [123, 124]. We use the scheme described in the previous section to evaluate the simulation data. The fit results for chains with $N = 20$ and different values of c_{max} are shown in figure 5.4 (a). The data for small values of c_{max} is not plotted because of the large statistical errors. The quadratic polynomial is fitted to the data in the range $0.2 < c_{max}R_e < 0.3$ to extrapolate to the value for $c_{max} = 0$. Data for polymers with $N = 10$, 20, 30, 40, 50, 100 and 200 has been evaluated. The results for the contributions to the curvature elastic constants are plotted against $N^{-1/2}$, see figure 5.5 (a). The corrections-to-scaling relations are given by:

$$\begin{aligned}
a_{sp} &= 0.1801\ \left(1 - 0.369\,N^{-1/2}\right) \\
a_\kappa &= 0.2130\ \left(1 - 0.870\,N^{-1/2}\right) \\
\bar{a}_\kappa &= -0.1682\ \left(1 - 1.179\,N^{-1/2}\right)
\end{aligned} \tag{5.7}$$

The statistical error of the amplitudes is of the order 10^{-3}. A positive a_{sp} — by definition — corresponds to the membrane bending away from the polymer. The finite size effects in all cases lead to a reduction of the amplitude of the

---

[5]For all functionalities investigated, the sign of the second order term in the functions is positive.
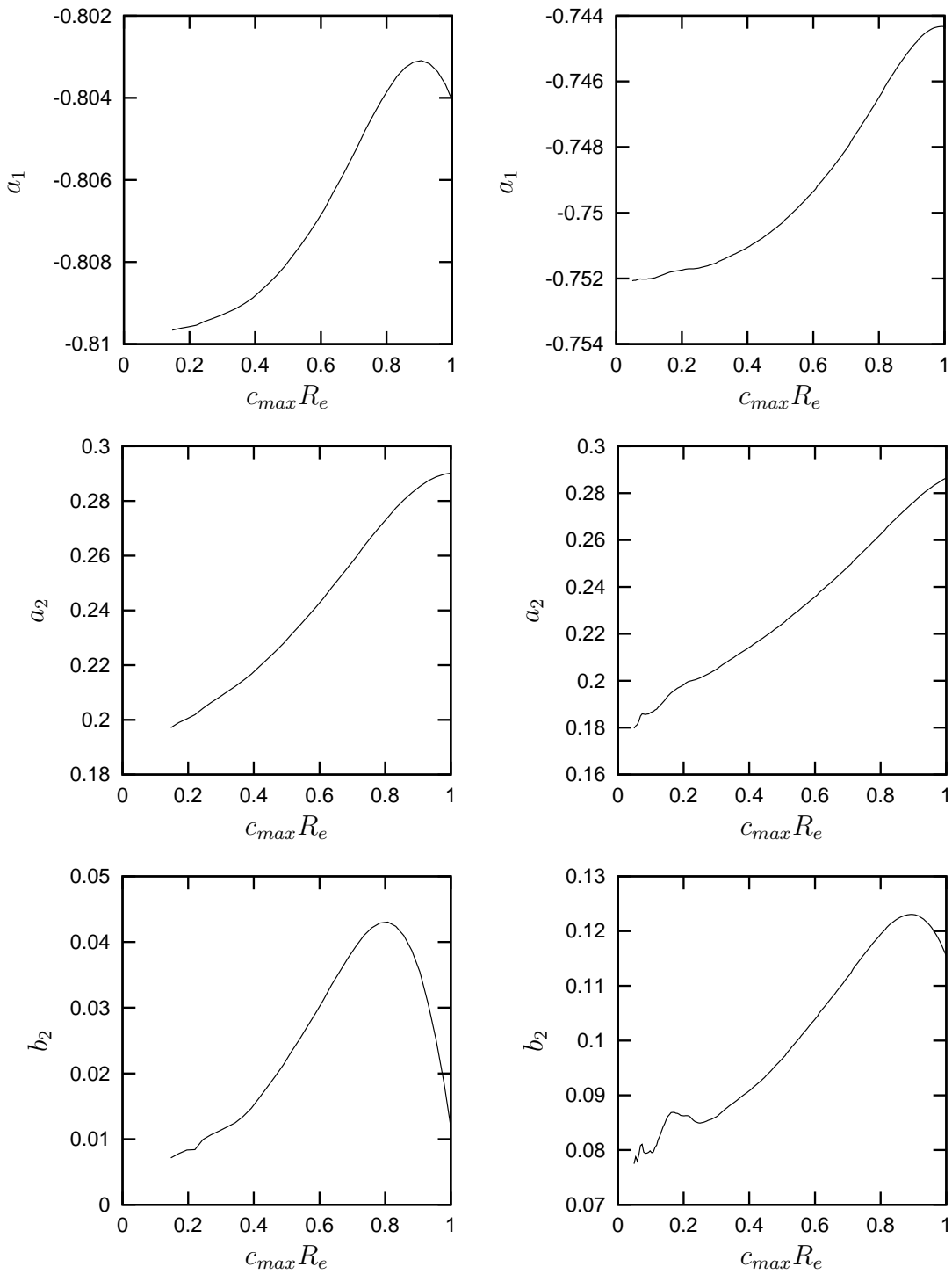
(a) ideal   (b) self-avoiding

Figure 5.4: Small-curvature expansion coefficients for the partition function ratios (20 bonds). The fits are performed from zero curvature up to c_{max}.
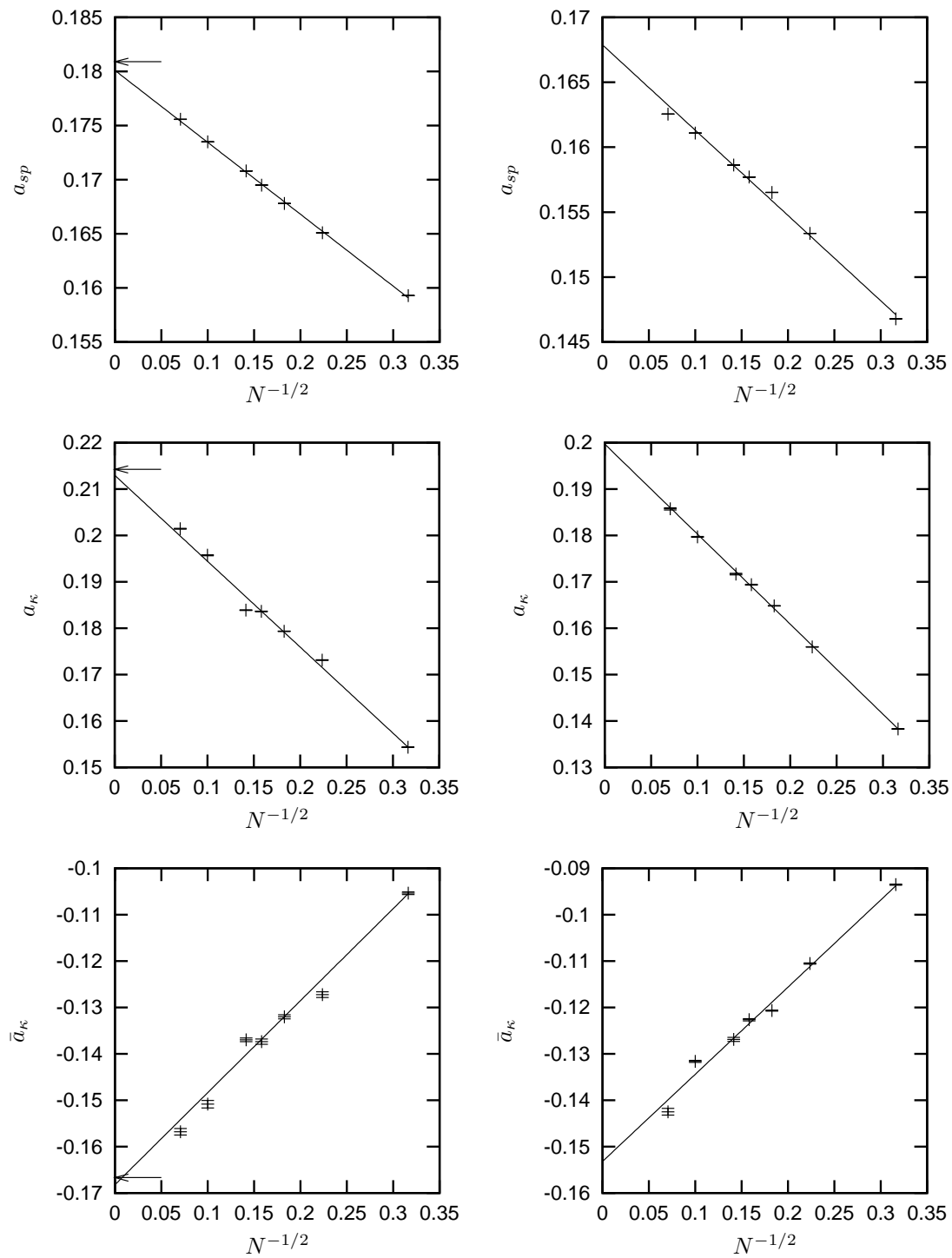
(a) ideal   (b) self-avoiding

Figure 5.5: Universal amplitudes a_{sp}, a_κ und $\bar{a}_\kappa$ for ideal and self-avoiding linear polymers with 10 to 200 bonds. The arrow indicates the analytical result.

	analytical		simulation
a_{sp}	$\sqrt{\pi}/(4\sqrt{6})$	$+0.1809$	$+0.1801$
a_{κ}	$(1 + \pi/2)/12$	$+0.2142$	$+0.2130$
$\bar{a}_{\kappa}$	$-1/6$	-0.1667	-0.1682

Table 5.1: Universal amplitudes for anchored ideal linear polymers. The statistical error is of the order 10^{-3}. The analytical values have been taken from [123, 124].

polymer effect. Note that the overall prefactor is universal in all equations, but the prefactor of the $N^{-1/2}$ term is model dependent. Even within the same model, the prefactor of the corrections-to-scaling varies for different ratios of the bead size to the bond length. The universal prefactors extracted from the simulations that describe the change of the membrane curvature elastic constants in the case of small membrane curvatures are listed in table 5.1, together with the analytically calculated values. The analytical results and the simulation results for Δc_0, $\Delta \kappa$ and $\Delta \bar{\kappa}$ agree nicely.

5.4   Self-avoiding linear chains

The simulation method which has been developed provides a straight forward way to investigate self-avoidance effects. Data of good quality can be obtained, so that the fit of the expansion coefficient data for different c_{max} can be done with a quadratic polynomial, compare figure 5.4 (b). A plot of the results for different bond numbers against $N^{-1/2}$, as shown for $N = 20$ in figure 5.5 (b), allows the conclusion that all data points fall on a linear curve. The coefficients obtained for the corrections-to-scaling prefactors as well as the resulting universal values for the curvature elastic constants have been found to be:

$$
\begin{aligned}
a_{sp} &= 0.168 \left(1 - 0.391 \, N^{-1/2}\right) \\
a_{\kappa} &= 0.120 \left(1 - 0.972 \, N^{-1/2}\right) \\
\bar{a}_{\kappa} &= -0.153 \left(1 - 1.221 \, N^{-1/2}\right)
\end{aligned}
\tag{5.8}
$$

Simulating self-avoiding chains is very time-consuming, especially for longer chains with $N > 50$. The statistical accuracy of the data is therefore not as good as for ideal chains. Thus the statistical errors of all values have been estimated to be of the order 10^{-2}. In table 5.2, the universal prefactors of the simulations for ideal and self-avoiding chains are listed. Self-avoidance has been shown to reduce the polymer effect, if ideal and self-avoiding chains of the same R_e are compared. If the bond length and bond number are kept fixed, the introduction of self-avoidance to the system leads to a swelling of the chain, as shown in figure 4.3. In the latter case, R_g as well as R_e increase, and thus also the polymer's effect on the membrane curvature elastic constants increases.

	ideal	self-avoiding
a_{sp}	+0.1801	+0.1679
a_{κ}	+0.2130	+0.1997
$\bar{a}_{\kappa}$	−0.1682	−0.1532

Table 5.2: Universal amplitudes for anchored linear polymers. The statistical error is of the order 10^{-3} for ideal and 10^{-2} for self-avoiding chains.

5.5 Star polymers

The effect of self-avoidance for a single linear chain is not very large, but for some polymer architectures self-avoidance is a necessary prerequisite to investigate even qualitative effects. One of these examples is the star polymer architecture. Let us assume that no membrane-mediated interactions between the polymer chains are present. This is the case if the polymer effect is small compared with the κ of the bare membrane. For ideal chains, therefore no differences in the polymer effects will be observed if the chains are attached to different points of the membrane or if several chains are anchored to the same point. Star polymer effects on κ and $\bar{\kappa}$ can only be investigated taking into account for self-avoidance!

Simulations

Star polymers of functionalities f between 2 and 5, i. e. polymers with two to five arms, have been attached at their centers to a wall. The pivot algorithm has been used for all functionalities to change the polymer conformation [233–236]. The performance of local algorithms [237, 238] has been tested, but they did not lead to an improved data quality. Unfortunately, the quality of the simulation data has not been good enough in order to extrapolate to zero curvature using a quadratic polynomial. The data has been fitted 'by eye' with a linear function. Most probably, systematic errors are present in the results due to the linear fit. The second order contribution is positive. The plots in figure 5.4 illustrate, that by a linear fit preferably a smaller value for all expansion coefficients is obtained. Finally, a set of universal amplitudes and a set of corrections-to-scaling prefactors have been obtained, determined by fits of the data to a function

$$a_x = a_{x,\infty} \left(1 - c_x N^{-1/2}\right) \quad . \tag{5.9}$$

The corrections-to-scaling prefactors generally do not vary with the arm number within the statistical error (table 5.3). The value for $f = 5$ seems to be a maverick.

In table 5.4, the data of the universal prefactors per chain for different functionalities is listed.[6] As discussed earlier, for ideal chains the same value for all

---

[6]A calculation of two ideal chains separated by a wall is found in literature [152]. The

f	c_{sp}	c_κ	$\bar{c}_\kappa$
1	0.39	0.97	1.22
2	0.39	0.93	1.20
3	0.37	0.94	1.28
4	0.39	0.82	1.13
5	0.39	0.85	0.44

Table 5.3: Amplitudes of the correction to scaling prefactors for anchored star polymers with functionality f. The statistical error is of the order 10^{-2} for c_{sp} and 10^{-1} for c_κ and $\bar{c}_\kappa$.

f	a_{sp}/f	a_κ/f	$\bar{a}_\kappa/f$
1	0.168	0.200	−0.153
2	0.193	0.224	−0.157
3	0.215	0.255	−0.169
4	0.235	0.272	−0.168
5	0.254	0.301	−0.141

Table 5.4: Universal amplitudes (per chain) for anchored star polymers of functionality f. The statistical error is of the order 10^{-2}.

functionalities would be obtained. In the case of self-avoiding chains, the polymer effects of spontaneous curvature c_0 and bending rigidity κ increase almost linearly with functionality and double at about $f = 10$. The saddle splay modulus $\bar{\kappa}$ does not change with f. All simulation results are illustrated in figure 5.6 (a). A descriptive argument why the bending rigidity changes with the arm number whereas the saddle splay modulus does not can be obtained in the context of a blob model calculation.

Blob model

Blob model calculations are used to derive scaling arguments. They have been successfully employed, for example, for polymers in constrained geometries [239, 240], to mimic intra- and interchain excluded volume interactions in dense polymer systems [123, 226, 241] and to study polymers in flow [242, 243]. Computer simulations for many-arm star polymers are rather expensive concerning CPU time, therefore the behaviour of star polymers with high functionalities has been calculated by the blob model. The polymer is modeled by blobs for all distances from the center of the polymer.[7]. In a naive picture, the star can be thought of consisting of cones, meeting at the center of the star and containing spherical blobs as sketched in figure 5.7. The free energy is then — according to the basic idea of blobs — given by the number of blobs in the system. In my calculations, a continuum version of the model is applied. The volume accessible to the polymer

---

authors obtain an effect on the spontaneous curvature of $\kappa_{eff}\Delta c_0 = (7/2)\left[\sqrt{\pi}/\left(4\sqrt{6}\right)\right]\sigma R_e$. This overestimates the effect, as the simulations show.

[7]Different regimes of a 'stretched conformation', a 'blob model' and a 'free chain' as in Ref. [241] have not been distinguished
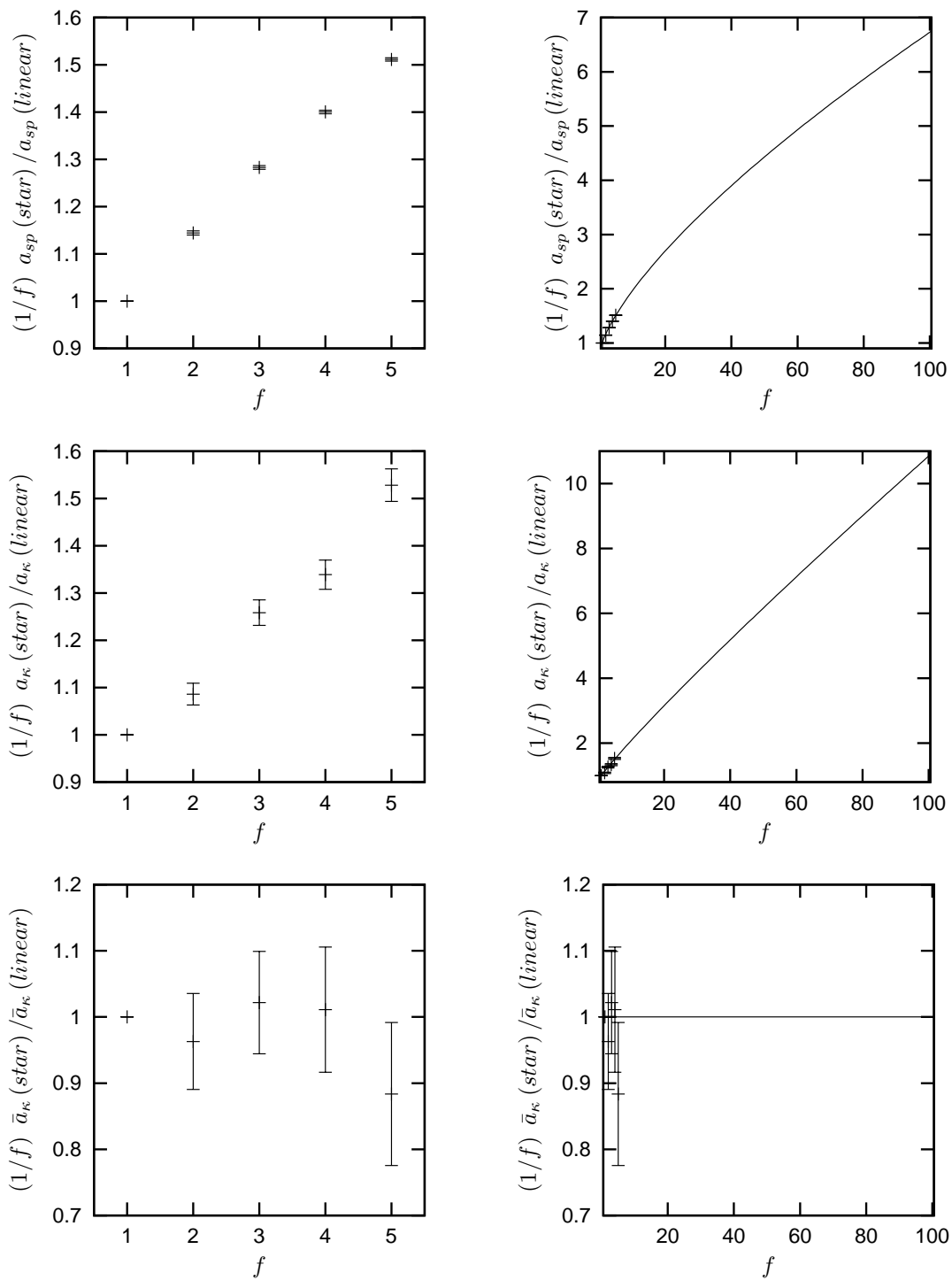
(a) simulation   (b) blob model and simulation

Figure 5.6: The star-polymer effect per chain as function of the functionality f.
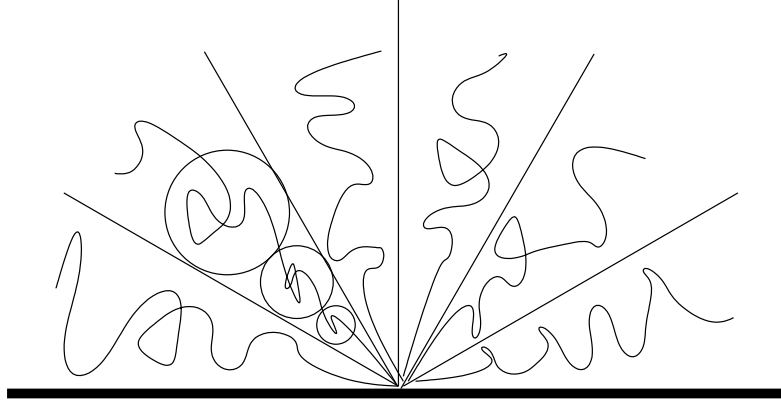
Figure 5.7: Two-dimensional sketch of the blob model describing a star anchored to a planar wall.

is given by an integral over the infinitesimal volumes determined by the areas $\xi_x^2(r)$ accessible to the polymer at distances r from the anchor point.

$$\xi_x^2(r) = \frac{1}{f} \int_0^{2\pi} d\phi \int_{\theta_{min,x}}^{\pi/2} d\theta \ r^2 \cos\theta \tag{5.10}$$

The geometrical constraints for the star are taken into account by the lower integration boundary $\theta_{min,x}$. For a free star polymer, $\theta_{min,f} = -\pi/2$ applies while for a star polymer anchored with its center to a planar wall, $\theta_{min,f} = 0$. If the polymer is anchored to the inside of a sphere or a cylinder, the intersections between the 'polymer' sphere which describes region in which the blobs are located and the deformed 'membrane' are determined to be

$$\sin\theta_{min,s} \quad = \quad \frac{r}{2R} \tag{5.11}$$

$$\sin\theta_{min,c}(\varphi) \quad = \quad \frac{R - (R^2 - r^2 \sin^2\varphi \cos^2\varphi)^{1/2}}{r\cos^2\varphi} \quad , \tag{5.12}$$

for a spherical resp. a cylindrical deformation. A cylindrical deformation is illustrated in figure 5.8. The integrals of Eq. 5.10 can be evaluated exactly for free stars and in the cases of the planar wall and a spherical deformation. For a cylindrical deformation, an expansion in terms of small membrane deformations has been employed. Besides the linear and the quadratic term, terms of orders $O\left[(r/R_c)^4\right]$ and of higher orders occur. However, contributions of orders beyond $O[(r/R_c)^2]$ are not relevant for the calculation of effective membrane curvature constants. Up to quadratic order, the areas of the polymer-sphere surfaces in the space region accessible to the polymer in the different scenarios are given by

$$\xi_x^2(r) = \frac{2\pi r^2}{f} \left(1 - q_x \frac{r}{R}\right) \tag{5.13}$$
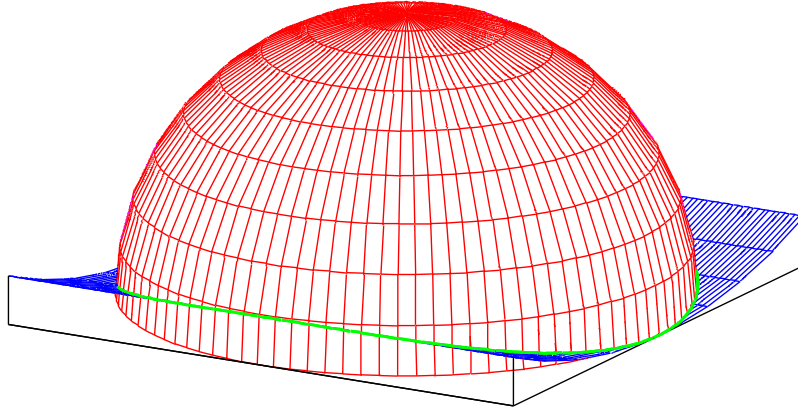
Figure 5.8: The intersection of the hemisphere describing the star polymer anchored to a planar wall and a cylinder further restricting the geometry is described by $\theta_{min,c}\,(\phi, r, R)$, indicated by the green curve.

with $q_p = 0$ for the planar wall, $q_s = 1/2$ for a spherical deformation and $q_c = 1/4$ for a cylindrical deformation. The typical length scale for the polymer is therefore $\xi_x\,(r)$ and corresponds to the number of monomers $n_x(r)$ in a blob of this radius. The value of $n_x(r)$ is determined by

$$n_x\,(r) = \left(\frac{\xi_x\,(r)}{l_0}\right)^{1/\nu} \tag{5.14}$$

due to the scaling laws $R_e \sim l_0 N^\nu$ and $R_g \sim l_0 N^\nu$ for a chain of bond length l_0. For known l_0 and total bond number N, the radius of the star polymer $R_{star,x}$ can be determined using the implicit equation

$$N = \int_0^{R_{star,x}} dr \frac{n_x(r)}{\xi_x(r)} \tag{5.15}$$

with the radial monomer density $n_x\,(r)\,/\xi_x\,(r)$. After evaluation of the integral, recursive substitution of $R_{star,x}$ and expansion of several expressions for small $l_0 N^\nu / R_x$ gives

$$R_{star,x} = f^{(1-\nu)/2}\ \ell_0 N^\nu\ \Gamma\left(f^{(1-\nu)/2}\,\frac{\ell_0 N^\nu}{R_x}\right) \tag{5.16}$$

with a scaling function $\Gamma(x) = Q_0 + Q_{x,1}x + Q_{x,2}x^2$ and positive constants Q_0, $Q_{x,1}$ and $Q_{x,2}$. The complete expressions can be found in appendix B. Using $R_{star,x}$, the free energies can be calculated. The idea of the blob model is that the free energy corresponds to the number of blobs, thus the upper integral boundary is $R_{star,x}$. A lower cutoff needs to be introduced in order to prevent the integral from diverging. A physical meaning of this lower cutoff might be provided by the

monomer size ℓ_0.[8] The radial number density of blobs is inverse proportional to the blob radius $\xi_x(r)$ and the free energy is given by:

$$\mathcal{F}_x = k_B T \int_{\ell_0}^{R_{star,x}} dr \frac{1}{\xi_x(r)} \tag{5.17}$$

For further details, please refer to appendix B. The final result shows that the polymer effect per chain scales nearly linearly with f for c_0 and κ. The polymer effect for $\bar{\kappa}$ is predicted to be constant with respect to f. The results nicely complement the simulation data.

$$
\begin{aligned}
\kappa_{eff}\Delta c_0/f &\sim& f^{1-\nu/2} \, \sigma\ell_0 N^\nu \sim f^{0.71} \\
\Delta\kappa/f &\sim& f^{3/2-\nu} \, \sigma\ell_0^2 N^{2\nu} \sim f^{0.91} \\
\Delta\bar{\kappa}/f &=& \text{const.} < 0
\end{aligned}
\tag{5.18}
$$

The scaling relations imply that $\Delta\kappa/\Delta\bar{\kappa} \sim -f^{3/2-\nu}$. Scaling applies for large functionalities. A fit of the simulation data to a function $c_1 + c_2 f^{c_3}$ is consistent with the scaling behaviour. The results of such a fit are

$$
\begin{aligned}
(\kappa_{eff}\Delta c_0/f)(f) &=& \left[0.79 + 0.23 \, f^{0.71}\right] \, (\kappa_{eff}\Delta c_0/f)(1) \\
(\Delta\kappa/f)(f) &=& \left[0.85 + 0.15 \, f^{0.91}\right] \, (\Delta\kappa/f)(1) \\
(\Delta\bar{\kappa}/f)(f) &=& (\Delta\bar{\kappa}/f)(1)
\end{aligned}
\tag{5.19}
$$

with the single chain values denoted by '(1)'. The fit curves are plotted in figure 5.6 (b).

Discussion

Concerning the validity of the results, some further discussion is needed. The spontaneous curvature has been evaluated for a polymer chain attached to a sphere. As discussed earlier, a pinch-like deformation is expected to occur for a real membrane. I have argued that for ideal linear chains the average mean curvature calculated within the pinch model and the spontaneous curvature calculated for a single chain anchored to a spherically deformed membrane coincide. This implies that the average mean curvature only depends on the total pressure exerted by an anchored polymer to a planar wall and not on the shape of the deformation — at least in the limit of bending rigidities κ of the bare membrane which are large compared to the effect of the polymer. Thus the analogy should also hold in the case of star polymers. Note that this interpretation problem for c_0 again does not occur for symmetrical polymers which are anchored to a membrane. In this case, the spontaneous curvature of the membrane vanishes.

---

[8]An exact definition is not needed because the results for the membrane curvature constants are independent from the cutoff value.
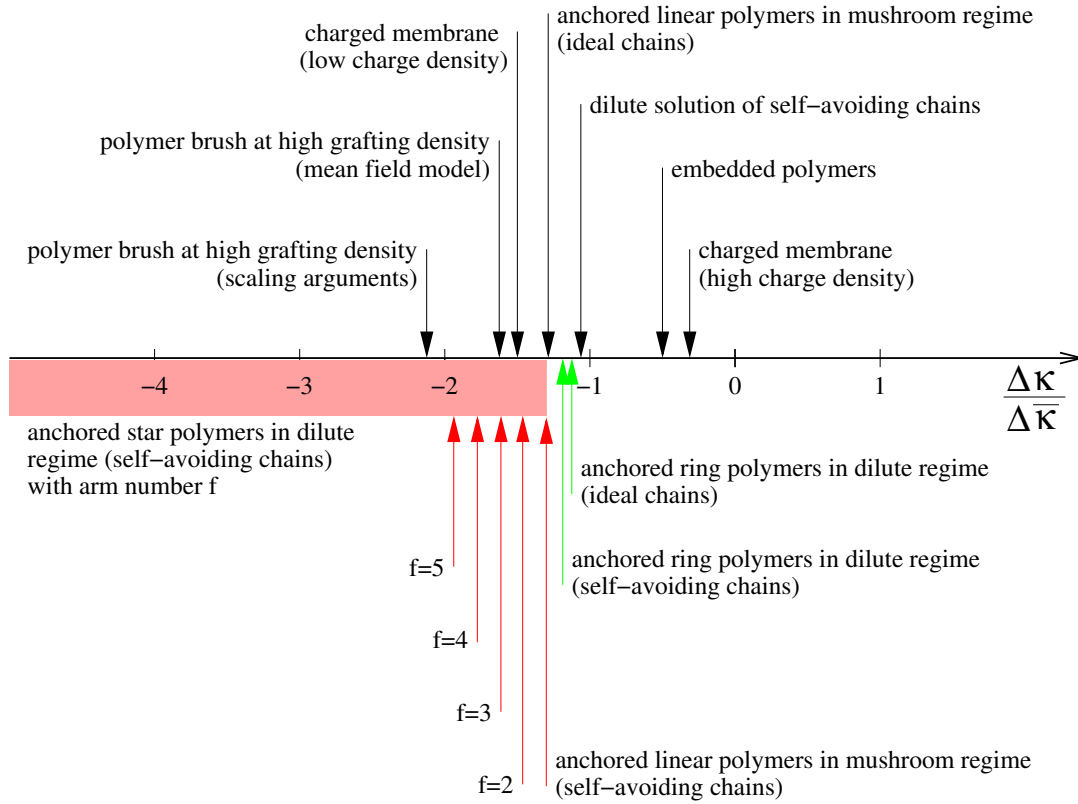
Figure 5.9: Ratios of $\Delta\kappa$ to $\Delta\bar{\kappa}$ for different systems [120, 123, 124, 134, 244–246]. Ring and star polymer values result from simulations presented in this work. To minimise the error, assuming that $\bar{a}_\kappa$ is constant, always the single-chain value of $\bar{a}_\kappa$ has been used.

The formation of stars at the membrane makes the polymer more efficient, an increased effect per chain on κ and c_0 is observed. However, the absolute value of the polymer effect can also be altered by a different number density of chains per membrane area. In my view, the fact that the star architecture allows to change the ratio $\Delta\kappa/\Delta\bar{\kappa}$ according to different functionalities is more important. This effect can be used to modify the phase behaviour of the system in a controlled fashion. There are of course also other possibilities to change the effective membrane curvature constants that allow to obtain different ratios of $\Delta\kappa/\Delta\bar{\kappa}$, see figure 5.9. The advantage of star polymers is the possibility to get different effects on both constants just by changing the functionality and without altering the type of the system.

The results of this chapter discussed so far, have been published recently in Ref. [247].

54

5.6   Ring polymers

Ring polymers are of special interest because the effect of knots can be investigated. Two cases have been considered in my thesis, ring polymers with an arbitrary number of knots and without knots. Ring polymers have been simulated employing the single-bead and the multiple-bead crankshaft algorithms [248, 249].[9]

Ring polymers of arbitrary knot number (phantom chains)

In the case of artificially synthesised polymers, an arbitrary knot number models the ensemble average of real systems [251–253]. The polymer effect is characterised by the anchor density σ, the root mean squared end-to-end distance R_e of a free linear chain with equal bond number and the set of prefactors a_{sp}, a_κ and $\bar{a}_\kappa$. Another view would be to characterise the polymer effect by the root mean squared radius of gyration of the ring polymers $R_{g,ring}$, which is connected by conversion factors of 12 for ideal polymers and 10.6 for self-avoiding chains to R_e [254]. The ratios between the radius of gyration of the ring and the end-to-end distance vary slightly due to finite-size effects [255] but — most essential — the scaling of both is the same [256, 257].[10] The finite-size effects for the membrane curvature elastic constants again can be described by a $N^{-1/2}$ term, as illustrated in figure 5.10. The fit functions are given by

$$
\begin{aligned}
a_{sp} &= 0.18 \left(1 - 0.74\,N^{-1/2}\right) \\
a_\kappa &= 0.13 \left(1 - 1.47\,N^{-1/2}\right) \\
\bar{a}_\kappa &= -0.12 \left(1 - 1.92\,N^{-1/2}\right)
\end{aligned}
\tag{5.20}
$$

in the case of ideal chains and by

$$
\begin{aligned}
a_{sp} &= 0.18 \left(1 - 0.77\,N^{-1/2}\right) \\
a_\kappa &= 0.12 \left(1 - 1.31\,N^{-1/2}\right) \\
\bar{a}_\kappa &= -0.10 \left(1 - 1.58\,N^{-1/2}\right)
\end{aligned}
\tag{5.21}
$$

for self-avoiding polymers. The errors of all amplitudes are of the order 10^{-2}. Figure 5.11 demonstrates that the universal amplitudes of self-avoiding chains in the limit $N \to \infty$ agree rather well for bead sizes of $0.25\,a_{pol}$ and $0.50\,a_{pol}$ within the simulation accuracies. This is consistent with the expectation that the universal amplitudes should be independent from the bead radius.

The universal amplitudes of the polymer effect for linear and self-avoiding polymers ($r_{bead} = 0.25\,a_{pol}$) are listed in table 5.5. The spontaneous curvature term is the same in both cases, up to the simulation accuracy. For the bending

---

[9]It is claimed that the so-called 'vector shuffling' method is much more efficient [250].

[10]Non-phantom ideal ring polymers have been shown to scale with $\nu \approx 0.588$ [258].

(a) ideal

(b) self-avoiding

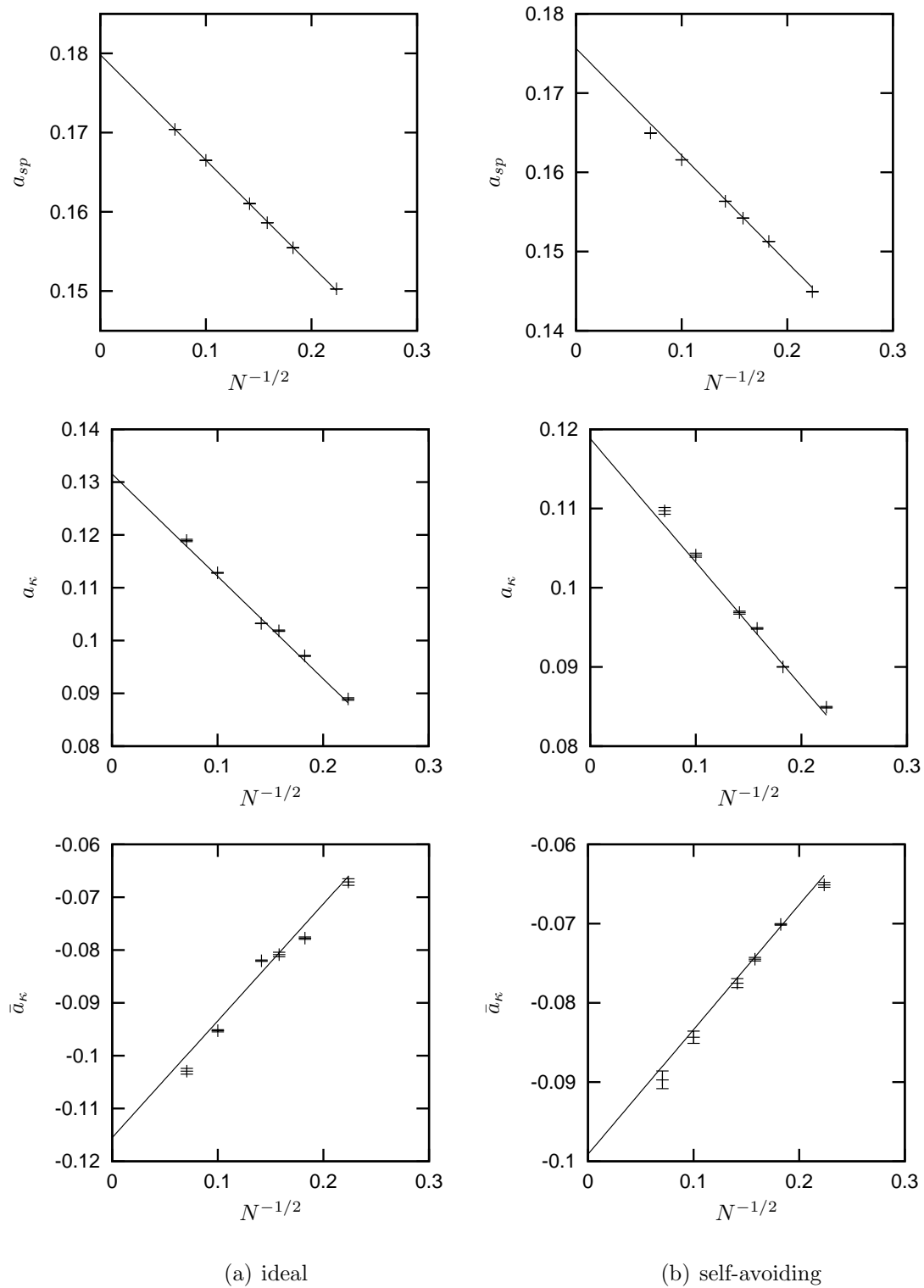Figure 5.10: Universal amplitudes a_{sp}, a_κ und $\bar{a}_\kappa$ for ideal and self-avoiding ring polymers with 20 to 200 bonds and a bead radius of $0.25\,a_{pol}$.
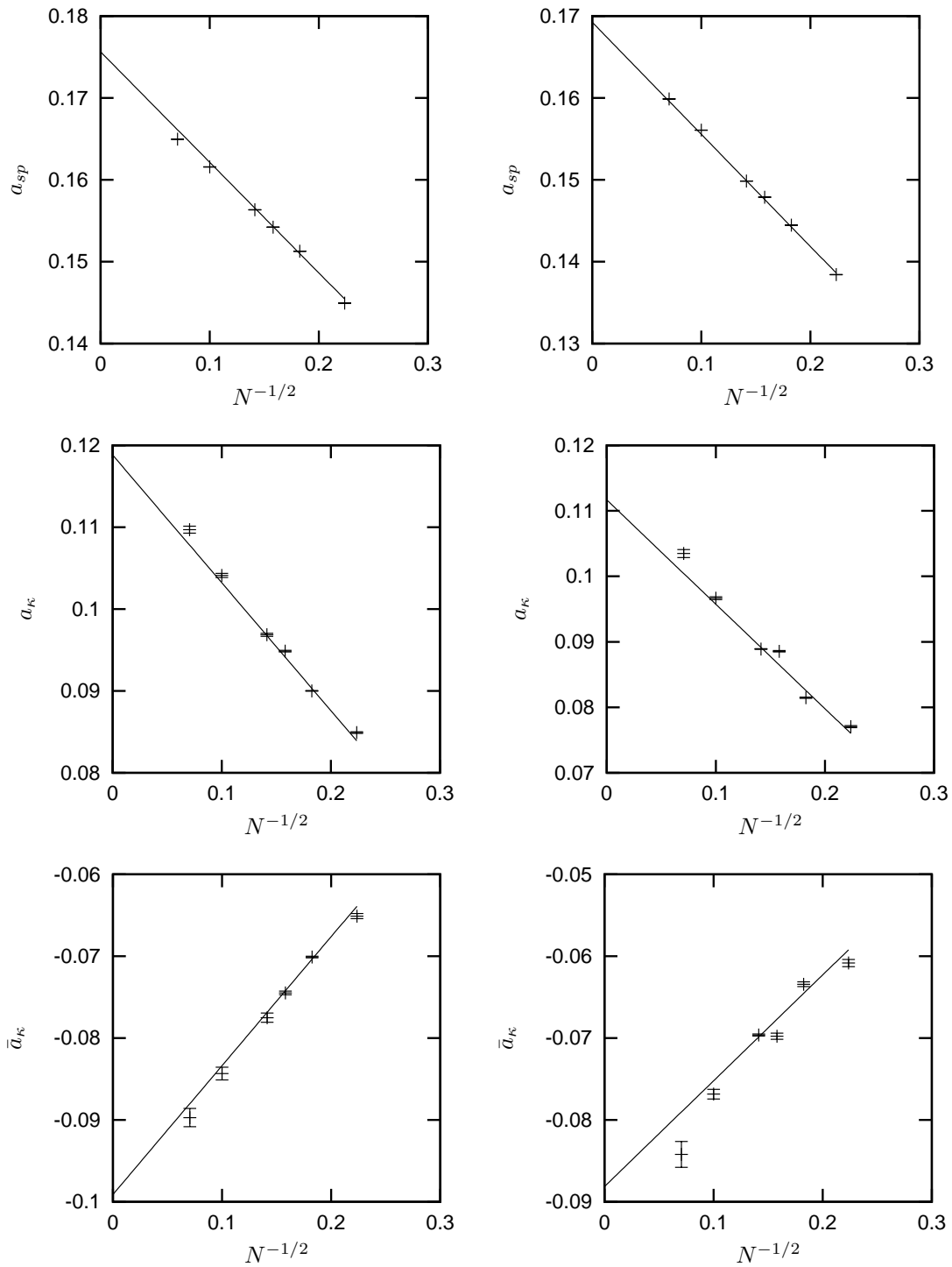
(a) $R_{bead} = 0.25\,l_0$

(b) $R_{bead} = 0.50\,l_0$

Figure 5.11: Universal amplitudes a_{sp}, a_{κ} und $\bar{a}_{\kappa}$ for self-avoiding polymers with 20 to 200 bonds and bead sizes $0.25\,a_{pol}$ and $0.50\,a_{pol}$.

	ideal	self-avoiding
a_{sp}	+0.18	+0.18
a_{κ}	+0.13	+0.12
$\bar{a}_{\kappa}$	−0.12	−0.10

Table 5.5: Universal amplitudes for anchored ring polymers. The statistical error is of the order 10^{-2}.

	(1)	(2)	(3)	(4)
$(\Delta c_0)_{ring}/(\Delta c_0)_x$	1.00	1.05	0.71	0.79
$(\Delta\kappa)_{ring}/(\Delta\kappa)_x$	0.62	0.60	0.62	0.67
$(\Delta\bar{\kappa})_{ring}/(\Delta\bar{\kappa})_x$	0.68	0.64	0.68	0.73

Table 5.6: Ratios of the effect of anchored ring polymers to the effect of other polymer geometries with equal contour length. The statistical error is of the order 10^{-2}. The following systems have been compared: (1) ideal ring polymer, ideal linear chain; (2) self-avoiding ring polymer, self-avoiding linear chain; (3) ideal ring polymer, two ideal linear chains of half length; (4) self-avoiding ring polymer, self-avoiding star with two arms of half length

rigidity and the saddle-splay modulus, the effects self-avoiding polymers have smaller amplitudes, which is consistent with the results obtained for linear chains. Note that for self-avoiding polymers the conversion factor between the ring's radius of gyration and the end-to-end radius of the linear chain is smaller than for ideal polymers. This partly 'cancels' the self-avoidance effect if it is presented in a notation of the ring-polymer effects in terms of σ and $R_{g,ring}$.

It is instructive to compare the effects of different polymer architectures with equal contour lengths. In table 5.6, the ring polymer effect is compared to the effect of a linear chain anchored at one end, and in its middle to the membrane. Both comparisons have been done for ideal and the self-avoiding polymers.

- The spontaneous curvature induced by a ring polymer is virtually the same as the spontaneous curvature induced by an end-grafted chain.

- Compared to chains that are grafted in the middle, ring polymers induce a spontaneous curvature which is about 30% smaller.

- For κ and $\bar{\kappa}$, the effect of the ring polymer is about $30 - 40\%$ smaller compared to the other architectures. The differences between self-avoiding and ideal chains as well as between end-grafted chains and those which are attached in the middle are basically not significant.[11] For the latter case

---

[11]In case the ring is compared with the two-arm star, self-avoidance seems to relatively increase the polymer effect due to the ring, compared to the effect of the star.
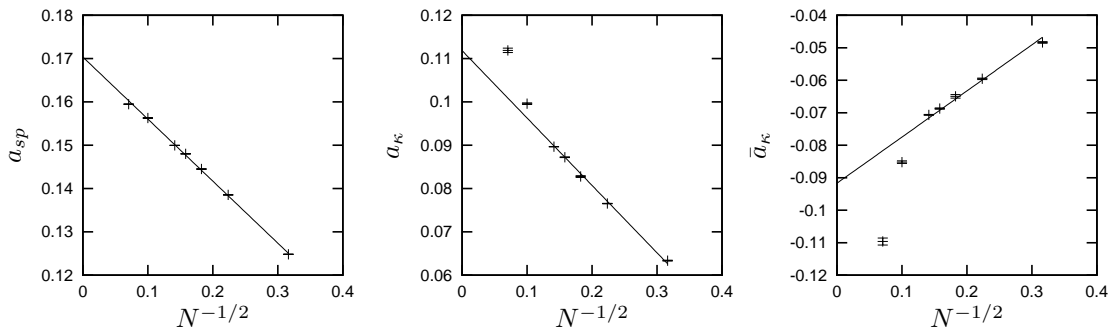
Figure 5.12: Universal amplitudes a_{sp}, a_κ und $\bar{a}_\kappa$ for self-avoiding non-phantom ring polymers with 10 to 200 bonds and a bead radius of 0.25 of the bond length.

it can be shown by simple calculations that the effects of ideal chains are even exactly the same.

Ring polymers without knots

An example for a ring polymer without knots is circular DNA [252]. In the simulation, the constraint can be implemented straightforward by geometric hindrance. There is a minimal bead radius of $r_{bead} = a_{pol}/\left(2\sqrt{2}\right)$ for which a part of the polymer chain cannot cross any other part of the chain in case the changes are only done by an one-bead crankshaft algorithm. The possible number of knots is preserved and can be controlled by the number of knots in the initial conformation.

Simulations for chains of up to 200 bonds without knots and with touching neighbouring beads ($r_{bead} = 0.5\,a_{pol}$) were performed in order to investigate the effect of knot-free rings. Especially changes in the slopes of $a_\kappa\left(N^{-1/2}\right)$ and $\bar{a}_\kappa\left(N^{-1/2}\right)$ seem to occur for $N > 50$, see figure 5.12.

For very small bond numbers, the probability of knots is probably very low due to the small flexibility of the chain. This might be the reason why there are no differences observed for a_{sp}, a_κ and $\bar{a}_\kappa$ between phantom and non-phantom ring polymers. I expect a threshold value of N at which knots become more probable for the phantom chain. This might be the reason for the differences observed in a_κ and $\bar{a}_\kappa$ for bond numbers larger than $N \approx 50$.

A further investigation would require a more thorough study of the knot probabilities. Tests of the knot numbers are computationally rather expensive [259] and have not been done yet. The tube inflation method has been strongly recommended to me [259, 260], because different kinds of knots can be distinguished unambiguously. For checking only for the occurrence of knots, the more common method using the Alexander polynomials should be sufficient [261].

Chapter 6

Polymer adsorption effects

Polymer adsorption is a phenomenon which is quite common in biological systems [262] and which is very important in many technical applications. One of the most prominent applications is probably glue. By theoretical studies on surfaces, a phase transition has been shown to occur between completely desorbed and completely adsorbed polymers for free chains in solution [263–266]. Effects of adsorbed polymers on the membrane curvature constants have already been discussed in chapter 3 by means of results that can be found in the literature. For an anchored chain and a weak attractive interaction between membrane and polymer, the bending rigidity increases while the saddle splay modulus decreases; vice versa for strong adsorption [126]. The results for free chains were based on calculations employing a mean-field approximation. Beyond these basic effects, two very recent papers are dealing with special aspects of adsorbed polymers. Breidenich, Netz and Lipowsky discuss the pinch induced by one-sided anchored polymers, the induced average mean curvature and the effect of an anchor length for ideal chains by means of simulations and analytical calculations [133]. Skau and Blokhuis have presented extended mean-field models to deal with adsorbed polymers which are in coexistence with a semi-dilute solution of free polymers [267]. Detailed studies for self-avoiding chains have not yet been done and results beyond mean-field approximations for the effects on κ and $\bar{\kappa}$ and for different adsorption strengths are not available in the literature.

6.1   Model, simulation and evaluation technique

I have implemented a simulation technique to investigate adsorption effects. Like in the case without adsorption, the polymer is anchored to a hard wall. Again a Pearson walk with and without excluded volume interaction is used to model the polymer chain. In addition to the model of the last chapter, a square-well potential of the membrane acting on the polymer's vertices is introduced. The potential can be used to model attractive and repulsive forces between the poly-

```
recursive subroutine STEP(X,N)
# X: location of last polymer bead (start at X=(0,0,0))
# N: number of bonds in polymer
# w_step : weight attached to placing the next bond
# w_total: total weight of the chain with N bonds

# Choose new position X'
  X -> X'

# Determine new weight connected with the choice of X'.
  w_step = p(allowed) * exp(-E(X')/k_B T)
  w_total(N) = w_total(N-1) * w_step(N)

# Determine partition functions for polymers attached to spheres/cylinders
# (choice given by the type variable) of curvatures c > c_min:
  for type=sphere,cylinder; for c_min < c < c_max
    if X' belongs to a valid conformation
      partition_function(type,c,N) = partition_function(type,c,N) + w_total
      ...
    end if
  end for; end for

# Add the current chain's contribution to the partition sum Z(N) of all N-bond
# chains generated up to now and calculate observables.
  Z(N) = Z(N) + w_total(N)
  r_e2e = r_e2e + X'^2 * w_total(N)
  ...

# Enrich, prune or grow the conformation in the next step according to the
# ratio of its weight to the mean weight of all previous conformations, if
# the chain has not yet reached its maximal length N_MAX (and if it has a
# finite weight). Z(N) counts the number of initial chains.
  if N < N_MAX and w_total(N) > 0 then
    w_upper_bound = c_upper * Z(N) / Z(1)
    w_lower_bound = c_lower * Z(N) / Z(1)
    if w_total(N) > w_upper_bound then
      w_total(N) = w_total(N) / 2
      call STEP(X',N+1); call STEP(X',N+1)
    else if w_total(N) < w_lower_bound then
      w_total(N) = w_total(N) / 2
      choose 0 <= random_number < 1
      if random_number < 1/2 then; call STEP(X',N+1); end if
    else
      call STEP(X',N+1)
    end if
  end if
  return
end subroutine STEP
```

Figure 6.1: Pseudocode of a PERM algorithm to evaluate the polymer effect (a more general PERM pseudocode can be found in the appendix of [268]).

mer chain and the membrane and thus allows to study adsorption effects. It is obvious that the use of the pivot algorithm probably still works fine in the system with a weak attractive interaction, but will certainly fail to generate a proper ensemble for a strong attractive interaction. The same applies for the evaluation technique of simulating a polymer chain anchored to a planar wall and applying virtual spheres and cylinders to determine ratios of partition functions. For adsorbed polymers, ensembles that are suitable to describe systems with differently curved walls simultaneously obviously do not exist.

The first problem of applying the simulation method described in the last chapter, that conformations of high statistical weight cannot be generated by the pivot algorithm, can certainly be overcome. A method that changes the conformation by local instead of global moves should be more suitable for this problem. However, the second problem that partition functions and free energies of one ensemble are not accessible by Metropolis Monte Carlo remains. These values are needed for the evaluation of the partition function ratios, because for each membrane shape one simulation run has to be performed. This second problem can be solved by a growth algorithm, which intrinsically delivers the free energy of each ensemble[1]: the growth of polymers attached to membranes of different shapes will deliver the desired values of the partition functions.

Unfortunately, naive growth of chains is not capable of handling strong adsorption with good statistics. A refined technique, the **P**runed **E**nriched **R**osenbluth **M**ethod (PERM), has been proven to generate proper ensembles for dense polymer systems and for strongly restricted geometries [269–271]. The partition function of a system and its free energy are a natural result of the simulation, as they are needed by PERM for its population control.

PERM is based on the growth algorithm introduced by Rosenbluth in the 1950s [210], which already provides a possibility to grow self-avoiding chains without facing the problem of severe attrition for large bond numbers. With the Rosenbluth algorithm, new bonds are always chosen in such a way that an allowed conformation results. In order to avoid unwanted bias, weights have to be introduced which correspond to the number of available growth possibilities in each step. Assume that a bond should be added on a 3D simple cubic lattice and only two of the five possible growth directions are available.[2] One of both possibilities is chosen randomly in order to obtain a new valid conformation, while the weight of this chain will be reduced by a factor of 2/6. The PERM algorithm adds an additional feature to the simple Rosenbluth method. A population control enriches the conformations with high statistical weight and prunes the ensemble from conformations of low weight. Pruning and enrichment enables PERM to keep those conformations which contribute most when calculating observables.

---

[1]A simple growth algorithm provides the free energy in terms of the fraction of conformations that succeeded to reach a certain bond number.
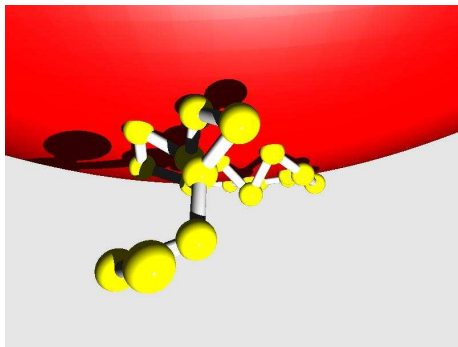
[2]Each grid point has six neighbours but one possibility is already occupied by the monomer grown in the previous step.
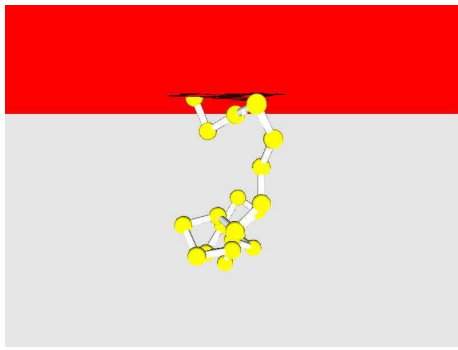
(a) no adsorption
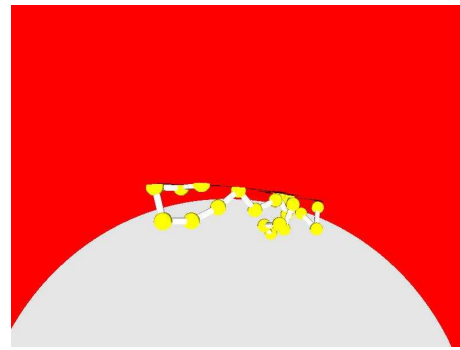
(b) adsorption energy: $3\,k_BT$ per bead

(c) adsorption energy: $3\,k_BT$ per bead
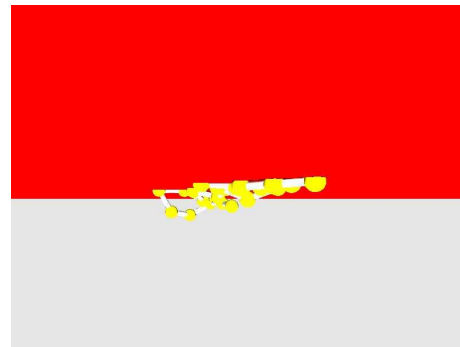
(d) adsorption energy: $10\,k_BT$ per bead

Figure 6.2: Simulation snapshots of polymers anchored to hard walls of different shape with $N = 20$, $a_{pol} = 1$ and $r_{bead} = 0.125\,a_{pol}$. The potential width is $0.125\,a_{pol}$. In all images, the wall is on the top.

This is the crucial feature of the algorithm, which leads to its good performance in highly confined geometries. PERM, as well as the original Rosenbluth algorithm, naturally applies for polymers on a lattice. However, off-lattice versions of both algorithms are also available. A set of possible growth vectors is provided before each growing step. All vectors are given by the polymer bond length and their direction chosen by random determination of points on a sphere. Thus for each growth step a 'local grid environment' is present[3] but the result of the total growth process will be an off-lattice chain.

PERM can be implemented in a recursive fashion which results in a rather short and simple program code. Figure 6.1 shows the pseudocode of a typical

---

[3]Obviously the concept of 'occupied lattice sites' to check for self-avoidance does not apply directly. Self-avoidance is checked for by the overlap of (virtual) spheres centered at the polymer vertices.

PERM implementation, used to determine the polymer effect.[4]

In the adsorbed regime, simulations for each curvature and membrane shape have to be done separately. At first glance the need of separate simulations for each membrane shape seems to be a major disadvantage compared to the method applied in the last chapter. However, note that PERM allows to generate ensembles for different chain lengths in one simulation run which is an advantage compared to the method of chapter 5.

6.2   Simulations

The method has been validated for systems without an attractive potential where the effects on the membrane curvature constants can be compared directly with the simulations done by the pivot algorithm. Long production runs to determine membrane constants for systems with adsorption have not yet been done, but simulation snapshots for different observables and different wall shapes are shown in figure 6.2.

---

[4]Choosing `c_lower` $= 0$ and `c_upper` $= \infty$ (or a sufficiently high value), neither pruning nor enrichment will occur and the code is just the usual Rosenbluth algorithm.

Chapter 7

Fluctuation spectrum of a decorated membrane

In the previous chapters, the effects of the polymer on the membrane curvature elastic constants have only been calculated in the limit where the wavelengths of the fluctuations are large compared to the polymer size. The simulation methods which have been employed are especially suitable for polymers attached symmetrically to the membrane and for membranes with a high bare membrane κ. For bending rigidities of the order of $k_B T$, which typically occur in surfactant systems, it becomes more important to gain insight into the polymer effect on the whole fluctuation spectrum of the membrane. Independently from my work, Bickel and Marques [151] have addressed this aspect recently for membrane-polymer systems with ideal end-grafted linear chains that decorate both sides of a membrane.

7.1 Modeling, simulation and evaluation

In order to evaluate the polymer effect on the whole fluctuation spectrum, we need to simulate a fluctuating membrane with an attached polymer. The Monge representation is used for the membrane (compare chapter 4) and periodic boundary conditions are applied. To avoid possible problems corresponding to the pinch which is formed at asymmetric polymer coverage, for the systematic studies chains have always been symmetrically attached to each side of the membrane. A picture of such a polymer-membrane system is shown in figure 7.1. The average mean curvature of the membrane will vanish due to the symmetry, and the saddle-splay contribution will be a constant because of the Gauss-Bonnet theorem[1]. Therefore only the influence on κ will be extracted from the simulation data, the effects on $\bar{\kappa}$ cannot be evaluated. For the evaluation of κ, 'cylinder-like' deformations are sufficient, i. e. a membrane that fluctuates only in one direction. This simplifi-

---

[1]Neglecting the fact that the polymer contribution is not exactly homogeneous on the membrane area. Further discussion is found in chapter 3.
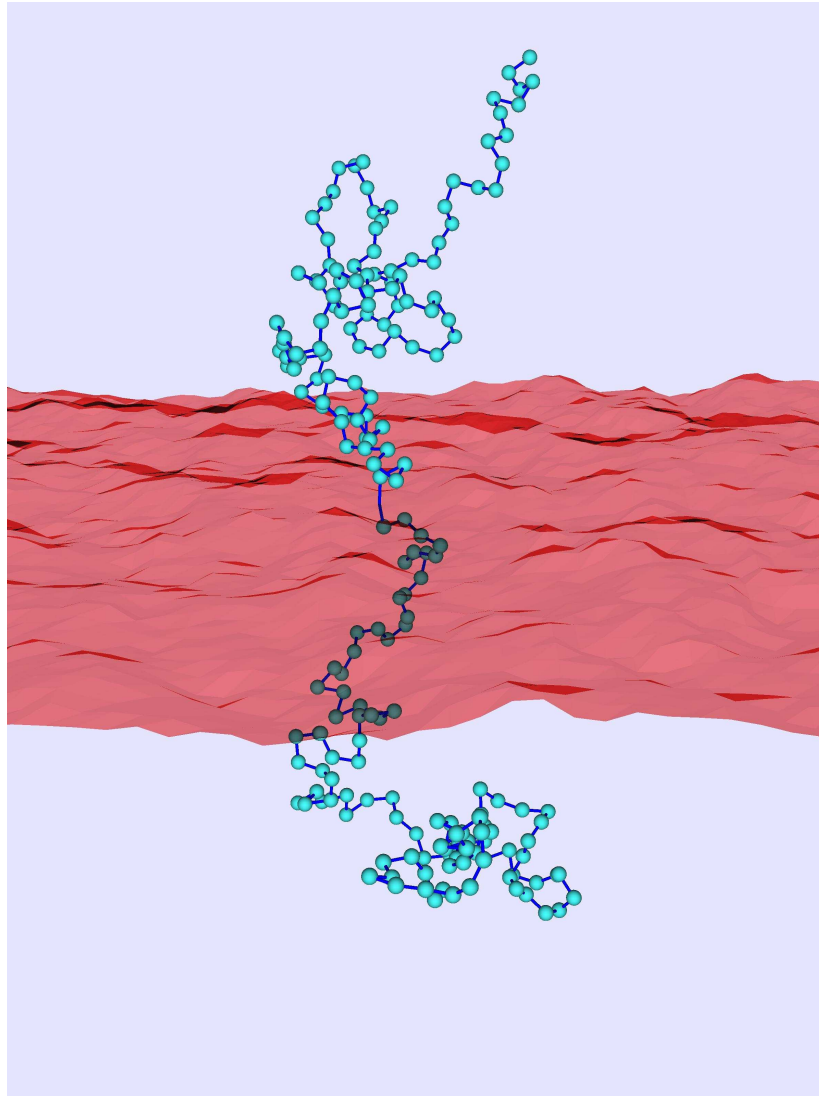
Figure 7.1: Simulation snapshot of a self avoiding polymer anchored to a fluctuating membrane. The chain is fixed to the membrane in such a way that the parts on both sides of the membrane have equal lengths.
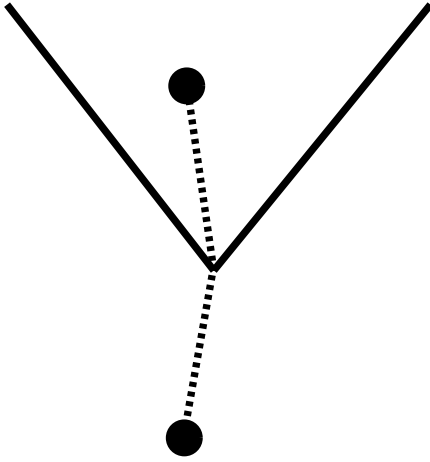
Figure 7.2: A bead fixed by a rod in the apex of an angle. This simple model helps to illustrate the polymer effect on the bending rigidity.

cation reduces the degrees of freedom of the system considerably and speeds up the simulations (see chapter 3).

Simple models

Simple models can be calculated analytically and might be helpful to understand why polymers anchored to a membrane increase the bending rigidity.

- A 2D clapper-wedge model is sketched in figure 7.2. Compared to the planar case, a clapper located at the outside of the wedge will gain entropy while the inner clapper will loose entropy. The entropy of the system is given by $S_{two} = -k_B T \ln(\phi(2\pi - \phi))$ for $\phi \in [0, 2\pi]$. The maximum of S_{two} occurs at $\phi = \pi$, which is thus the preferred state of the system.

- In a histogram model, the membrane is assumed to consist of height levels which are constant in one direction (figure 7.3). In the perpendicular direction, all levels have the width of the clapper length (taken to be 1) and periodic boundary conditions apply. The partition function of the system is given by the integral over the membrane height differences of adjacent strips with the proper weights, and integrals over the steradians available to the clapper ends for the polymer. For a system of three strips, the clapper integrals can be evaluated in the limit of small height differences h_{ij} of the strips and incorporated in the Boltzmann factors

$$
\begin{aligned}
Z(\kappa) \;=\; & \int dh_{12} \int dh_{23} \int dh_{31} \quad \delta\left(h_{31} - h_{12} - h_{13}\right) \qquad\qquad (7.1)\\
& \int_{\Omega_1(h_{12},h_{23})} d\tilde{\Omega}_1 \int_{\Omega_2(h_{12},h_{23})} d\tilde{\Omega}_2 \\
& \exp\left[-\frac{3}{2}\kappa\left(\left(h_{12} - h_{23}\right)^2 + \left(h_{23} - h_{31}\right)^2 + \left(h_{31} - h_{12}\right)^2\right)\right]
\end{aligned}
$$

69
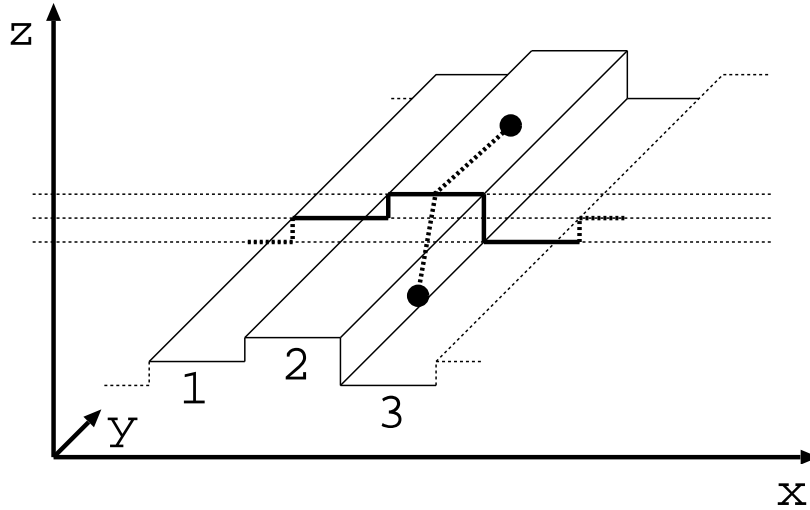
Figure 7.3: The membrane fluctuates only in one direction and is discretised using three heights with periodic boundary conditions. It interacts with a bead, fixed in unit distance from a membrane point via a histogram shape.

$$
\begin{aligned}
\approx \quad & 4\pi^2 \int dh_{12} \int dh_{23} \int dh_{31} \quad \delta\left(h_{31} - h_{12} - h_{13}\right) \\
& \exp\left[-\frac{3}{2}\kappa\left(\left(1 + \frac{2}{27}\right)(\Delta h_{12,23})^2 + (\Delta h_{23,31})^2 + (\Delta h_{31,12})^2\right)\right]
\end{aligned}
$$

where $\Delta h_{ij,jk} = h_{ij} - h_{jk}$. Thus the clapper contribution can be interpreted as an effective bending rigidity

$$
\kappa_{eff} \approx \kappa + \frac{1}{3}\left(\frac{2}{27}\right) \approx \kappa + 0.025 \tag{7.2}
$$

if the anchor point is equally distributed over all strips.

The model calculation has been presented for three levels but can be generalised to L height levels for any $L > 2$. The corresponding effect on κ is then given by $\Delta\kappa = 2/(9L^2)$. Analytical values and simulation results are listed in table 7.1. The simulations have been done with the code which is has also been used to simulate the polymer chains of several bonds. Thus this model serves as a test of the code. For high κ, it is rather time-consuming to obtain a proper statististical accuracy (and therefore these values have been skipped for large L) while for very small κ the approximations used in the analytical calculation do not hold. The simulation results are consistent with the analytical values.

L	$2/(9L^2)$	$\kappa = 0.1$	$\kappa = 1$	$\kappa = 10$	$\kappa = 20$	$\kappa = 50$
2	0.055	0.013	0.054	0.055	0.048	0.04
3	0.025	0.003	0.023	0.026	0.023	0.03
4	0.013	0.003	0.013	0.013	0.012	0.01
5	$8.9\,10^{-3}$	$2\,10^{-3}$	$8.1\,10^{-3}$	$1\,10^{-2}$	$1\,10^{-2}$	-
8	$3.5\,10^{-3}$	-	$3.4\,10^{-3}$	-	-	-

Table 7.1: Analytical and simulation results for the clapper-wedge model. The error is of the order of magnitude of the last digit. Simulations have been performed for a membranes with different bare κ values.

Modeling the membrane-polymer interaction

The membrane representation can be discretised either in Fourier space or in real space. If it is discretised in Fourier space, it is continuous in real space and calculations of the avoidance of the polymers with the smooth membrane height field are computationally rather time-consuming. All membrane fluctuation modes need to be evaluated for each coordinate pair (x, y) which describes a polymer location. The smooth membrane representation thus seems to be not favourable, because typically 10^8 Monte Carlo steps have to be generated. As it will be discussed later, the membrane has been discretised in Fourier space for generating the membrane conformations and an additional discretisation has been employed in real space to model the interaction with the polymer.

The simplest polymer-membrane model used for the simulations is a histogram representation of the membrane and attached Pearson walks to simulate the polymer chains. The membrane-polymer interaction is given by the requirement that the vertices of the polymer cannot cross the 'staircase' of height levels. Two discretisations are involved in this model: the polymer bond length, and the histogram representation used to evaluate the membrane-polymer interaction. While the effects of the polymer discretisation have already been extensively discussed for smooth membrane shapes in chapter 5, the additional discretisation effects due to the membrane discretisation are investigated in this chapter. On the one hand, the height levels of the histogram model are a crude approximation to the smooth membrane shape shown in figure 7.4. On the other hand, the use of height levels is very fast concerning computation time. Only the integer parts of the x and y coordinates of the vertices need to be determined (as the membrane grid constant is 1) and the z coordinate can be compared to the corresponding height level, the value of the height is stored in an array.

A membrane representation with an linear interpolation between the grid points is only slightly more time-consuming than the histogram model. The membrane coordinates of neighbouring grid points are joined by straight lines for a membrane fluctuating only in one direction. A triangulation is applied for more
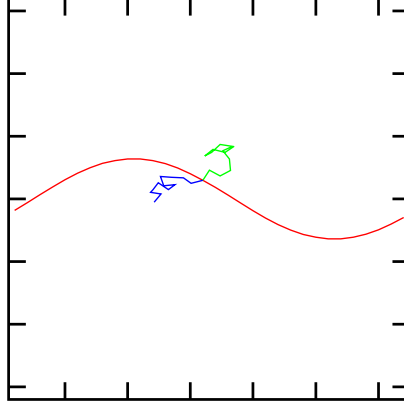
Figure 7.4: A diblock copolymer and the membrane: exact membrane shape.

general fluctuations. The applicability of both approximate models is discussed in section 7.2.

Generating membrane conformations and evaluation

The membrane Hamiltonian in Monge representation can be written in terms of Fourier-transformed variables instead of the membrane height field. Using the expressions in Fourier space which were discussed in section 4.2 and in appendix C, several observables can be calculated analytically for pure membrane systems. For the discretised membrane model of size $L \times L$, with $\mathbf{q} = (2\pi k_x/L, 2\pi k_y/L)$, the ensemble averages read

$$\left\langle \sum_{\mathbf{x}} \left[h_{\mathbf{x}} - \bar{h} \right]^2 \right\rangle_c = \frac{1}{L^2} \sum_{\mathbf{q}; \mathbf{q} \neq 0} \langle H_{\mathbf{q}} H_{-\mathbf{q}} \rangle_c \tag{7.3}$$

for the mean squared deviations from the average value of the height field and

$$\left\langle \sum_{\mathbf{x}} \left[\nabla h \left(\mathbf{x} \right) \right]_{\mathbf{x}}^2 \right\rangle_c = \frac{2}{L^2} \sum_{\mathbf{q}; \mathbf{q} \neq 0}^{L-1} \langle H_{\mathbf{q}} H_{-\mathbf{q}} \rangle_c \left\{ \left[\cos \left(\mathbf{q}_x \right) \right] + \left[\cos \left(\mathbf{q}_y \right) \right] - 2 \right\} \tag{7.4}$$

for the mean squared gradients of the height field. Both observables comprise membrane fluctuations on all length scales and in all directions. They employ sums over the ensemble averages of

$$\langle H_{\mathbf{q}} H_{-\mathbf{q}} \rangle_c = \frac{1}{4\kappa} \left[\cos \left(\mathbf{q}_x \right) + \cos \left(\mathbf{q}_y \right) - 2 \right]^{-2} \tag{7.5}$$

which characterise fluctuations of wavelengths determined by $\mathbf{q}$. The values $\langle H_{\mathbf{q}} H_{-\mathbf{q}} \rangle_c$ can be reproduced exactly by simulations for pure membrane systems. If these observables are extracted from the data of membrane-polymer simulations, effective values of κ can be calculated. Of special interest is Eq. (7.5) which has been employed to calculate the length-scale dependent polymer effect on the bending rigidity.

There are two different strategies to change the membrane conformation in a Metropolis Monte Carlo simulation algorithm: Either the membrane height of one grid point is varied and the energy of the new conformation[2] is determined by Eq. (4.5), or the value of one $H_{\mathbf{q}}$ is varied, which affects one of the terms in the sum occurring in Eq. (4.9). The observables of most interest (Eq. (7.5)) can be directly deduced from the $H_{\mathbf{q}}$ (Eq. (7.5)). In order to reduce the correlation time of consecutive observable snapshots, a method that generates the conformations in Fourier space has been chosen.

7.2   Results and discussion

Ideal and self-avoiding polymers anchored to a membrane have been simulated.

Ideal chains

Simulations have been done for membrane grids of the sizes $L = 16$, 32 and 64, for polymer bond numbers N between 12 and 100 and for bare membrane κ values of 1.6, 2.0, 3.2 and 6.4. In most simulations, the polymer bond length a_{pol} has been chosen to equal the membrane grid constant a_{mem}. To check for discretisation effects, systems with $a_{pol} = 2\, a_{mem}$ and $a_{pol} = 0.5\, a_{mem}$ have also been investigated. The membrane-polymer interaction has been modeled by the histogram and the straight-line membrane representations. Simulations have been done for the coupled case where modes change on all length scales, as well as for the decoupled case with only one active fluctuation mode. All systematic studies have been done for symmetric polymer coverage, but one system with a single end-grafted chain has also been simulated.

In the case of symmetric polymer coverage and large-scale fluctuations, the polymer effect is expected to match the values discussed in chapter 5, i. e. for the ideal chains the analytical values that have been calculated by Eisenriegler and Hiergeist/Lipowsky [123, 124].

A comparison of the results obtained by the histogram and the straight-line model is shown in figure 7.5 for a membrane grid size $L = 32$ (32×32 grid points). The bare membrane bending rigidity is $\kappa_{mem} = 2$. The polymer coverage is symmetric with one chain anchored to each side of the membrane, each chain consists of $N = 12$ bonds of length $a_{pol} = a_{mem}$. Note that the value of the

---

[2]In practice, the energy change is evaluated only on five grid points, see Eq. (4.6)

(a) histogram model

(b) linear-connection model
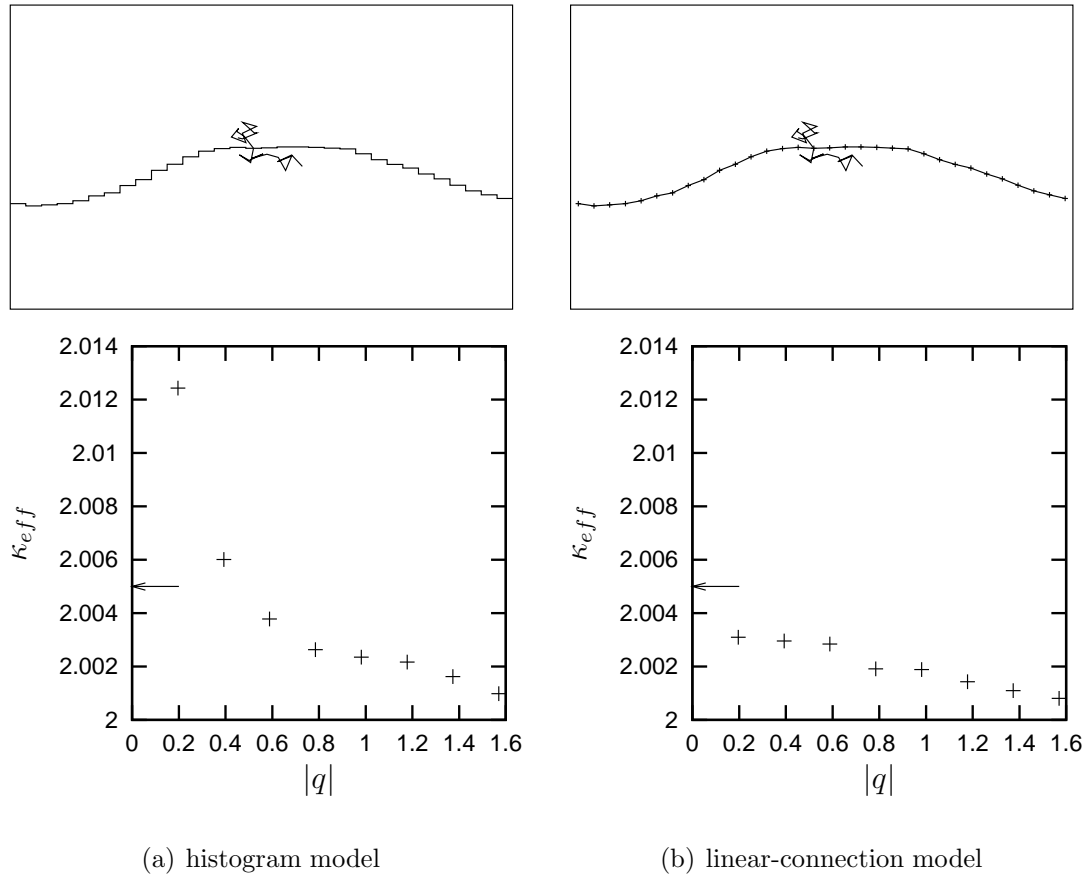
Figure 7.5: The simulation snapshots show the same conformation using different membrane representations to model the membrane-polymer interaction. In the histogram case, the bending rigidity increases strongly for $|q| \to 0$. The dashed lines denote the analytical value for $q \to 0$ [123, 124]. Note that the amplitudes of the membrane fluctuations in the simulation snapshots are not realistic. An extremely low bare membrane κ has been chosen for the snapshots.

polymer effect is only about 0.1% of κ_{mem}.[3] This requires a high accuracy of the simulation data and a large number of observable snapshots.

- The histogram model extrapolates for $|q| \rightarrow 0$ to a much too high value compared to the analytical calculations. The strong increase of the polymer effect for small $|q|$ becomes less pronounced if larger ratios of a_{pol}/a_{mem} are chosen, but does not vanish for reasonable sizes of the membrane grid.[4]

- The data obtained by simulations with the straight-line approximation allows for a proper extrapolation to $|q| \rightarrow 0$, but the data seems to extrapolate to a somewhat too small value.

The strongly increased polymer effect for large-scale fluctuations in the histogram model could be traced back to be mostly due to those conformations where the polymer is anchored to a 'planar' part of the membrane which is tilted against the plane defining the membrane grid, compare figure 7.6 (a). For these conformations, the 'staircase' effect is most pronounced. This has been investigated by attaching a polymer chain to a membrane with a fluctuation length larger than the radius of gyration of the polymer. The membrane has been chosen to fluctuate like $a \sin(x)$ and the polymer chain has been attached at $x = 0$ in one simulation and at $x = \pi/2$ in another simulation. The amplitude a has been varied by simulations in order to comply with the membrane curvature energy. It has been found, that in the histogram model the polymer-damping of the fluctuation is much stronger if the chain is anchored at $x = 0$ than if it is anchored at $x = \pi/2$. This behaviour is opposite to the behaviour which is expected to occur for a smooth membrane representation. In the smooth case, the membrane remains flat around $x = 0$ despite of the fluctuations. The polymer should therefore have no influence on the fluctuations, if it is anchored to this part of the membrane. Obviously this problem does not occur if the membrane height values on the grid are connected by straight lines. In order to get rid of the staircase artefact, the straight-line representation of the membrane has been applied for all further studies.

Figure 7.7 shows simulations for several membrane sizes and chain lengths. The results for finite q are normalised by $a_\kappa(0)$, denoting the universal amplitudes discussed in chapter 5. For dimensionality reasons, $a_\kappa(q)/a_\kappa(0)$ is plotted against $|q| R_e$, so the data for different chain lengths scales properly. The polymer effect is large for small values of $|q|$. This is compliant with an intuitive picture because the fluctuation amplitudes scale like $1/q^4$ (compare appendix C). Surprisingly, a

---

[3]It is not possible to choose a much lower κ of the bare membrane for two reasons: 1. The Hamiltonian employed is valid only for small curvatures. 2. With larger curvatures the connection to the known limiting values is not possible any more.

[4]Increasing the ratio a_{pol}/a_{mem} requires an enlarged membrane grid size in oder to avoid spurious effects due to the periodic boundary conditions — and thus leads to an increase of the simulation time.

System snapshot # 12 (a)
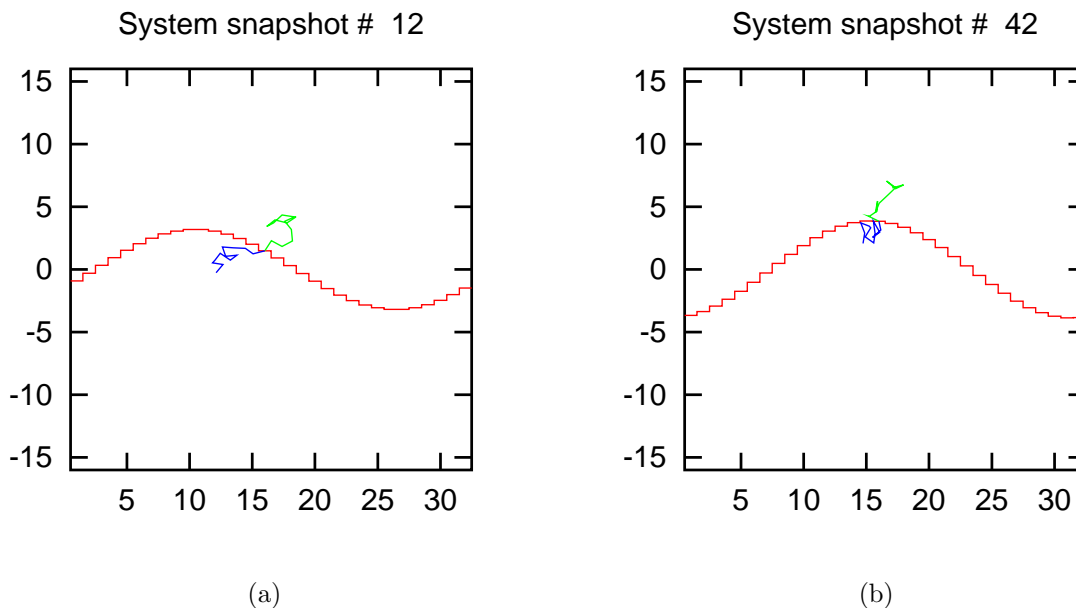
System snapshot # 42 (b)

Figure 7.6: The histogram model for the polymer-membrane interaction. The κ value chosen to obtain the snapshots is much smaller than the value used for the simulations.
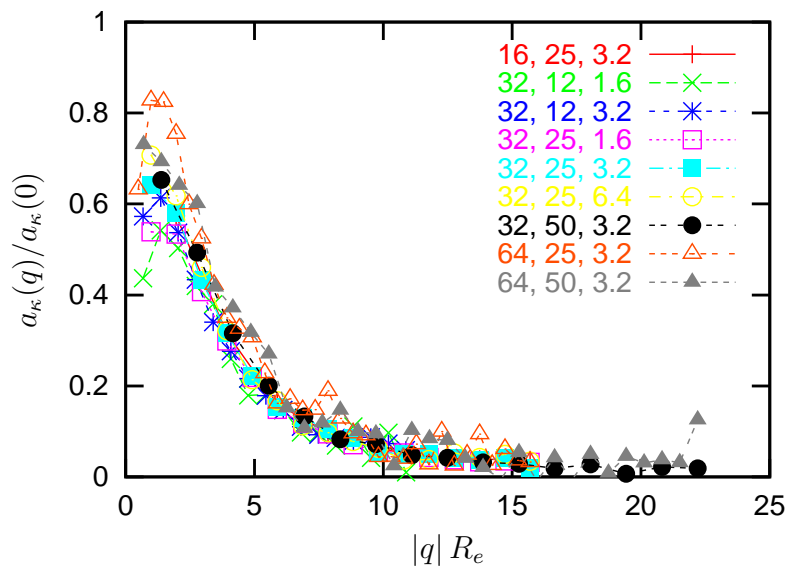

Figure 7.7: Simulation results for ideal chains without finite size corrections. Labels are given by the set of values for L, N and κ_{mem}.
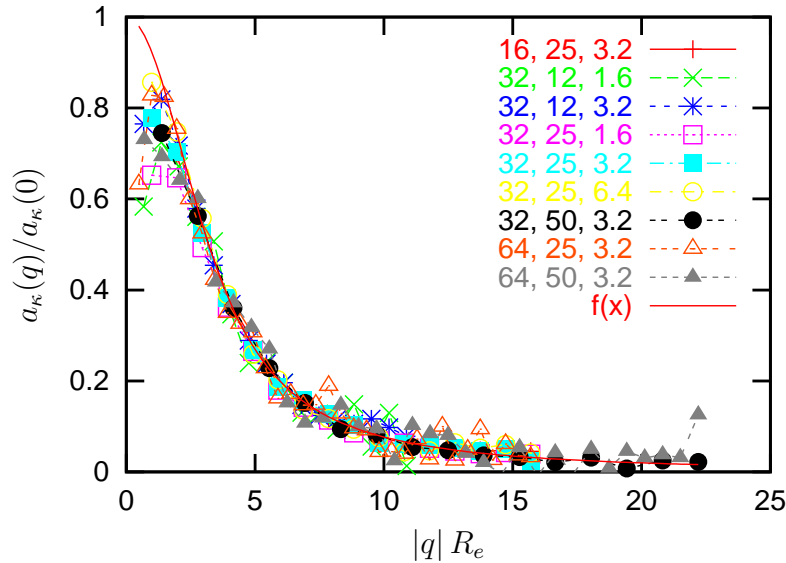
Figure 7.8: Simulation results for ideal chains with the finite size corrections obtained in chapter 5. Labels are given by the set of values L, N and κ_{mem}. The function is $f(x) = 2.0 \left\{ \exp(-x^2) - 1 + x^2 \right\}/x^4$ where $x = |q|\,R_e/2$.

decrease of $a_\kappa(q)$ at the lowest $|q|$ value on the grid is observed in several cases. The decrease occurs especially for low κ_{mem} and for polymer chains which are short compared to the membrane size. At least partly this behaviour is due to mode coupling, as will be discussed later. The statistical errors become rather large compared to the effect for high absolute values of q. However, the simulation results for different chain lengths and membrane sizes fall on a single master curve reasonably well, even though the bond number of some of the chains is extremely small and huge finite-size effects might have been expected ($N = 12$). If the finite-size effects given by Eq. (5.7) are taken into account, the consistency of the data improves considerably, see figure 7.8. Neglecting the decrease for the low $|q|$, an extrapolation of the data to 1 now seems to be possible. Postulating that the data extrapolates to 1 for small $|q|$ and assuming that the functional form is the same as for the system of Bickel and Marques [151], we find that the simulations results can be very well described by:

$$f\left(q\,R_e\right) = 2 \left\{ \exp\left(-\left[\frac{q\,R_e}{2}\right]^2 \right) - 1 + \left[\frac{q\,R_e}{2}\right]^2 \right\} \bigg/ \left[\frac{q\,R_e}{2}\right]^4 \qquad (7.6)$$

Note that a priori there is no reason to expect that our simulation data is described exactly by the calculations of Bickel and Marques. Both systems differ: in Ref. [151] on both sides single chains are anchored at one end to the membrane, whereas in the simulation symmetric polymers have been anchored. Indeed the

authors propose that the ratio $a_\kappa(q)/a_\kappa(0)$ in their system is given by [5]

$$f_{BM}\left(q\,R_e\right) = A_{BM} \left\{ \exp\left(-\left[\frac{q\,R_e}{\sqrt{6}}\right]^2 \right) - 1 + \left[\frac{q\,R_e}{\sqrt{6}}\right]^2 \right\} \bigg/ \left[\frac{q\,R_e}{\sqrt{6}}\right]^4 \qquad (7.7)$$

and is *not* extrapolating to 1. They calculate that for $q \to 0$ the function extrapolates to $1/(1 + \pi/2)$ and the function decays more slowly with increasing qR_e. Note the different scale factors $1/2$ and $1/\sqrt{6}$. The different behaviour is due to the different system responses to the spontaneous curvature terms. The distributions of end-grafted polymers on the membrane will adjust to the membrane shape, driven by an effect which is linear in the membrane's curvature. The end-grafted single chains prefer locations where the membrane is curved away from the polymer. Due to the symmetric coverage, in the system investigated in this work the polymers prefer planar parts of the membrane rather than those which are highly curved.[6] I have observed a similar effect as Bickel and Marques have found, if the membrane has been decorated by one end-grafted polymer chain (figure 7.9).[7] However, quantitatively the simulation data of this asymmetric system does not confirm the results in the publication. For my system, the data is well described if the prefactor A_{BM} would be only half the value given in the reference. A decrease of κ due to polymer redistribution is consistent with more general studies on asymmetric membrane components [272]. In my simulation, asymmetry has only been introduced in one direction because the polymer molecule is attached only to one side of the membrane. This might explain the mismatch of a factor 2.

I have studied the effect of different ratios a_{pol}/a_{mem} (figure 7.10) and have found the simulation data for ratios of 0.5, 1 and 2 to be consistent for a wide range of $|q|R_e$. This supports that Eq. (7.6) is independent from discretisation effects.

Finally, I have checked for mode coupling effects by simulating the different modes separately. The results for single q-modes in figure 7.11 imply that the observed decrease of the polymer effect for low $|q|$ is at least partly due to mode coupling.

Self-avoiding chains

Self-avoiding chains of $N = 50$ and $N = 100$ bonds have been simulated. The bond length has been chosen to equal the membrane grid constant and a bead

---

[5]see Eq. 3.10

[6]The free energy term corresponding to this redistribution is already of quadratic order in the curvature and thus the resdistribution should not affect the value of the bending rigidity. This is also the reason why I expect my simulations to extrapolate to 1.

[7]For more detailed studies of this architecture, the effect of the pinch would have to be discussed.
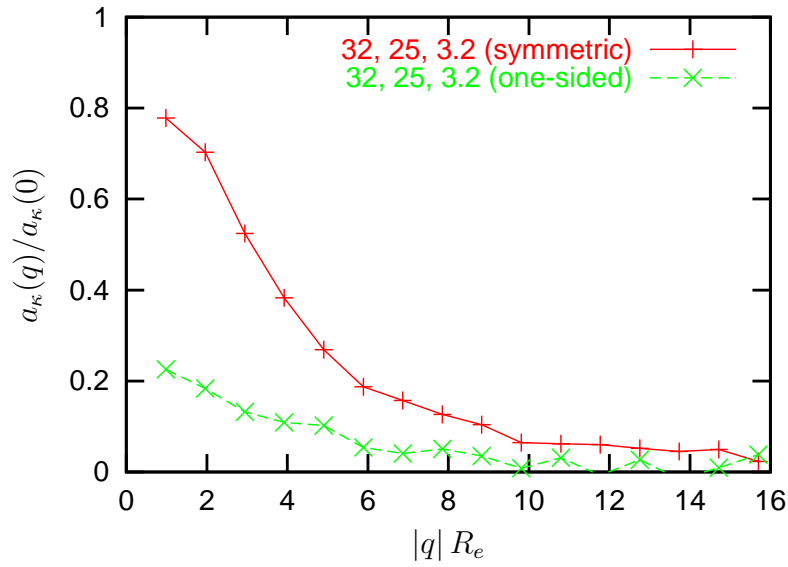
Figure 7.9: Simulation results for a symmetric polymer attachment to the membrane and a chain anchored only to one side. Labels are given by the set of values L, N and κ_{mem}.
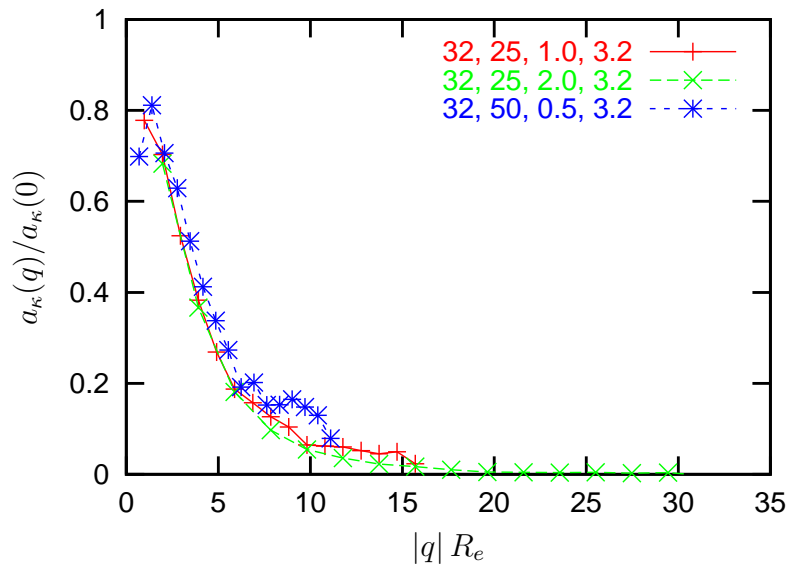
Figure 7.10: Simulation results for different ratios a_{bond}/a_{mem}. Labels are given by the set of values L, N, a_{pol}/a_{mem} and κ_{mem}.
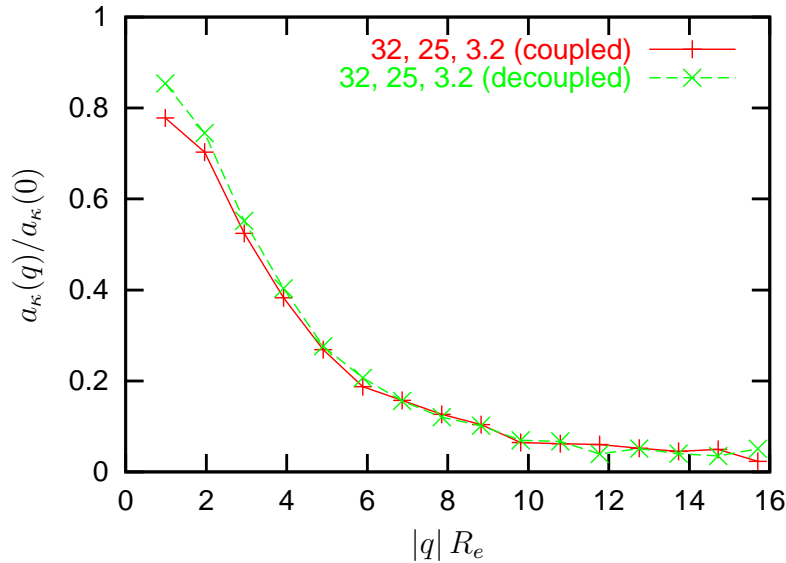
Figure 7.11: Simulation results for coupled and decoupled modes of different q. Labels are given by the set of values L, N and κ_{mem}.

size of $0.25\,a_{pol}$ is used. The values for R_e have been determined by calculations for free chains. The effects for the membrane's curvature elastic constants on the whole fluctuation spectrum have been normalised by those for the limit of large fluctuation length scales, $a_\kappa(0)$, that have been obtained in chapter 5. Up to the simulation accuracy, self-avoidance has no influence on the functional dependence of the polymer effect on $|q|$ (figure 7.12).

Self-avoiding chains have much larger values of R_e and R_g compared to ideal chains of the same bond numbers and bond lengths. The average chain conformation therefore needs to be much more stretched in the self-avoiding case. Already for 200 bonds the radius of gyration for the self-avoiding chain is a factor of 1.5 larger than for the ideal case, compare figure 4.3. In addition, as discussed in chapter 5, the amplitude of the polymer effect for large κ_{mem} changes if self-avoidance effects are taken into account. Therefore it is very remarkable that the proper normalised functions $a_\kappa(q)$ coincide for ideal and self-avoiding chains. However, this is consistent with the results of an recent investigation for the pressure exerted by ideal and self-avoiding chains in Ref. [147], and it confirms the simulation results for $a_\kappa(0)$, obtained in the limit of large scale fluctuations.
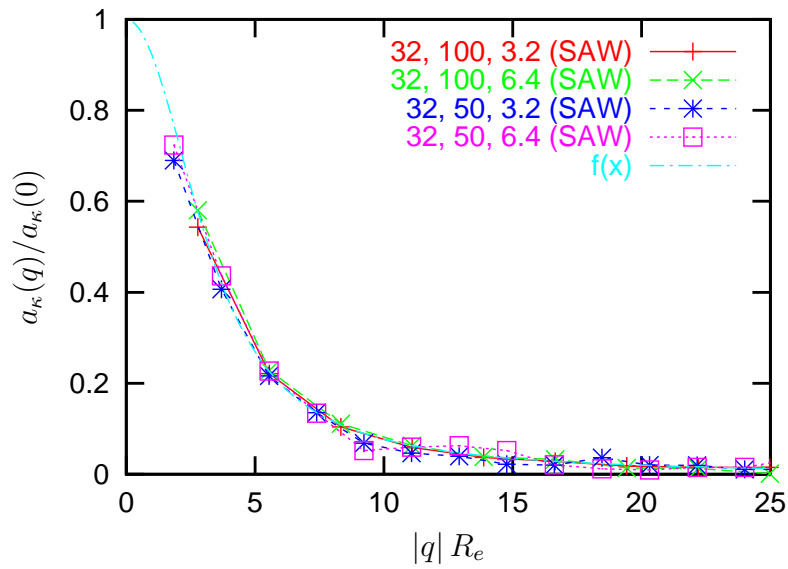
Figure 7.12: Simulation results for ideal and self-avoiding chains. Labels are given by the set of values L, N and κ_{mem}. The function $f(x)$ is the same as in figure 7.8.

Chapter 8

Linear polymers in the lamellar phase

8.1 Model and simulation technique

In this chapter, the effects of an anchored linear polymer in the lamellar phase are discussed. The polymer is modeled by a freely-jointed chain confined between two parallel walls. The chain is end-grafted to one of the walls. The evaluation technique is very similar to the one described in chapter 5. In addition to the one-wall case, virtual spheres and cylinders will be applied to both walls.

For wall distances which are very small compared to the size of the polymer, a new algorithm generating conformations of the chain needs to be introduced. Apart from the one-bead crankshaft algorithm, conformations generated by 3D pivot, multiple-bead crankshaft, one-bond changes and simple growth all have very low acceptance rates. Subsequent conformations generated by a one-bead crankshaft algorithm are correlated to a very high degree. Therefore I have introduced a 2D pivot algorithm that operates only in the plane parallel to the walls. In combination with the one-bead crankshaft algorithm, 2D pivot moves are capable to generate all possible conformations. I have validated the 2D pivot algorithm by comparing the results with those which were obtained with the standard pivot algorithm for chains of length 20 and not too small interlayer distances.

8.2 Polymer-wall simulations

An ideal chain of $N = 100$ bonds with bond length 0.245, i. e. $R_g = 1$ and $R_e = \sqrt{6} = 2.45$, has been simulated. For large distances of the parallel walls, the polymer does not notice the additional constraint and the results equal those of chapter 5. For distances between $d = 5\,R_g$ and $d = 1.5\,R_g$, the polymer effect increases for all membrane constants, see figure 8.1 (a). For $d = 3\,R_g$, the effect

(a)   (b)
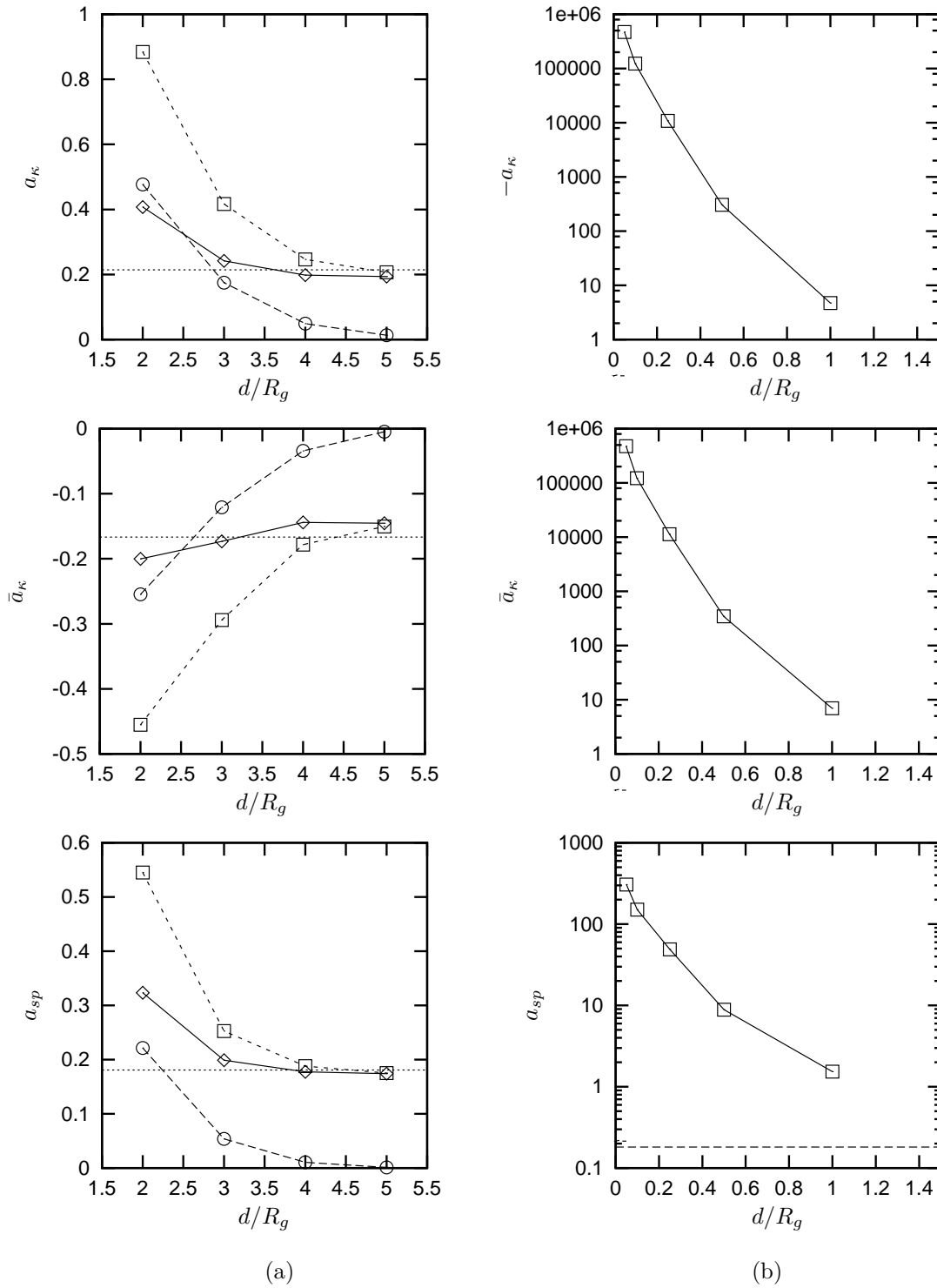
Figure 8.1: Universal amplitudes a_{sp}, a_κ und $\bar{a}_\kappa$ for an ideal linear polymer ($N = 100$, $R_g = 1$) constrained between parallel walls of distance d. Diamonds denote the effect on the wall the chain is attached to, circles the effect on the opposite wall and squares the total effect. The dashed line indicates the analytical value without confinement.

d/R_g	$a_{sp,d}$	$a_{sp,o}$	$a_{sp,a}$	$a_{\kappa,d}$	$a_{\kappa,o}$	$a_{\kappa,a}$	$\bar{a}_{\kappa,d}$	$\bar{a}_{\kappa,o}$	$\bar{a}_{\kappa,a}$
1	1.28	1.39	2.67	-8	-8	-16	11	11	23
2	0.37	0.26	0.63	0.49	0.50	0.99	-0.25	-0.27	-0.52
3	0.21	0.06	0.28	0.27	0.23	0.50	-0.20	-0.18	-0.38
4	0.19	0.01	0.20	0.22	0.06	0.29	-0.17	-0.04	-0.21
5	0.18	0.00	0.18	0.21	0.01	0.22	-0.17	0.00	-0.17

Table 8.1: Membrane constants obtained for a polymer constrained between two parallel walls. Data is presented for the wall the chain is directly anchored to (index d), the opposite wall (index o) and the sum of both (index a). The statistical error is of the order of magnitude of the last digit.

almost doubles for κ and $\bar{\kappa}$, compared to $d = \infty$ and it increases by about $1/3$ for c_0. For $d = 2\,R_g$, the model predicts enhancement factors of about 4.2 for κ, and 3 for $\bar{\kappa}$ and c_0. The enhanced effects are due to two different reasons:

- The effect on the anchoring wall increases.

- The polymer also affects the fluctuations of the opposite wall.

Surprisingly, at $d \approx 1.5\,R_g$ the polymer effect changes qualitatively, compare figure 8.1 (b). The absolute values of a_κ and $\bar{a}_\kappa$ increase strongly if the interlayer distance is decreased, but with reversed sign.[1] The effect on a_{sp} continues to increase and remains positive. For $d > 0.5\,R_g$, the universal amplitudes can be calculated with reasonable accuracy and the $N^{1/2}$ extrapolation holds for bond lengths smaller than the interlayer distance. The extrapolated data is listed in table 8.1. The strong negative values at small interlayer distances have been observed for all finite chain lengths, but the for $d < 0.5\,R_g$ extrapolation errors in the limit $N \to \infty$ become too large to decide about the sign of a_{sp}, a_κ and $\bar{a}_\kappa$.

8.3 Discussion

An ensemble has been investigated where the distance between the polymer anchor point and the opposite wall has been kept fixed.[2] In this model, a strong decrease of the bending rigidity and a strong increase of the saddle-splay modulus have been observed. It is obvious that we do not expect a sign change of the total effective membrane constants, because an instability of the lamellar phase is expected to occur at somewhat larger distances. The results of the wall model

---

[1]In the figure, only the total values are shown. The values for anchor and opposite wall are both half of the total effect.

[2]For a real membrane, a relaxation of this distance should be taken into account.

should be valid if the bare membrane κ is sufficiently larger than the $\Delta\kappa$ induced by the polymer.

The results for the polymers in the lamellar phase are rather surprising. However, it is obvious that the anchor looses its effect on the polymer conformations when the interlayer distance becomes small. Therefore the effect of free and anchored chains should be the same for strong confinement and one of both effects thus has to change sign.

In a blob model calculation, the most naive ansatz is the assumption of a cylindrical symmetry of the polymer extension around the anchor point. With this assumption, the sizes of the blobs are changed if the membrane is curved, but a blob redistribution will not take place. An increase of the absolute values for a_κ and $\bar{a}_\kappa$ is found in the calculations if the lamellar spacings decrease. However, the model cannot explain the sign change in a_κ, because all expansion coefficients for the free energy turn out to be positive for arbitrary values of d (compare Eqs. (5.6)). The model is obviously not capable to take into account for changes of an asymmetric shape of the polymers, which are due to a finite membrane curvature. Indeed, figure 8.2 shows that (a) the polymer has a mean shape which is not cylindrically symmetric and (b) that the monomer density redistributions for a small change of the curvature of the anchoring wall are large. The response of the polymer chain to this asymmetry thus seems to be an important effect for the determination of the values of a_κ and $\bar{a}_\kappa$ at small interlayer distances.

The dependence of the polymer effect on the interlayer distance might explain some of the effects described for the lamellar-phase experiments in chapter 2. Especially it might explain two effects observed in the microemulsion experiments[3]:

- Confinement effects might explain the missing factor of about 2 in the measurements of a_κ and $\bar{a}_\kappa$ in the microemulsion experiment [13,16]. Note that the average structural size of a microemulsion in Ref. [16] has about twice the value of the interlayer spacing where confinement effects are expected.[4] However, due to fluctuations which have not been taken into account by the wall model, also smaller intermembrane distances will occur.

- Confinement effects might explain the occurrence of a lamellar island in the microemulsion experiments [9, 17]. The effect has been observed for high polymer additions and the structural size of the microemulsion is of the order of magnitude where confinement effects are expected. The ratio $-\kappa/\bar{\kappa}$ has a maximum at about $d = 2R_g$. This might favour a lamellar phase, compare appendix D. The decrease of the amplitudes of the polymer effect

---

[3]Note that in both cases data obtained for the *lamellar* phase is used to argue for *microemulsion* experiments.

[4]Compare Fig. 1 in Ref. [16] and use the formula $d = 2.05\,nm/\phi_s$ to determine the domain size [273]. With $R_g(PEP_5 - PEO_5) = 3\,nm$, we obtain $d = 6.3\,R_g$ for the measurement at $\phi_s = 0.11$ and $d = 10.5\,R_g$ for $\phi_s = 0.71$.
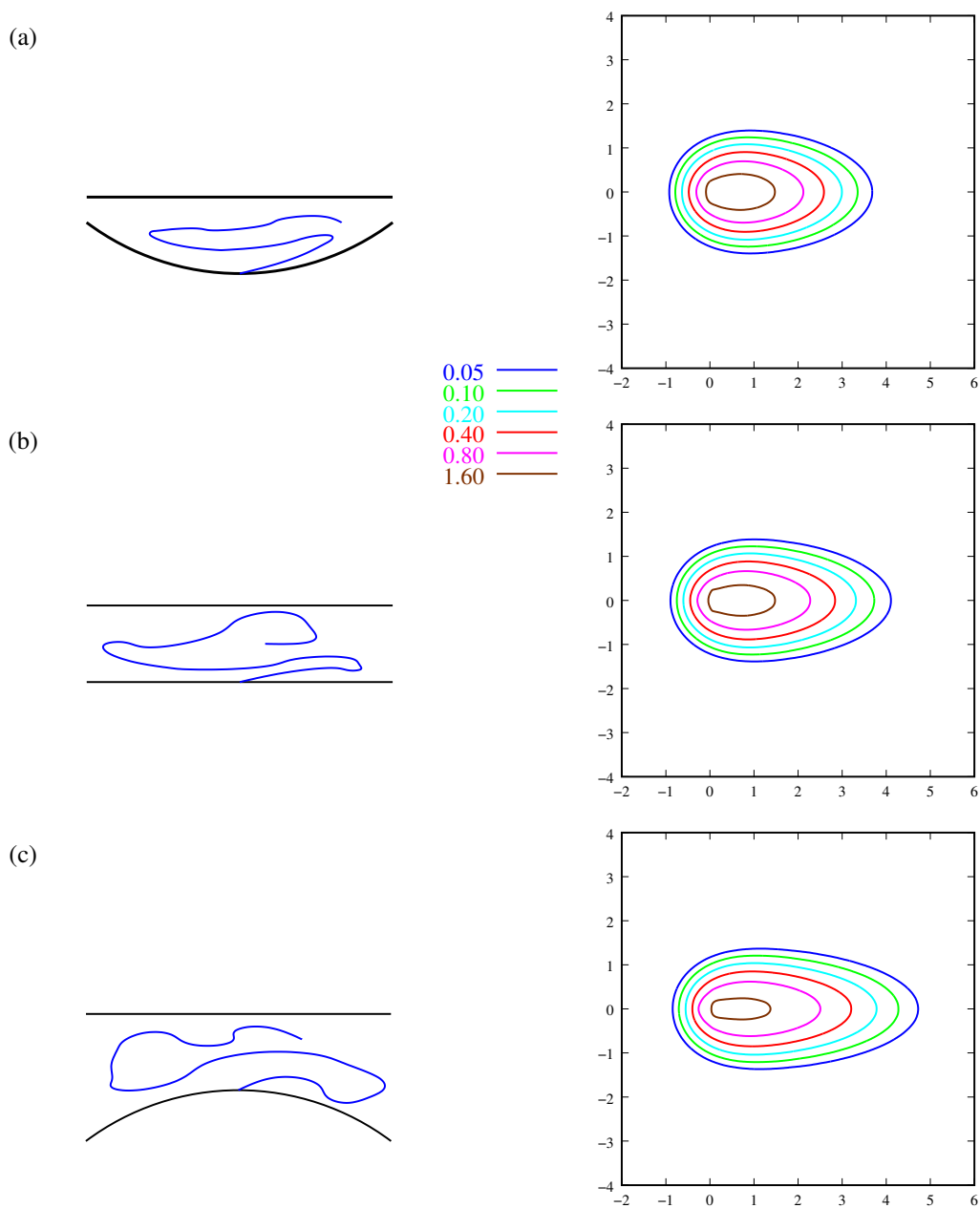
Figure 8.2: Contour plot of monomer densities of an ideal linear polymer with 100 bonds and bond length $a_{pol.} = 0.2449$ which is constrained by two walls. The anchor point is fixed at $(0, 0)$ and the center of gravity is always oriented in positive x direction by turning the confirmation around an axis perpendicular to the walls through the anchor point. Bond lengths and number of bonds correspond to a free chain of mean squared radius of gyration 1. All density values are given in units of $1/a_{pol.}^2$. The sketches are strongly exaggerated. The distance between the walls is 0.25 and the curvature in cases (a) and (c) equals 8.3169×10^{-4}.
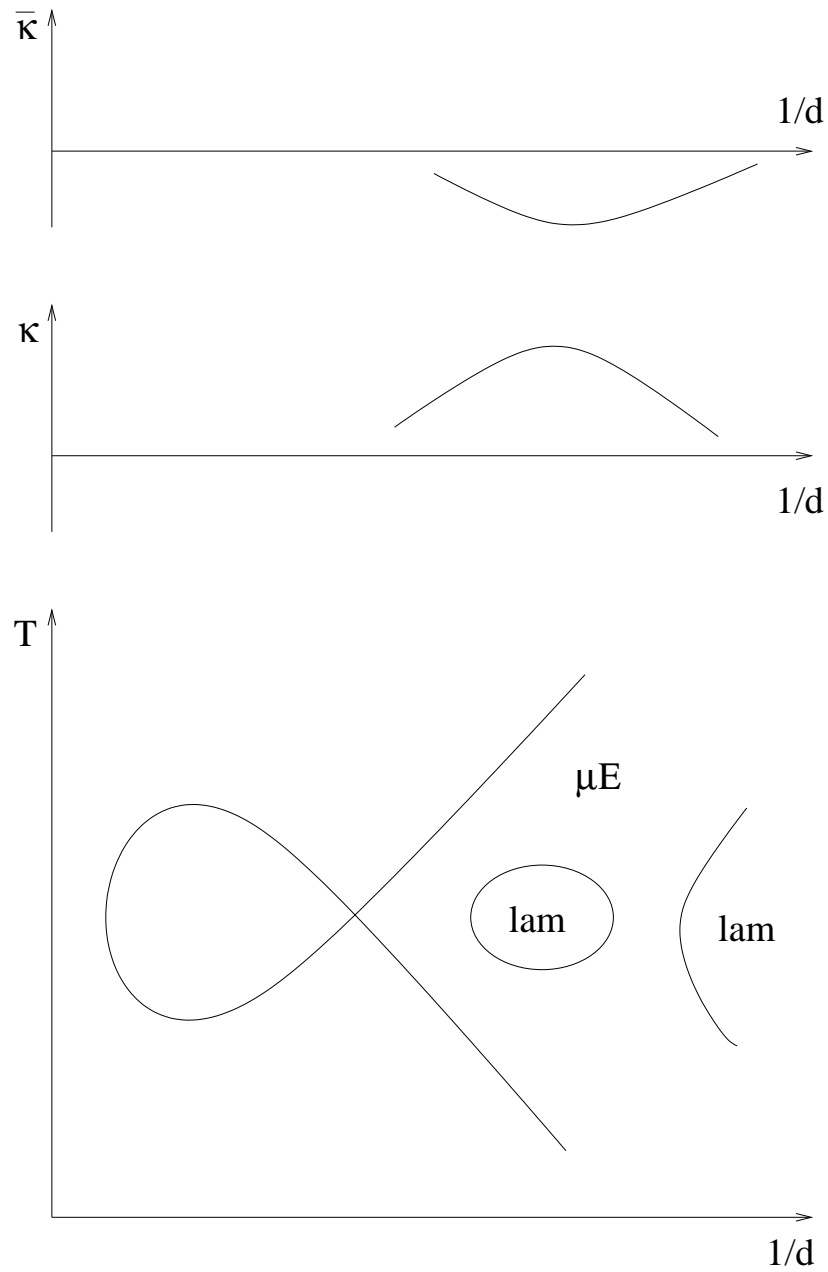
Figure 8.3: The lamellar island observed in oil-water-amphiphile microemulsion experiments by addition of block-copolymers (identifying the amphiphile volume fraction ϕ with $1/d$) [9, 17]. The island might be due to confinement effects of the anchored polymer chains which act differently on κ and $\bar{\kappa}$.

might also explain why the lamellar phase at high values of $1/d$ has been observed not to shift upon polymer addition [9]. This hypothetical scenario is sketched in figure 8.3. Note that the relation of the theoretical data for the extrema of $a_\kappa(1/d)$ and $\bar{a}_\kappa(1/d)$ with the position of the lamellar island in the phase diagram, as indicated in the figure, still has to be investigated in more detail.

In this chapter, confinement effects have been investigated for the limit of bare membrane κ values that are large compared to the polymer effect. Experimental evidence for this limiting case has not yet been found. It would be therefore interesting to extend the studies in order to connect them quantitatively to experiments with smaller membrane κ, e. g. surfactant systems like the microemulsions.

Chapter 9

Conclusions

Several experiments on different kinds of polymer-membrane systems have been discussed. With microemulsion experiments, the polymer effect on the bending rigidity and the saddle-splay modulus have been measured recently. While the scaling behaviour agrees very well, the values do not coincide with the analytical theories of ideal chains. The measurements are about a factor of 1.5 to 2 larger than current theoretical predictions.

I have developed a Monte Carlo simulation technique for polymers anchored to membranes and was able to reproduce the analytical results for ideal linear chains. Finite-size effects as well as universal system properties have been studied. Two fit steps are involved to obtain the universal constants from simulations of chains with up to 200 bonds. After validation of the method, the effects of self-avoidance have been determined with high accuracy. The self-avoidance effects for linear chains have been found to be rather small. Star polymers with up to 5 arms, anchored at their centers to the membrane, have been simulated. I have found that

1. A star increases the efficiency of the polymer with respect to the bending rigidity and the spontaneous curvature.

2. The ratio of the polymer effects on κ and $\bar{\kappa}$ can be chosen by the functionality.

Both properties of star polymers have been confirmed analytically by blob model calculations. Ring polymers with and without self-avoidance have been studied. For a self-avoiding ring polymer without knots, I have observed a change in the effect on the membrane curvature elastic constants, if the number of bonds increases over a threshold number of about 50.

Polymers in a multilayer system have been investigated, modeled as one chain constrained between two parallel walls. I have found the effect of an anchored polymer to increase significantly for interlayer distances d of 2 to 4 times the radius of gyration of the chain. For smaller interlayer distances, the effects on κ

91

and $\bar{\kappa}$ have been found to change their signs and to increase much more strongly in magnitude. A sign change of the effective membrane constants is not supposed to be found in real systems because an instability is supposed to occur for a somewhat larger value d. The confinement effects are of the right order of magnitude that they might explain the missing factor of about 2 for the bending rigidity and the saddle splay modulus if the microemulsion measurements are compared to the analytical theory.

I have modified the simulation method in order to make it capable to investigate adsorption effects. Simulation results have not yet been obtained.

The polymer effect on the bending rigidity has been evaluated for the whole fluctuation spectrum of the membrane. The chain has therefore been attached to a fluctuating surface. In compliance with intuitive arguments, the effect is most pronounced for fluctuations on length scales large compared to the size of the chain. Using the calculated finite-size effects, scaling works very well for different system sizes. We were able to describe the data by a single master curve. Self-avoidance effects have been determined, and the data is found to be described by the same master curve obtained for ideal chains. This allows to make the point that there are no effects of self-avoidance on the functional form of the fluctuation spectrum of a membrane.

Appendix A

Fourier transformation of the membrane height field

A 2D discrete Fourier transform is needed to transform the membrane height field. The fact that the data is real allows to simplify and fasten the transformation by about a factor of two [274]. The discrete Fourier transformation of a field $X[j_1, j_2]$ of dimension $L \times L$ is defined by

$$Y[i_1, i_2] = \frac{1}{N} \sum_{j_1=0}^{L-1} \sum_{j_2=0}^{L-1} X[j_1, j_2] \exp\left(\frac{2\pi i}{L} i_1 j_1\right) \exp\left(\frac{2\pi i}{L} i_2 j_2\right) \qquad \text{(A.1)}$$

with an appropriate normalization factor N and for $0 \leq i_1 < L$, $0 \leq i_2 < L$. In general, the $Y[i_1, i_2]$ are complex; for real X, the array Y has hermitian symmetry, i. e. $Y[i_1, i_2] = Y^*[L - i_1, L - i_2]$. It is easy to see that hermitian symmetry corresponds to a real value: If $a = a_r + i\, a_i$, $a \exp(i\, kx) + a^* \exp(-i\, kx) = 2a_r \cos(kx) + 2a_i \sin(kx)$.

Contrary to the impression one might get in reading textbooks on numerical mathematics, it is not essential to choose the size of the data field to powers of

l ↓ m →	0	1	2	3
0	r	c_2	r	c_2^*
1	c_3	c_4	c_5	c_6
2	r	c_1	r	c_1^*
3	c_3^*	c_6^*	c_5^*	c_4^*

l ↓ m →	0	1	2	3	4
0	r	c_1	c_2	c_2^*	c_1^*
1	c_3	c_5	c_8	c_{10}	c_{11}
2	c_4	c_7	c_6	c_9	c_{12}
3	c_4^*	c_{12}^*	c_9^*	c_6^*	c_7^*
4	c_3^*	c_{11}^*	c_{10}^*	c_8^*	c_5^*

Table A.1: The structure of the fourier transformed 2D real array. The marked region is the data that `rfftw2d` prints out. Here, r stands for a real data entry, c for a complex one. Complex entries always occur together with their complex conjugate counterpart.

two — needed for a conventional fast Fourier transformation — in order to get reasonable performance. Program libraries as for example the freely available FFTW are fast also for other array sizes [275–277]. The FFTW library is commonly used for scientific computations but the structure of the output of a 2D real transform is somewhat intriguing. For the special cases of $N = 4$ and $N = 5$, table A.1 lists the structure of the arrays. Note that there are four real values if L is even: $(0,0)$, $(0, L/2)$, $(L/2, 0)$ and $(L/2, L/2)$. In case of odd L, only the value with index $(0,0)$ is real.

For my membrane height field data, the value with the index $(0,0)$ is not of interest because it corresponds to an overall shift of the membrane. The values with indices $(1,0)$ and $(0,1)$ correspond to the amplitude of the longest wavelength fluctuations which are possible in the system. The values with indices $(L-1, 0)$ and $(0, L-1)$ analogously give the amplitudes of fluctuations with the smallest fluctuation lengths (parallel to one of the coordinate axes).

Appendix B

The blob model for star polymers

In this appendix, detailed equations for the blob model calculation for star polymers discussed in chapter 5 can be found. These expressions are not necessary for a basic understanding of the problem and are presented for completeness.

Evaluating integral 5.15 radius of the star polymer is found to be

$$
\begin{aligned}
R_{star,x} &= l_0 N^\nu \left(\frac{f}{2\pi}\right)^{\frac{1-\nu}{2}} \nu^{-\nu} \left\{ 1 + \left(\frac{1}{2} - \frac{1}{2\nu}\right) \frac{1}{1+\nu} a_x \frac{R_{star,x}}{R_x} \right. \\
&\left. + \frac{1}{2}\left(\frac{1}{2} - \frac{1}{2\nu}\right)\left(\frac{3}{2} - \frac{1}{2\nu}\right)\frac{1}{1+2\nu} a_x^2 \frac{R_{star,x}^2}{R_x^2} \right\}^{-\nu}
\end{aligned}
\tag{B.1}
$$

in exact representation. Expansion of the terms in curled brackets gives

$$
\begin{aligned}
R_{star,x} &= l_0 N^\nu \left(\frac{f}{2\pi}\right)^{\frac{1-\nu}{2}} \nu^{-\nu} \left\{ 1 + \left(\frac{1}{2\nu} - \frac{1}{2}\right)\frac{\nu}{1+\nu} a_x \frac{R_{star,x}}{R_x} + \frac{1}{2}\left[\left(\frac{1}{2\nu} - \frac{1}{2}\right) \right.\right. \\
&\left.\left. \left(\frac{3}{2} - \frac{1}{2\nu}\right)\frac{1}{1+2\nu} + \left(\frac{1}{2\nu} - \frac{1}{2}\right)^2 \frac{1}{1+\nu}\right] \nu a_x^2 \frac{R_{star,x}^2}{R_x^2} \right\} \quad .
\end{aligned}
\tag{B.2}
$$

Recursive substitution of $R_{star,x}$ leads to Eq. (5.16) and

$$
Q_0 = \nu^{-\nu}
\tag{B.3}
$$

$$
Q_{x,1} = a_x \left(\frac{1}{2\nu} - \frac{1}{2}\right)\frac{\nu^{1-2\nu}}{1+\nu}
\tag{B.4}
$$

$$
Q_{x,2} = a_x^2 \nu^{1-3\nu}\left[\frac{1}{2}\left(\frac{1}{2\nu} - \frac{1}{2}\right)\left(\frac{3}{2} - \frac{1}{2\nu}\right)\frac{1}{1+2\nu} + \frac{1}{2}\left(\frac{1}{2\nu} - \frac{1}{2}\right)^2 \frac{1+3\nu}{(1+\nu)^2}\right]
\tag{B.5}
$$

Inserting $\xi_x(r)$, the free energy (Eq. (5.17)) reads

$$\mathcal{F}_x = k_B T \left(\frac{f}{2\pi}\right)^{\frac{1}{2}} \int_{l_0}^{R_{star,x}} dr \frac{1}{r} \left(1 - a_x \frac{r}{R_x}\right)^{-\frac{1}{2}} \tag{B.6}$$

and valuation of the integral leads to

$$\mathcal{F}_x = k_B T \left(\frac{f}{2\pi}\right)^{\frac{1}{2}} \left\{ \ln\left(\frac{R_{star,x}}{l_0}\right) + \frac{1}{2} a_x \frac{R_{star,x}}{R_x} + \frac{3}{16} a_x^2 \frac{R_{star,x}^2}{R_x^2} \right\} . \tag{B.7}$$

Now the value for $R_{star,x}$ determined previously needs to be inserted. After several steps one ends up with

$$
\begin{aligned}
\mathcal{F}_x &= k_B T \left(\frac{f}{2\pi}\right)^{\frac{1}{2}} \left\{ \ln\left(\frac{l_0 N^\nu}{l_0} \left(\frac{f}{2\pi}\right)^{\frac{1-\nu}{2}} \nu^{-\nu}\right) \right. \\
&\quad + \left(\left(\frac{1}{2\nu} - \frac{1}{2}\right)\left(\frac{f}{2\pi}\right)^{\frac{1-\nu}{2}}\right) \nu^{-\nu} a_x \frac{l_0 N^\nu}{R_x} \\
&\quad + \left(\frac{1}{2}\left(\frac{1}{2\nu} - \frac{1}{2}\right)\left(\frac{3}{2} - \frac{1}{2\nu}\right)\frac{\nu}{1+2\nu} + \frac{1}{2}\left(\frac{1}{2\nu} - \frac{1}{2}\right)^2 \frac{\nu(1+2\nu)}{(1+\nu)^2}\right. \\
&\quad \left.\left. + \frac{1}{2}\left(\frac{1}{2\nu} - \frac{1}{2}\right)\left(\frac{1}{2\nu} - \frac{1}{2}\right)\frac{\nu}{1+\nu} + \frac{3}{16}\right)\left(\frac{f}{2\pi}\right)^{1-\nu} \nu^{-2\nu} a_x^2 \frac{l_0^2 N^{2\nu}}{R_x^2} \right\}
\end{aligned}
\tag{B.8}
$$

for the free energy of the whole star polymer. It is easy to show analogously that the expansion also holds for spheres and cylinders that are curved away from the membrane. Comparison of the free energy with Eq. (5.5) gives the scaling relations for a_{sp}/f, a_κ/f and $\bar{a}_\kappa/f$:

$$
\begin{aligned}
\frac{a_{sp}}{f} &= -\frac{1}{4}\left(\left(\frac{1}{2\nu} - \frac{1}{2}\right)\frac{\nu}{1+\nu} + \frac{1}{2}\right) a_s \left(\frac{f}{2\pi}\right)^{1-\frac{\nu}{2}} \\
\frac{a_\kappa}{f} &= \left(\left(\frac{1}{2\nu} - \frac{1}{2}\right)\left(\frac{3}{2} - \frac{1}{2\nu}\right)\frac{\nu}{1+2\nu} + \left(\frac{1}{2\nu} - \frac{1}{2}\right)^2 \frac{\nu(1+2\nu)}{(1+\nu)^2}\right. \\
&\quad \left. + \left(\frac{1}{2\nu} - \frac{1}{2}\right)\frac{\nu}{1+\nu} + \frac{3}{8}\right)\nu^{-2\nu}\left(\frac{f}{2\pi}\right)^{\frac{3}{2}-\nu} a_c^2 \\
\frac{\bar{a}_\kappa}{f} &= 0 \tag{B.9}
\end{aligned}
$$

Appendix C

Analytical calculation of membrane observables

Observables of the pure 2D membrane system in Monge representation with small fluctuation amplitudes can be calculated analytically. The most accurate calculation seems to be a continuum model, but to compare with the simulation results a grid model is needed. Continuum as well as grid model employ the representation of the height field in Fourier space.

Continuum model

The membrane is represented in real space by a height field $h(x)$. This corresponds to an amplitude

$$H(\mathbf{q}) = \frac{1}{2\pi} \int_{-\infty}^{\infty} d\mathbf{x}\, h(\mathbf{x}) \exp\left(-i\mathbf{q} \cdot \mathbf{x}\right) \tag{C.1}$$

in Fourier space and the backwards transformation is given by

$$h(\mathbf{x}) = \frac{1}{(2\pi)^2} \int_{-\infty}^{\infty} d\mathbf{q}\, H(\mathbf{q}) \exp\left(\mathbf{q} \cdot \mathbf{x}\right) \tag{C.2}$$

for two-dimensional vectors $\mathbf{q}$ and $\mathbf{x}$. The membrane Hamiltonian

$$\mathcal{H} = \frac{1}{2} \int_{-\infty}^{\infty} d\mathbf{x}\, \kappa\, \left(\nabla^2 h\left(\mathbf{x}\right)\right)^2 \tag{C.3}$$

thus reads[1]:

$$\mathcal{H} = \frac{\kappa}{2} \int_{-\infty}^{\infty} d\mathbf{q} \int_{-\infty}^{\infty} d\mathbf{q}'\, \mathbf{q}^2 \mathbf{q}'^2\, H(\mathbf{q})H(-\mathbf{q}')\delta(\mathbf{q} + \mathbf{q}') \tag{C.5}$$

---

[1]

$$\delta(x) = \frac{1}{(2\pi)^2} \int_{-\infty}^{\infty} d\mathbf{t} \exp\left(i\mathbf{x} \cdot \mathbf{t}\right) \qquad (2D) \tag{C.4}$$

Using the equipartition theorem [186], one gets for the ensemble average:

$$\frac{\kappa}{2}\mathbf{q}^2\mathbf{q'}^2\left\langle H(\mathbf{q})H(-\mathbf{q'})\right\rangle_c = \frac{1}{2}k_B T\delta(\mathbf{q}+\mathbf{q'}) \tag{C.6}$$

The mean squared deviations of $h(\mathbf{x})$ from the average membrane height can be calculated using polar coordinates and taking into account for the physical restrictions of the model. The system size is given by L_{max} and the molecular length scale is a_{mol}. They determine the range of the integral in $|q|$ to $[2\pi/L_{max}, 2\pi/a_{mol}]$.

$$
\begin{aligned}
\left\langle h^2\left(\mathbf{x}\right)\right\rangle_c &= \frac{1}{(2\pi)^2}\int_\infty^\infty d\mathbf{q}\int_\infty^\infty d\mathbf{q'}\,\left\langle H(\mathbf{q})H(-\mathbf{q'})\right\rangle_c \exp\left[i\left(\mathbf{q}+\mathbf{q'}\right)\cdot\mathbf{x}\right] \\
&= \frac{1}{(2\pi)^2}\int_\infty^\infty d\mathbf{q}\,\frac{1}{\kappa\mathbf{q}^4} \\
&= \frac{1}{(2\pi)^2}\int_0^{2\pi\kappa}d\phi\int_0^\infty dq\frac{q}{q^4} \\
&\approx \frac{1}{2\pi\kappa}\int_{2\pi/L_{max}}^{2\pi/a_{mol}}\frac{dq}{q^3} \\
&\approx \frac{1}{16\pi^3}\frac{L_{max}^2}{\kappa} \tag{C.7}
\end{aligned}
$$

In a similar calculation, $\left\langle\left(\nabla h\left(x\right)\right)^2\right\rangle_c$ evaluates to:

$$\left\langle\left(\nabla h\left(x\right)\right)^2\right\rangle_c \approx \frac{1}{2\pi\kappa}\ln\left(\frac{L_{max}}{a_{mol}}\right) \tag{C.8}$$

Grid model

In this section, the discretised membrane model with periodic boundary conditions, i. e. $h(\mathbf{x}+L a,\mathbf{y}+L a)=h(\mathbf{x},\mathbf{y})$, and discretisation length 1 will be discussed. The Fourier transformation of the height field is given by

$$H_{n_x,n_y} = \frac{1}{L}\sum_{k_x=0}^{L-1}\sum_{k_y=0}^{L-1}h_{k_x,k_y}\exp\left[-2\pi i\left(k_x n_x + k_y n_y\right)/L\right] \tag{C.9}$$

and the reverse transformation reads

$$h_{k_x,k_y} = \frac{1}{L}\sum_{n_x=0}^{L-1}\sum_{n_y=0}^{L-1}H_{n_x,n_y}\exp\left[+2\pi i\left(k_x n_x + k_y n_y\right)/L\right] \tag{C.10}$$

for a square grid of size $L \times L$ and $n_x, n_y, k_x, k_y \in \{0, 1, ..., L-1\}$. The Hamiltonian becomes (compare Eq. (4.6))[2]:

$$
\begin{aligned}
\mathcal{H} &= \frac{\kappa}{2} \sum_{j,k=1}^{L-1} \left(h_{j+1,k} + h_{j-1,k} + h_{j,k+1} + h_{j,k-1} - 4h_{j,k} \right) \\
&= 2\kappa \sum_{l,m=0}^{L-1} H_{l,m} H_{-l,-m} \left[\cos\left(\frac{2\pi m}{L}\right) + \cos\left(\frac{2\pi l}{L}\right) - 2 \right]^2 \quad \text{(C.12)}
\end{aligned}
$$

The equipartition theorem gives[3]:

$$
\langle H_{l,m} H_{l',m'} \rangle_c = \frac{\delta_{l,l'} \delta_{m,m'}}{4\kappa} \left[\cos\left(\frac{2\pi m}{L}\right) + \cos\left(\frac{2\pi l}{L}\right) - 2 \right]^{-2} \quad \text{(C.13)}
$$

We get the observables:

$$
\begin{aligned}
\left\langle \sum_{j,k=1}^{L} (\nabla h_{j,k})^2 \right\rangle_c &= \frac{2}{L^2} \sum_{l,m=0;(l,m)\neq 0}^{L-1} < H_{l,m} H_{-l,-m} >_c \left\{ \left(1 - \cos\left(\frac{2\pi l}{L}\right) \right) \right. \\
&\left. + \left(1 - \cos\left(\frac{2\pi m}{L}\right) \right) \right\} \quad \text{(C.14)}
\end{aligned}
$$

$$
\left\langle \sum_{j,k=1}^{L} \left(h_{j,k} - \bar{h} \right)^2 \right\rangle_c = \frac{1}{L^2} \sum_{l,m=0;(l,m)\neq 0}^{L-1} < H_{l,m} H_{-l,-m} >_c \quad \text{(C.15)}
$$

---

[2]
$$
\delta_{m_x,m_x'} \delta_{m_y,m_y'} = \frac{1}{L^2} \sum_{t_x,t_y=0}^{L-1} \exp\left[\frac{2\pi i}{L} \left\{ (m_x - m_x') t_x + (m_y - m_y') t_y \right\} \right] \quad \text{(C.11)}
$$

[3]As $h_{j,k}$ consists of real numbers, $< H_{l,m} H_{-l,-m} > = < H_{l,m} H_{l,m}^* >$.

Appendix D

Free energy functions

Simple free energy functions might be used to calculate phase diagrams, based on the effective membrane curvature elastic constants, compare [278]. The basic variables of a phase diagram are the amphiphile concentration ϕ and the ratio of diblock-copolymer to amphiphile δ_p^2. We start with membrane-curvature expressions and rewrite the equations in terms of ϕ and δ_p^2.

Microemulsion phase

At vanishing spontaneous curvature, the microemulsion phase can be modeled by a minimal surface with $c_1 + c_2 = 0$, but $c_1 = -c_2 \neq 0$ [279]. The curvature Hamiltonian reduces to the $\bar{\kappa}$ term:

$$\mathcal{H} = \int dS \, \bar{\kappa} c_1 c_2 \tag{D.1}$$

The curvatures are inverse proportional to the typical system length scale and are proportional to the amphiphile concentration ϕ. As $c_1 = -c_2$, $c_1 c_2 < 0$. The integration over the whole interfacial area divided by the volume is proportional to the amphiphile concentration ϕ. We obtain

$$\mathcal{F}_{\mu e} = -c_{\mu e} \phi^3 \quad \bar{\kappa} \tag{D.2}$$

with $c_{\mu e} > 0$.

Lamellar phase

The lamellar phase is characterised by the bending rigidity κ of the membrane. The free energy density of a membrane confined between two parallel walls reads

$$\Delta \mathcal{F}_{walls} = c_1 \frac{(k_B T)^2}{\kappa} \xi^{-2} \tag{D.3}$$

where ξ is the length scale on which the fluctuations are analysed [279]. The free energy density per volume goes like $\Delta \mathcal{F}/\xi$ due to the membrane periodicity. The free energy density is given by

$$\Delta \mathcal{F}_{lam} = c_1 \frac{(k_B T)^2}{\kappa} \xi^{-3} \tag{D.4}$$

and connected with the concentration by a proportionality constant $c_{lam} > 0$

$$\Delta \mathcal{F}_{lam} = c_{lam} c_\infty \frac{(k_B T)^2}{\kappa} \phi^{-3} \tag{D.5}$$

with a different prefactor $c_\infty = 0.106$, if the membrane is confined by other membranes instead of walls.

Renormalisation due to fluctuations on smaller length scales

Fluctuations on smaller length scales than ξ should be taken into account by renormalisation of κ and $\bar{\kappa}$ (compare Eq. 2.5; see [278]). A lower cutoff a_{cut} is approximately the molecular size.

$$\kappa_R(\xi) = \kappa(\xi) - 3 \ln \left(\frac{\xi}{a_{cut}} \right)$$

$$\bar{\kappa}_R(\xi) = \bar{\kappa}(\xi) + \frac{10}{3} \ln \left(\frac{\xi}{a_{cut}} \right) \tag{D.6}$$

The polymer effect

The polymer effects on the membrane curvature constants are given by

$$\kappa_{eff} = \kappa + a_\kappa(d)\, \sigma \left(R_{e,w}^2 + R_{e,o}^2 \right)$$

$$\bar{\kappa}_{eff} = \bar{\kappa} + \bar{a}_\kappa(d)\, \sigma \left(R_{e,w}^2 + R_{e,o}^2 \right) \tag{D.7}$$

where $a_\kappa(\infty) = k_B T \left(1 + \frac{\pi}{2} \right)/12$, $\bar{a}_\kappa(\infty) = k_B T/6$ and the root mean squared end-to-end radii $R_{e,o}$ and $R_{e,w}$ of the oil and the water part respectively (compare Eq. 3.4). The area density of the polymers σ can be replaced by the δ_p^2, again introducing a proportionality factor which will be neglected in the following.

In the case of the lamellar phase we assume that the polymer renormalises the bilayer thickness in addition to the changes of the membrane's curvature elastic constants. This changes the membrane free energy expression to

$$\Delta \mathcal{F}_{lam} = c_{lam} c_\infty \frac{(k_B T)^2}{\kappa} \phi \left(\frac{1}{\phi} - \delta \right)^{-2} \tag{D.8}$$

The additional thickness can be estimated to be proportional to the radius of gyration and the amount of polymer to be $\delta = \delta_p^2(R_{e,o} + R_{e,w})/\sqrt{6}$.

Summary

Finally, we end up with a set of equations which can be used to calculate the phase diagrams:

- free energy of lamellar phase with renormalisation

$$F_{lam} = \frac{0.106\,\phi^3}{\kappa + 3\,\ln(\phi)} \tag{D.9}$$

- free energy of lamellar phase with renormalisation and polymer effect

$$
\begin{aligned}
F_{lam,p} \;=\;& 0.106\,\phi \\
& / \left[\kappa + a_\kappa(d)\delta_p^2(R_{e,o}^2 + R_{e,w}^2) + 3\,\ln(\phi)\right] \\
& / \left[1/\phi - (R_{e,o} + R_{e,w})\delta_p^2/\sqrt{6}\right]^2
\end{aligned} \tag{D.10}
$$

- free energy of microemulsion phase with renormalisation

$$F_{\mu e} = -\phi^3\left(\bar{\kappa} - \frac{10}{3}\ln(\phi)\right) \tag{D.11}$$

- free energy of microemulsion phase with renormalisation and polymer effect

$$F_{\mu e,p} = -\phi^3\left(\bar{\kappa} + \delta_p^2\bar{a}_\kappa(d)\left(R_{e,o}^2 + R_{e,w}^2\right) - \frac{10}{3}\ln(\phi)\right) \tag{D.12}$$

Bibliography

[1] K. H. Meyer, G. v. Susich, and E. Valko, *Die elastischen Eigenschaften der organischen Hochpolymeren und ihre kinetische Deutung*, Kolloid-Z. **59**, 208 (1932).

[2] E. Guth and H. Mark, *Zur innermolekularen Statistik, insbesondere bei Kettenmolekülen I*, Monatshefte für Chemie **65**, 93 (1934).

[3] W. Kuhn, *Über die Gestalt fadenförmiger Moleküle in Lösungen*, Kolloid-Z. **68**, 2 (1934).

[4] W. Kuhn, *Beziehungen zwischen Molekülgröße, statistischer Molekülgestalt und den elastischen Eigenschaften hochpolymerer Stoffe*, Kolloid-Z. **76**, 258 (1936).

[5] W. Kuhn and F. Grün, *Beziehungen zwischen elastischen Konstanten und Dehnungsdoppelbrechung hochelastischer Stoffe*, Kolloid-Z. **101**, 248 (1942).

[6] W. J. C. Orr, *Statistical Treatment of Polymer Solutions at infinite Dilution*, Trans. Faraday Soc. **43**, 12 (1947).

[7] L. Peliti and S. Leibler, *Effects of Thermal Fluctuations on Systems with Small Surface Tension*, Phys. Rev. Lett. **54**, 1690 (1985).

[8] N. K. Adam and D. G. Stevenson, Endeavour XII **45**, 25 (1953).

[9] B. Jakobs, *Amphiphile Blockcopolymere als 'Efficiency Booster' für Tenside: Entdeckung und Aufklärung des Effekts*, PhD thesis, Universität zu Köln, 2001.

[10] H. Endo, *Small Angle Neutron Scattering Investigation on the Emulsification Efficiency of Amphiphilic Block Copolymer in Microemulsions*, PhD thesis, Westfälische Wilhelms-Universität Münster, 2001.

[11] M. Mihailescu, *A study of the structural and dynamical properties of microemulsions with amphiphilic block-copolymers*, PhD thesis, Westfälische Wilhelms-Universität Münster, 2001.

[12] B. Jakobs et al., *Amphiphilic Block Copolymers as Efficiency Boosters for Microemulsions*, Langmuir **15**, 6707 (1999).

[13] H. Endo et al., *Membrane Decoration by Amphiphilic Block Copolymers in Bicontinuous Microemulsions*, Phys. Rev. Lett. **85**, 102 (2000).

[14] H. Endo et al., *Effect of amphiphilic block copolymers on the structure and phase behavior of oil-water-surfactant mixtures*, J. Chem. Phys. **115**, 580 (2001).

[15] M. Mihailescu et al., *Dynamics of bicontinuous microemulsion phases with and without amphiphilic block-copolymers*, J. Chem. Phys. **115**, 9563 (2001).

[16] G. Gompper et al., *Measuring bending rigidity and spatial renormalization in bicontinuous microemulsions*, Europhysics Letters **56**, 683 (2001).

[17] C. Stubenrauch, C. Frank, R. Strey, D. Burgemeister, and C. Schmidt, *Lyotropic Mesophases Next to Highly Efficient Microemulsions: A ^2H NMR Study*, Langmuir **18**, 5027 (2002).

[18] H. Endo et al., *Amphiphilic block compolymers as efficiency boosters in microemulsions: a SANS investigation of the role of polymers*, Appl. Phys. A **74**, S392 (2002).

[19] M. Mihailescu et al., *Neutron spin-echo investigation of the microemulsion dynamics in bicontinuous, lamellar and droplet phases*, Appl. Phys. A **74**, S414 (2002).

[20] H. Endo, J. Allgaier, and D. Richter, private communication.

[21] W. Jahn and R. Strey, *Microstructure of microemulsions by freeze fracture microscopy*, J. Phys. Chem. **92**, 2294 (1988).

[22] R. Strey, private communication.

[23] H. Endo and G. Gompper, private communication.

[24] W. D. Bancroft and C. W. Tucker, *Gibbs on emulsification*, J. Phys. Chem. **31**, 1681 (1927).

[25] T. P. Hoar and J. H. Schulman, *Transparent Water-in-Oil Dispersions: the Oleopathic Hydro-Micelle*, Nature **152**, 102 (1943).

[26] J. H. Schulman and T. S. McRoberts, *On the structure of transparent water and oil dispersions (solubilised oils)*, Trans. Faraday Soc. **42B**, 165 (1946).

106

[27] H. Saito and K. Shinoda, *The Solubilization of Hydrocarbons in Aqueous Solutions of Nonionic Surfactants*, Journal of Colloid and Interface Science **24**, 10 (1967).

[28] L. E. Scriven, *Equilibrium bicontinuous structure*, Nature **263**, 123 (1976).

[29] R. Ober and C. Taupin, *Interactions and Aggregation in Microemulsions. A Small-Angle Neutron Scattering Study*, J. Phys. Chem. **84**, 2418 (1980).

[30] M. Teubner and R. Strey, *Origin of the scattering peak in microemulsions*, J. Chem. Phys. **87**, 3195 (1987).

[31] S. Kline, *http://www.ncnr.nist.gov/resources/sansmodels/TeubnerStrey.html*, National Institute of Standards and Technology (October 14th, 2003).

[32] K.-V. Schubert, R. Strey, S. R. Kline, and E. W. Kaler, *Small angle neutron scattering near Lifshitz lines: Transition from weakly structured mixtures to microemulsions*, J. Chem. Phys. **101**, 5343 (1994).

[33] M. Gradzielski, D. Langevin, T. Sottmann, and R. Strey, *Small angle neutron scattering near the wetting transition: Discrimination of microemulsions from weakly structured mixtures*, J. Chem. Phys. **104**, 3782 (1996).

[34] T. Sottmann, R. Strey, and S.-H. Chen., *A small-angle neutron scattering study of nonionic surfactant molecules at the water-oil interface: Area per molecule, microemulsion size and rigidity*, J. Chem. Phys. **106**, 6483 (1997).

[35] N. F. Berk, *Scattering Properties of a Model Bicontinuous Structure with a Well Defined Length Scale*, Phys. Rev. Lett. **58**, 2718 (1987).

[36] N. F. Berk, *Scattering properties of the leveled-wave model of random morphologies*, Phys. Rev. A **44**, 5069 (1991).

[37] G. Gompper and M. Schick, *Scattering from internal interfaces in microemulsion and sponge phases*, Phys. Rev. E **49**, 1478 (1994).

[38] R. Granek and M. E. Cates, *Sponge phase of surfactant solutions: An unusual dynamic structure factor*, Phys. Rev. A **46**, 3319 (1992).

[39] G. Gompper and M. Hennes, *Dynamic Structure Factor of Microemulsions*, Phys. Rev. Lett. **73**, 1114 (1994).

[40] A. G. Zilman and R. Granek, *Undulations and Dynamic Structure Factor of Membranes*, Phys. Rev. Lett. **77**, 4788 (1996).

[41] M. Nonomura and T. Ohta, *Decay rate of concentration fluctuations in microemulsions*, J. Chem. Phys. **110**, 7516 (1999).

[42] J. S. Huang, S. T. Milner, B. Farago, and D. Richter, *Study of Dynamics of Microemulsion Droplets by Neutron Spin-Echo Spectrocopy*, Phys. Rev. Lett. **59**, 2600 (1987).

[43] P. Pieruschka and S. Marcelja, *Statistical mechanics of random bicontinuous phases*, J. Phys. II France **2**, 235 (1992).

[44] H. Leitao, A. M. Somoza, M. M. T. d. Gama, T. Sottmann, and R. Strey, *Scaling of the interfacial tension of microemulsions: A phenomenological description*, J. Chem. Phys. **105**, 2875 (1996).

[45] M. Gradzielski, D. Langevin, T. Sottmann, and R. Strey, *Droplet microemulsions at the emulsification boundary: The influence of the surfactant structure on the constants of the amphiphilic film*, J. Chem. Phys. **106**, 8232 (1997).

[46] T. Sottmann and R. Strey, *Ultralow interfacial tensions in water-n-alkane-surfactant systems*, J. Chem. Phys. **106**, 8606 (1997).

[47] T. Hellweg and D. Langevin, *Bending elasticity of the surfactant monolayer in droplet microemulsions: Determination by a combination of dynamic light scattering and neutron spin-echo spectroscopy*, Phys. Rev. E **57**, 6825 (1998).

[48] W. Helfrich, *Effect of thermal undulations on the rigidity of fluid membranes and interfaces*, J. Phys. France **46**, 1263 (1985).

[49] W. Helfrich, *Stiffening of fluid membranes and entropy loss of membrane closure: Two effects of thermal undulations*, Eur. Phys. J. B **1**, 481 (1998).

[50] G. Gompper and D. M. Kroll, *Membranes with Fluctuating Topology: Monte Carlo Simulations*, Phys. Rev. Lett. **11**, 2284 (1998).

[51] M. Maugey and A.-M. Bellocq, *Effect of Added Salt and Poly(ethylene glycol) on the Phase Behavior of a Balanced AOT-Water-Oil System*, Langmuir **15**, 8602 (1999).

[52] A. Holmberg, P. Hansson, L. Piculell, and P. Linse, *Effects of an Amphiphilic Graft Copolymer on an Oil-Continuous Microemulsion. Viscosity, Droplet Size, and Phase Behavior*, J. Phys. Chem. B **103**, 10807 (1999).

[53] N. Gov, A. G. Zilman, and S. Safran, *Cytoskeleton Confinement and Tension of Red Blood Cell Membranes*, Phys. Rev. Lett. **90**, 228101 (2003).

[54] E. Evans and W. Rawicz, *Elasticity of "'Fuzzy"' Biomembranes*, Phys. Rev. Lett. **79**, 2379 (1997).

[55] W. Rawicz, K. C. Olbrich, T. McIntosh, D. Needham, and E. Evans, *Effect of Chain Length and Unsaturation on Elasticity of Lipid Bilayers*, Biophys. J. **79**, 328 (2000).

[56] J.-B. Fournier, A. Ajdari, and L. Peliti, *Effective-Area Elasticity and Tension of Micromanipulated Membranes*, Phys. Rev. Lett. **86**, 4970 (2001).

[57] T. M. Allen and A. Chonn, *Large unilamellar liposomes with low uptake into the reticuloendothelial system*, FEBS Lett. **223**, 42 (1987).

[58] A. Gabizon and D. Papahadjopoulos, *Liposome formulations with prolonged circulation time in blood and enhanced uptake by tumors*, Proc. Natl. Acad. Sci. USA **85**, 6949 (1988).

[59] D. D. Lasic, F. J. Martin, A. Gabizon, S. K. Huang, and D. Papahadjopoulos, *Sterically stabilized liposomes: a hypothesis on the origin of the extended circulations times*, Biochim. Biophys. Acta **1070**, 187 (1991).

[60] D. D. Lasic, *Sterically Stabilized Vesicles*, Angew. Chem. Int. Ed. Engl. **33**, 1685 (1994).

[61] D. D. Lasic and D. Papahadjopoulos, *Liposomes Revisited*, Science **267**, 1275 (1995).

[62] T. W. Secomb and A. R. Pries, *Mechanics of shear transmission to endothelial cells in blood vessels lined with an endothelial surface layer*, BED-Vol. 50, 2001 Bioengineering Conference; ASME (2001).

[63] T. L. Kuhl, D. E. Leckband, D. D. Lasic, and J. N. Israelachvili, *Modulation of interaction forces between bilayers exposing short-chained ethylene-oxide headgroups*, Biophys. J. **66**, 1479 (1994).

[64] R. Joannic, L. Auvray, and D. D. Lasic, *Monodisperse Vesicles Stabilized by Grafted Polymers*, Phys. Rev. Lett. **78**, 3402 (1997).

[65] A. Schalchli-Plaszczynski and L. Auvray, *Vesicle-to-micelle transition induced by grafted diblock copolymers*, Eur. Phys. J. E **7**, 339 (2002).

[66] G. Massiera, L. Ramos, E. Pitard, and C. Ligoure, *The steric polymer layer of hairy wormlike micelles*, J. Phys.: Condens. Matter **15**, S225 (2003).

[67] E. Melzer, J. Kreuter, and R. Daniels, *Ethylcellulose: a new type of emulsion stabilizer*, Eur. J. Pharm. Biopharm. **56**, 23 (2003).

[68] R. Daniels, private communication.

[69] S. Rimpler and R. Daniels, *In Situ-Particle Sizing in Highly Concentrated Oil-in-Water Emulsions*, Pharmaceutical Technology Europe **8**, 72 (1996).

[70] E. Melzer, *Herstellung und physikochemische Charakterisierung von W/O-Emulsionen unter Verwendung von Ethylcellulose als nichtionischem Polymeremulgator*, PhD thesis, Technische Universität Carolo-Wilhelmina zu Braunschweig, 2000.

[71] C. Wollenweber, A. V. Makievsky, R. Miller, and R. Daniels, *Adsorption of hydroxypropyl methylcellulose at the liquid/liquid interface and the effect on the emulsion stability*, Colloids Surf. **172**, 91 (2000).

[72] M. B. Schulz and R. Daniels, *Hydroxypropylmethylcellulose (HPMC) as emulsifier for submicron emulsions: influence of molecular weight and substitution type on the droplet size after homogenization*, Eur. J. Pharm. Biopharm. **49**, 231 (2000).

[73] R. Daniels, *Neuartige Gelsysteme*, DermoTopics **2** (2002).

[74] R. J. Hunter, *Foundations of colloid science*, volume 1, chapter 8, pages 450–493, Oxford university press, 1st edition, 1992.

[75] W. Helfrich, *Steric Interaction of Fluid Membranes in Multilayer Systems*, Z. Naturforsch. **33a**, 305 (1978).

[76] J. Als-Nielsen et al., *Observation of algebraic decay of positional order in a smectic liquid crystal*, Phys. Rev. B **22**, 312 (1980).

[77] C. R. Safinya et al., *Steric Interactions in a Model Multimembrane System: A Synchrotron X-Ray Study*, Phys. Rev. Lett. **57**, 2718 (1986).

[78] W. Janke and H. Kleinert, *Fluctuation Pressure of a Stack of Membranes*, Phys. Rev. Lett. **58**, 144 (1987).

[79] W. Janke, H. Kleinert, and M. Meinhard, *Monte Carlo study of a stack of self-avoiding surfaces with extrinsic curvature stiffness*, Phys. Lett. B **217**, 525 (1989).

[80] G. Gompper and D. M. Kroll, *Steric Interactions in Multimembrane Systems: a Monte Carlo Study*, Europhysics Letters **9**, 59 (1989).

[81] H. Kleinert, *Fluctuation pressure of membrane between walls*, Phys. Lett. A **257**, 269 (1999).

[82] M. Bachmann, H. Kleinert, and A. Pelster, *Strong-coupling calculation of fluctuation pressure of a membrane between walls*, Phys. Lett. A **261**, 127 (1999).

[83] B. Kastening, *Fluctuation pressure of a membrane between walls through five loops*, Phys. Rev. E **66**, 061102 (2002).

[84] P. Kekicheff, B. Cabane, and M. Rawiso, *Macromolecules Dissolved in a Lamellar Lyotropic Mesophase*, Journal of Colloid and Interface Science **102**, 51 (1984).

[85] C. Ligoure, G. Bouglet, and G. Porte, *Polymer Induced Phase Separation in Lyotropic Smectics*, Phys. Rev. Lett. **71**, 3600 (1993).

[86] T. Zemb, D. Gazeau, M. Dubois, and T. Gulik-Krzywicki, *Critical Behaviour of Lyotropic Liquid Crystals*, Europhys. Lett. **21**, 759 (1993).

[87] M.-F. Ficheux, A.-M. Bellocq, and F. Nallet, *Experimental Study of a Lyotropic Lamellar Phase Swollen with Polymer Solutions*, J. Phys. II France **5**, 823 (1995).

[88] I. Javierre, A. M. Bellocq, and F. Nallet, *Effect of Confinement of a Polymer on the Phase Behavior of Ternary and Quaternary Lyotropic Mixtures*, Langmuir **17**, 5417 (2001).

[89] C. Ligoure, G. Bouglet, G. Porte, and O. Diat, *Smectic Compressibility of Polymer-Containing Lyotropic Lamellar Phases: An Experimental Tool to Study the Thermodynamics of Polymer Confinement*, J. Phys. II France **7**, 473 (1997).

[90] J. T. Brooks, C. M. Marques, and M. E. Cates, *Role of Adsorbed Polymer in Bilayer Elasticity*, Europhys. Lett. **14**, 713 (1991).

[91] J. T. Brooks, C. M. Marques, and M. E. Cates, *The effect of adsorbed polymer on the elastic moduli of surfactant bilayers*, J. Phys. II (France) **1**, 673 (1991).

[92] J. T. Brooks and M. E. Cates, *The role of added polymer in dilute lamellar surfactant phases*, J. Chem. Phys. **99**, 5467 (1993).

[93] G. Bouglet and C. Ligoure, *Polymer-mediated interactions of fluid membranes in a lyotropic lamellar phase: a small angle X-ray and neutron scattering study*, Eur. Phys. J. B **9**, 137 (1999).

[94] H. E. Warriner, S. H. J. Idziak, N. L. Slack, P. Davidson, and C. R. Safinya, *Lamellar Biogels: Fluid-Membrane-Based Hydrogels Containing Polymer Lipids*, Science **271**, 969 (1996).

[95] H. E. Warriner et al., *The Influence of Polymer Molecular Weight in Lamellar Gels Based on PEG-Lipids*, Biophys. J. **75**, 272 (1998).

[96] F. Castro-Roman, G. Porte, and C. Ligoure, *Renormalization of Helfrich's Interactions between Fluid Membranes in a Lyotropic Lamellar Phase by Addition of Amphiphilic Copolymers*, Phys. Rev. Lett. **82**, 109 (1999).

[97] F. Castro-Roman, P. Gr'egoire, and C. Ligoure, *Smectic Phase of Fluid Membranes Decorated by Amphiphilic Copolymers*, Langmuir **17**, 5045 (2001).

[98] Y. Yang, R. Prudhomme, K. M. McGrath, P. Richetti, and C. M. Marques, *Confinement of Polysoaps in Membrane Lyotropic Phases*, Phys. Rev. Lett. **80**, 2729 (1998).

[99] G. Bouglet, C. Ligoure, A. M. Bellocq, E. Dufourc, and G. Mosser, *Bending moduli of a nonadsorbing-polymer-containing lyotropic lamellar phase: An experimental study*, Phys. Rev. E **57**, 834 (1998).

[100] N. Tsapis, W. Urbach, and R. Ober, *Dramatic rigidification of a peptide-decorated lamellar phase*, Phys. Rev. E **63**, 041903 (2001).

[101] R. R. Netz and P. Pincus, *Inhomogeneous fluid membranes: Segregation, ordering, and effective rigidity*, Phys. Rev. E **52**, 4114 (1995).

[102] C.-M. Chen, *Theory of the bending rigidity of protein-coated lipid membranes*, Physica A **281**, 41 (2000).

[103] N. Taulier et al., *Behavior of a Reverse Lamellar Phase in the Presence of Low Molecular Weight Triblock Molecules*, Langmuir **18**, 68 (2002).

[104] E. Z. Radlinska et al., *Polymer Confinement in Surfactant Bilayers of a Lyotropic Lamellar Phase*, Phys. Rev. Lett. **74**, 4237 (1995).

[105] E. Z. Radlinska et al., *Modification of the Lamellar Phase in $C_{12}E_5$/Water System by a Random Hydrophilic-Hydrophobic Polyelectrolyte*, J. Phys. II France **7**, 1393 (1997).

[106] L. Porcar, C. Ligoure, and J. Marignan, *Layer Compression Modulus of Electrostatically Stabilized Lyotropic Lamellar Phases Revisited: Application to the Quantitative Analysis of a Polymer Induced Critical SmA-SmA Phase Separation*, J. Phys. II France **7**, 493 (1997).

[107] V. Frette et al., *Coiling of Cylindrical Membrane Stacks with Anchored Polymers*, Phys. Rev. Lett. **83**, 2465 (1999).

[108] W. Meier, *Polymer Networks with Lamellar Structure*, Macromolecules **31**, 2212 (1998).

[109] K. M. Palmer, M. Goulian, and P. Pincus, *Fluctuation-induced forces in stacked fluid membranes*, J. Phys. II (France) **4**, 805 (1994).

[110] E. M. Blokhuis, K. I. Skau, and J. B. Avalos, *Free energy formalims for polymer adsorption: Self-consistent field theory for weak adsorption*, J. Chem. Phys. **119**, 3483 (2003).

112

[111] P. B. Canham, *The Minimum Energy of Bending as a Possible Explanation of the Biconcave Shape of the Human Red Blood Cell*, J. Theoret. Biol. **26**, 61 (1970).

[112] W. Helfrich, *Elastic Properties of Lipid Bilayers: Theory and Possible Experiments*, Z. Naturforsch. **28 c**, 693 (1973).

[113] E. A. Evans, *Bending resistance and chemically induced moments in membrane bilayers*, Biophys. J. **14**, 923 (1974).

[114] R. Cantor, *Nonionic Diblock Copolymers as Surfactants between Immiscible Solvents*, Macromolecules **14**, 1186 (1981).

[115] F. David, Geometry and field theory of random surfaces and membranes, in *Statistical Mechanics of Membranes and Surfaces*, edited by S. W. D. Nelson, T. Piran, pages 157–223, World Scientific, Singapore, 1989.

[116] R. Lipowsky, *Adhesion of Membranes via Anchored Stickers*, Phys. Rev. Lett. **77**, 1652 (1996).

[117] R. Lipowsky, *Flexible membranes with anchored polymers*, Colloids and Surfaces A: Physicochemical and Engineering Aspects **128**, 255 (1997).

[118] K. Yaman, P. Pincus, and C. M. Marques, *Membranes in Rod Solutions: A System with Spontaneously Broken Symmetry*, Phys. Rev. Lett. **78**, 4514 (1997).

[119] K. Yaman, M. Jeng, P. Pincus, C. Jeppesen, and C. M. Marques, *Rods near curved surfaces and in curved boxes*, Physica A **247**, 159 (1997).

[120] A. Hanke, E. Eisenriegler, and S. Dietrich, *Polymer depletion effects near mesoscopic particles*, Phys. Rev. E **59**, 6853 (1999).

[121] Y. W. Kim and W. Sung, *Membrane curvature induced by polymer adsorption*, Phys. Rev. E. **63**, 041910 (2001).

[122] R. Lipowsky, *Bending of Membranes by Anchored Polymers*, Europhys. Lett. **30**, 197 (1995).

[123] C. Hiergeist and R. Lipowsky, *Elastic Properties of Polymer-Decorated Membranes*, J. Phys. II France **6**, 1465 (1996).

[124] E. Eisenriegler, A. Hanke, and S. Dietrich, *Polymers interacting with spherical and rodlike particles*, Phys. Rev. E **54**, 1134 (1996).

[125] M. Müller and G. Gompper, *Elastic properties of polymer interfaces: Aggregation of pure diblock, mixed diblock and triblock copolymers*, Phys. Rev. E **66**, 041805 (2002).

[126] C. Hiergeist, V. A. Indrani, and R. Lipowsky, *Membranes with anchored polymers at the adsorption transition*, Europhys. Lett. **36**, 491 (1996).

[127] R. Podgornik, *Polymer-Boundary Surface Interactions and Bilayer Curvature Elasticity*, Europhys. Lett. **21**, 245 (1993).

[128] F. Clement and J.-F. Joanny, *Curvature Elasticity of an Adsobed Polymer Layer*, J. Phys. II (France) **7**, 973 (1997).

[129] M. Laradji, *Polymer adsorption on fluctuating surfaces*, Europhys. Lett. **47**, 694 (1999).

[130] P. G. d. Gennes, *Interactions between Polymers and Surfactants*, J. Phys. Chem. **94**, 8407 (1990).

[131] T. Garel, M. Kardar, and H. Orland, *Adsorption of Polymers on a Fluctuating Surface*, Europhys. Lett. **29**, 303 (1995).

[132] W. Sung and E. Oh, *Membrane Fluctuation and Polymer Adsorption*, J. Phys II France **6**, 1195 (1996).

[133] M. Breidenich, R. R. Netz, and R. Lipowsky, *Adsorption of polymers anchored to membranes*, Eur. Phys. J. E **5**, 403 (2001).

[134] S. T. Milner and T. A. Witten, *Bending moduli of polymeric surfactant interfaces*, J. Phys. (France) **49**, 1951 (1988).

[135] N. Dan and S. A. Safran, *Spontaneous Curvature of Mixed-Copolymer Bilayers*, Europhys. Lett. **21**, 975 (1993).

[136] G. Porte and C. Ligoure, *Mixed amphiphilic bilayers: Bending elasticity and formation of vesicles*, J. Chem. Phys. **102**, 4290 (1995).

[137] I. Bivas, M. Winterhalter, P. M'el'eard, and P. Bothorel, *Elasticity of bilayers containing PEG lipids*, Europhys. Lett. **41**, 261 (1998).

[138] D. Marsh, *Elastic Constants of Polymer-Grafted Lipid Membranes*, Biophys. J. **61**, 2154 (2001).

[139] M. Laradji, *Elasticity of polymer-anchored membranes*, Europhys. Lett. **60**, 594 (2002).

[140] B. Groh, *Vesicles in solutions of hard rods*, Phys. Rev. E **59**, 5606 (1999).

[141] B. Groh and S. Dietrich, *Fluids of rodlike particles near curved surfaces*, Phys. Rev. E **59**, 4216 (1999).

114

[142] C. S. Hiergeist, *Elastische Eigenschaften Polymer-dekorierter Membranen*, PhD thesis, Universität Potsdam, 1997.

[143] M. Breidenich, R. R. Netz, and R. Lipowsky, *The shape of polymer-decorated membranes*, Europhys. Lett. **49**, 431 (2000).

[144] T. Bickel, C. Marques, and C. Jeppesen, *Grafted polymers are miniaturized pressure tools*, C. R. Acad. Sci. Paris **1**, 661 (2000).

[145] M. Breidenich, *Polymers at Membranes*, PhD thesis, Universität Potsdam, 2000.

[146] T. Bickel, *Interactions polymer-membranes: une approche locale*, PhD thesis, Université Louis Pasteur Strasbourg I, 2001.

[147] T. Bickel, C. Jeppesen, and C. M. Marques, *Local entropic effects of polymers grafted to soft interfaces*, Eur. Phys. J. E **4**, 33 (2001).

[148] F. Brochard and J. F. Lennon, *Frequency spectrum of the flicker phenomenon in erythrocytes*, J. Phys. France **36**, 1035 (1975).

[149] A. R. Evans, M. S. Turner, and P. Sens, *Interactions between proteins bound to biomembranes*, Phys. Rev. E **67**, 041907 (2003).

[150] R. Lipowsky, *The conformation of membranes*, Nature **349**, 475 (1991).

[151] T. Bickel and C. M. Marques, *Scale-dependent rigidity of polymer-ornamented membranes*, Eur. Phys. J. E **9**, 349 (2002).

[152] C. M. Marques and J. B. Fournier, *Deviatoric spontaneous curvature of lipid membranes induced by Siamese macromolecular cosurfactants*, Europhys. Lett. **35**, 361 (1996).

[153] J. B. Fournier, *Nontopological Saddle-Splay and Curvature Instabilities from Anisotropic Membrane Inclusions*, Phys. Rev. Lett. **76**, 4436 (1996).

[154] G. Gompper, J. K. G. Dhont, and D. Richter, *Komplexe Materialien auf mesoskopische Skala*, Phys. Unserer Zeit **34**, 12 (2003).

[155] G. Gompper, J. K. G. Dhont, and D. Richter, *Eine Welt zwischen Fest und Flüssig*, Phys. Unserer Zeit **34**, 19 (2003).

[156] G. Gompper, *Modellierung von Knautschprozessen*, Spektrum der Wissenschaft , 29 (1997).

[157] G. Gompper and D. M. Kroll, *Statistische Physik von Zufallsflächen*, Physikalische Blätter **6**, 557 (1994).

[158] H. E. Stanley, *Scaling, universality, and renormalization: Three pillars of modern critical phenomena*, Rev. Mod. Phys. **71**, S358 (1999).

[159] B. J. Alder and T. E. Wainwright, *Studies in Molecular Dynamics. I. General Method*, J. Chem. Phys. **31**, 459 (1959).

[160] A. Bellemans, J. Orban, and D. V. Belle, *Molecular dynamics of rigid and non-rigid necklaces of hard discs*, Molecular Physics **39**, 781 (1980).

[161] N. Metropolis and S. Ulam, *The Monte Carlo Method*, Journal of the American Statistical Association **44**, 335 (1949).

[162] O. Narayan and A. P. Young, *Convergence of Monte Carlo Simulations to Equilibrium*, arXiv: cond-mat/0008046 (2000).

[163] N. Metropolis, A. W. Rosenbluth, M. N. Rosenbluth, A. H. Teller, and E. Teller, *Equation of State Calculations by Fast Computing Machines*, J. Chem. Phys. **21**, 1087 (1953).

[164] D. P. Landau and K. Binder, *A guide to Monte Carlo Simulations in Statistical Physics*, Cambridge University Press, 2000.

[165] I. Vattulainen, K. Kankaala, J. Saarinen, and T. Ala-Nissila, *A comparative study of some pseudorandom number generators*, Comp. Phys. Comm. **86**, 209 (1995).

[166] F. J. Resende and B. V. Costa, *Using random number generators in Monte Carlo simulations*, Phys. Rev. E **58**, 5183 (1998).

[167] D. Stauffer, F. W. Hehl, V. Winkelmann, and J. G. Zabolitzky, *Computer Simulation and Computer Algebra*, chapter 2, pages 55–81, Springer-Verlag, Heidelberg, 1988.

[168] M. E. J. Newman and G. T. Barkema, *Monte Carlo Methods in Statistical Physics*, chapter 16 and B.5, pages 382–409 and 451–453, Clarendon Press, Oxford, 1999.

[169] M. Luescher, *A portable high-quality random number generator for lattice field theory simulations*, Comp. Phys. Comm. **79**, 100 (1994).

[170] F. James, *RANLUX: A Fortran implementation of the high-quality pseudorandom number generator of Lüscher*, Comp. Phys. Comm. **79**, 111 (1994).

[171] F. James, *RANLUX: a Fortran implementation of the high-quality pseudorandom number generator of Luscher (Erratum)*, Comp. Phys. Comm. **97**, 357 (1996).

[172] K. G. Hamilton and F. James, *Acceleration of RANLUX*, Comp. Phys. Comm. **101**, 241 (1997).

[173] K. G. Hamilton, *Assembler RANLUX for PCs*, Comp. Phys. Comm. **101**, 249 (1997).

[174] L. N. Shchur and P. Butera, *The RANLUX Generator: Resonances in a Random Walk Test*, International Journal of Modern Physics C **9**, 607 (1998).

[175] W. Janke, Statistical analysis of simulations: Data correlations and error estimation, in *Quantum Simulations of Complex Many-Body Systems: From Theory to Algorithms*, edited by J. Grotendorst, D. Marx, and A. Muramatsu, volume 10 of *NIC Series*, pages 423–445, NIC-Directors, Jülich, 2002.

[176] R. M. Servuss, W. Harbich, and W. Helfrich, *Measurement of the curvature-elastic modulus of egg lecithin bilayers*, Biochim. Biophys. Acta **436**, 900 (1976).

[177] F. Brochard, P. G. d. Gennes, and P. Pfeuty, *Surface tension and deformations of membrane structures: Relation to two-dimensional phase transitions*, J. Phys. France **37**, 1099 (1976).

[178] M. B. Schneider, J. T. Jenkins, and W. W. Webb, *Thermal fluctuations of large cylindrical phospholipid vesicles*, Biophys. J. **45**, 891 (1984).

[179] M. B. Schneider, J. T. Jenkins, and W. W. Webb, *Thermal fluctuations of large quasi-spherical bimolecular phospholipid vesicles*, J. Phys. France **45**, 1457 (1984).

[180] A. Zilker, H. Engelhardt, and E. Sackmann, *Dynamic reflection interference contrast (RIC-) microscopy: a new method to study surface excitations of cells and to measure membrane bending elastic moduli*, J. Phys. France **48**, 2139 (1987).

[181] W. K. den Otter and W. J. Briels, *The bending rigidity of an amphiphilic bilayer from equilibrium and nonequilibrium molecular dynamics*, J. Chem. Phys. **118**, 4712 (2003).

[182] C. Loison, private communication.

[183] R. Lipowsky, H.-G. Döbereiner, C. Hiergeist, and V. Indrani, *Membrane curvature induced by polymers and colloids*, Physica A **249**, 536 (1998).

[184] U. Schwarz and G. Gompper, Bicontinuous surfaces in self-assembling amphiphilic systems, in *Lecture Notes in Physics*, edited by K. R. Mecke and D. Stoyan, pages 107–151, Springer, Berlin, 2002.

[185] P. G. d. Gennes and C. Taupin, *Microemulsions and the Flexibility of Oil/Water Interfaces*, J. Phys. Chem. **86**, 2294 (1982).

[186] G. Gompper, Statistical mechanics of membranes, in *Soft Matter: Complex Materials on Mesoscopic Scales*, edited by J. K. G. Dhont, G. Gompper, and D. Richter, chapter B 9, Forschungszentrum Jülich, 2002.

[187] O. Kratky and G. Porod, *Röntgenuntersuchung gelöster Fadenmoleküle*, Recueil **68**, 1106 (1949).

[188] G. Porod, *Zusammenhang zwischen mittlerem Endpunktabstand und Kettenlänge bei Fadenmolekülen*, Monatsh. Chem. **80**, 251 (1949).

[189] P. J. Flory, *Statistical Mechanics of Chain Molecules*, chapter IV.4, page 111, Wiley, New York, 1969.

[190] S. F. Edwards, The configurations and dynamics of the polymer chain, in *Molecular Fluids*, edited by R. Balian and G. Weill, pages 151–208, London, 1973, Gordon and Breach.

[191] E. Loftus and P. J. Gans, *Geometric Properties of Off-Lattice Self-Avoiding Random Walks*, J. Chem. Phys. **49**, 3828 (1968).

[192] D. Kienle, private communication.

[193] S. D. Stellman and P. J. Gans, *Computer Simulation of Polymer Conformation. II. Distribution Function for Polymers with Excluded Volume*, Macromolecules **5**, 720 (1972).

[194] S. D. Stellman and P. J. Gans, *Efficient Computer Simulation of Polymer Conformation. I. Geometric Properties of the Hard-Sphere Model*, Macromolecules **5**, 516 (1972).

[195] K. Pearson, *The Problem of the Random Walk*, Nature **72**, 294 (1905).

[196] E. W. Montroll, *Markoff Chains and Excluded Volume Effect in Polymer Chains*, J. Chem. Phys. **18**, 734 (1950).

[197] C. Domb, *Excluded-Volume Effect for Two- and Three-Dimensional Lattice Models*, J. Chem. Phys. **38**, 2957 (1963).

[198] J. D. Cloizeaux, R. Conte, and G. Jannink, *Swelling of an isolated polymer chain in a solvent*, J. Physique Lett. **46**, L595 (1985).

[199] M. Muthukumar and B. G. Nickel, *Expansion of a polymer chain with excluded volume interaction*, J. Chem. Phys. **86**, 460 (1987).

[200] F. T. Wall, L. A. Hiller (Jr.), and D. J. Wheeler, *Statistical Computation of Mean Dimensions of Macromolecules. I*, J. Chem. Phys. **22**, 1036 (1954).

[201] F. T. Wall, L. A. Hiller (Jr.), and W. F. Atchison, *Statistical Computations of Mean Dimensions of Macromolecules. III*, J. Chem. Phys. **23**, 2314 (1955).

[202] F. T. Wall, L. A. Hiller (Jr.), and W. F. Atchison, *Statistical Computation of Mean Dimensions of Macromolecules. II*, J. Chem. Phys. **23**, 913 (1955).

[203] F. T. Wall, L. A. Hiller (Jr.), and W. F. Atchison, *Statistical Computation of Mean Dimensions of Polymer Molecules. IV*, J. Chem. Phys. **26**, 1742 (1957).

[204] F. T. Wall and J. J. Erpenbeck, *New Method for the Statistical Computation of Polymer Dimensions*, J. Chem. Phys. **30**, 634 (1959).

[205] F. T. Wall and J. J. Erpenbeck, *Statistical Computation of Radii of Gyration and Mean Internal Dimensions of Polymer Molecules*, J. Chem. Phys. **30**, 637 (1959).

[206] F. T. Wall, S. Windwer, and P. J. Gans, *Monte Carlo Procedures for Generation of Nonintersecting Chains*, J. Chem. Phys. **37**, 1461 (1962).

[207] S. Windwer, *Monte Carlo Generation of a Restricted Random Walk and the Excluded-Volume Problem*, J. Chem. Phys. **43**, 115 (1965).

[208] P. J. Gans, *Self-Avoiding Random Walks. I. Simple Properties of Intermediate-Length Walks*, J. Chem. Phys. **42**, 4159 (1965).

[209] D. C. Rapaport, *Molecular dynamics simulation of polymer chains with excluded volume*, J. Phys. A: Math. Gen. **11**, L213 (1978).

[210] M. N. Rosenbluth and A. W. Rosenbluth, *Monte Carlo Calculation of the Average Extension of Molecular Chains*, J. Chem. Phys. **23**, 356 (1955).

[211] M. Lal, *'Monte Carlo' computer simulation of chain molecules*, Molecular Physics **17**, 57 (1969).

[212] B. MacDonald, N. Jan, D. L. Hunter, and M. O. Steinitz, *Polymer conformations through 'wiggling'*, J. Phys. A: Math. Gen. **18**, 2627 (1985).

[213] G. Marsaglia, *Choosing a point from the surface of a sphere*, Ann. math. Stat. 43 **43**, 645 (1972).

[214] M. P. Allen and D. J. Tildesley, *Computer Simulation of Liquids*, chapter G.4, page 349, Oxford University Press, 1st edition, 1987.

[215] N. Madras and A. D. Sokal, *The Pivot Algorithm: A Highly Efficient Monte Carlo Method for the Self-Avoiding Walk*, Journal of Statistical Physics **50**, 109 (1988).

[216] A. J. Barrett and B. C. Benesch, *Direct Monte Carlo measurement of excluded volume for Pearson walks*, J. Chem. Phys. **97**, 9454 (1992).

[217] B. Li, N. Madras, and A. D. Sokal, *Critical Exponents, Hyperscaling, and Universal Amplitude Ratios for Two- and Three-dimensional Self-Avoiding Walks*, J. Stat. Phys. **80**, 661 (1995).

[218] O. F. Olaj, B. Neubauer, and G. Zifferer, *Monte Carlo investigations of dense copolymer systems, 1; Pivot algorithm and pair distribution function*, Macromol. Theory Simul. **7**, 381 (1998).

[219] S. Caraciollo, M. S. Causo, and A. Pelissetto, *End-to-end distribution function for dilute polymers*, J. Chem. Phys. **112**, 7693 (2000).

[220] M. S. Causo, *Cut-and-Permute Algorithm for Self-Avoiding Walks in the Presence of Surfaces*, J. Stat. Phys. **108**, 247 (2002).

[221] K. Kremer and K. Binder, *Monte Carlo Simulations of Lattice Models for Macromolecules*, Comput. Phys. Rep. **7**, 259 (1988).

[222] K. Kremer, Computer simulation of polymers, in *Computer Simulation in Chemical Physics*, edited by M. P. Allen and D. J. Tildesley, NATO ASI Series C, pages 397–459, Dordrecht, 1993, Kluwer Academic Publishers.

[223] L. A. Johnson, A. Monge, and R. A. Friesner, *A hierarchical algorithm for polymer simulations*, J. Chem. Phys. **97**, 9355 (1992).

[224] P. Grassberger, P. Sutter, and L. Schäfer, *Field theoretic and Monte Carlo analysis of the Domb-Joyce model*, J. Phys. A: Math. Gen. **30**, 7039 (1997).

[225] P. Sutter, L. Schäfer, and P. Grassberger, *Applicability of the standard renormalized field theory to the strong coupling regime for the Domb-Joyce model*, Int. J. Mod. Phys. B **12**, 1397 (1998).

[226] P.-G. d. Gennes, *Scaling Concepts in Polymer Physics*, Cornell University Press, Ithaca, 1979.

[227] S. P. Obukhov, *The efficiency of the Flory approximation*, J. Phys. A: Math. Gen. **17**, L965 (1984).

120

[228] D. L. Hunter, N. Jan, and B. MacDonald, *On the correction-to-scaling exponent of linear polymers in two dimensions*, J. Phys. A: Math. Gen. **19**, L543 (1986).

[229] K. Kelly, D. L. Hunter, and N. Jan, *Critical properties of the three-dimensional self-avoiding walk*, J. Phys. A: Math. Gen. **20**, 5029 (1987).

[230] B. G. Nickel, *One-Parameter Recursion Model for Flexible-Chain Polymers*, Macromolecules **24**, 1358 (1991).

[231] E. Eisenriegler, Polymers near surfaces, in *Soft Matter: Complex Materials on Mesoscopic Scales*, edited by J. K. G. Dhont, G. Gompper, and D. Richter, chapter B 10, Forschungszentrum Jülich, 2002.

[232] B. Dünweg, D. Reith, M. Steinhauser, and K. Kremer, *Corrections to scaling in the hydrodynamic properties of dilute polymer solutions*, J. Chem. Phys. **117**, 914 (2002).

[233] M. Bishop, J. H. R. Clarke, and J. J. Freire, *Computer simulation study of the validity of scaling and renormalization group theories for two-dimensional star polymers*, J. Chem. Phys. **98**, 3452 (1993).

[234] M. Bishop, J. H. R. Clarke, and J. J. Freire, *Structure function of linear and star polymers in the small wave vector regime*, J. Chem. Phys. **102**, 5094 (1995).

[235] A. M. Rubio and J. J. Freire, *Monte Carlo Calculation of Second Virial Coefficients for Linear and Star Chains in a Good Solvent*, Macromolecules **29**, 6946 (1996).

[236] P. Romiszowski and A. Sikorski, *Temperature dependance of properties of star-branched polymers: A computer simulation study*, J. Chem. Phys. **109**, 2912 (1998).

[237] L. A. Molina and J. J. Freire, *Monte Carlo Simulation of Many-Chain Star Polymer Solutions*, Macromolecules **32**, 499 (1999).

[238] G. Zifferer, *Monte Carlo simulation of the size and shape of linear and star-branched polymers embedded in the tetrahedral lattice*, Macromol. Theory Simul. **8**, 433 (1999).

[239] F. T. Wall, W. A. Seitz, J. C. Chin, and P. G. de Gennes, *Statistics of self-avoiding walks confined to strips and capillaries*, Proc. Natl. Acad. Sci. USA **75**, 2069 (1978).

[240] M. Aubouy, G. H. Frederickson, P. Pincus, and E. Rapha"el, *End-Tethered Chains in Polymeric Matrices*, Macromolecules **28**, 2979 (1995).

[241] M. Daoud and J. P. Cotton, *Star shaped polymers: a model for the conformation and its concentration dependence*, J. Phys. France **43**, 531 (1982).

[242] P. Pincus, *Excluded Volume Effects and Stretched Polymer Chains*, Macromolecules **9**, 386 (1976).

[243] E. M. Sevick and D. R. M. Williams, *Polymer Brushes as Pressure-Sensitive Automated Microvalves*, Macromolecules **27**, 5285 (1994).

[244] K. Yaman, P. Pincus, F. Solis, and T. A. Witten, *Polymers in Curved Boxes*, Macromolecules **30**, 1173 (1997).

[245] H. N. W. Lekkerkerker, *Contribution of the electric double layer to the curvature elasticity of charged amphiphilic monolayers*, Physica A **159**, 319 (1989).

[246] H. N. W. Lekkerkerker, *The electric contribution to the curvature elastic moduli of charged fluid interfaces*, Physica A **167**, 384 (1990).

[247] T. Auth and G. Gompper, *Self-Avoiding Linear and Star Polymers Anchored to Membranes*, Phys. Rev. E **68**, 051801 (2003).

[248] P. H. Verdier and W. H. Stockmayer, *Monte Carlo Calculations of Polymers in Dilute Solution*, J. Chem. Phys. **36**, 227 (1962).

[249] A. Baumgärtner and K. Binder, *Monte-Carlo studies on the freely jointed polymer-chain with excluded volume interaction*, J. Chem. Phys. **71**, 2541 (1979).

[250] K. Koniaris, *Modelling large Gaussian ring polymers*, J. Chem. Phys. **101**, 731 (1994).

[251] D. W. Sumners and S. G. Whittington, *Knots in self-avoiding walks*, J. Phys. A: Math. Gen. **21**, 1689 (1988).

[252] K. Koniaris and M. Muthukumar, *Knottedness in Ring Polymers*, Phys. Rev. Lett. **66**, 2211 (1991).

[253] R. Metzler, *Localization behaviour in a phenomenological model of three-dimensional knots*, New Journal of Physics **4**, 91.1 (2002).

[254] J. J. Prentis, *Spatial correlations in a self-repelling ring polymer*, J. Chem. Phys. **76**, 1574 (1982).

[255] Y.-d. Chen, *Monte-Carlo study of freely jointed ring polymers. III. The generation of undistorted perfect ring polymers*, J. Chem. Phys. **75**, 5160 (1981).

[256] J. J. Prentis, *Crossover between random and self-avoiding behaviour in a ring polymer*, J. Phys. A: Math. Gen. **17**, 1723 (1984).

[257] M. Bishop and C. J. Saltiel, *Universal properties of linear and ring polymers*, J. Chem. Phys. **89**, 1159 (1988).

[258] A. Y. Grosberg, *Critical Exponents for Random Knots*, Phys. Rev. Lett. **85**, 3858 (2000).

[259] A. Y. Grosberg, private communication.

[260] A. Y. Grosberg, A. Feigel, and Y. Rabin, *Flory-type theory of a knotted ring polymer*, Phys. Rev. E **54**, 6618 (1996).

[261] A. Grosberg and S. Nechaev, *Polymer Topology*, Adv. Pol. Sci. **106**, 1 (1993).

[262] A. F. Xie and S. Granick, *Phospholipid membranes as substrates for polymer adsorption*, Nature Materials **1**, 129 (2002).

[263] G. M. Torrie, K. M. Middlemiss, S. H. P. Bly, and S. G. Whittington, *Self-avoiding walks interacting with an interface*, J. Chem. Phys. **65**, 1867 (1976).

[264] P. Mark and S. Windwer, *Polymer Adsorption on a Surface by an Exact Enumeration Study*, Macromolecules **7**, 690 (1974).

[265] J. M. Hammersley, G. M. Torrie, and S. G. Whittington, *Self-avoiding walks interacting with a surface*, J. Phys. A: Math. Gen. **15**, 539 (1982).

[266] E. Eisenriegler, K. Kremer, and K. Binder, *Adsorption of polymer chains at surfaces: Scaling and Monte Carlo analyses*, J. Chem. Phys. **77**, 6296 (1982).

[267] K. I. Skau and E. M. Blokhuis, *Mean-field theory for polymer adsorption on curved surfaces*, Eur. Phys. J. E **7**, 13 (2002).

[268] P. Grassberger, *Pruned-enriched Rosenbluth method: Simulations of Θ polymers of chain length up to 1 000 000*, Phys. Rev. E **56**, 3682 (1997).

[269] P. Grassberger, *Recursive sampling of random walks: self-avoiding walks in disordered media*, J. Phys. A: Math. Gen. **26**, 1023 (1993).

[270] P. Grassberger, *Go with the winners: a general Monte Carlo strategy*, Comp. Phys. Comm. **147**, 64 (2002).

[271] H.-P. Hsu, V. Mehra, W. Nadler, and P. Grassberger, *Growth algorithms for lattice heteropolymers at low temperature*, J. Chem. Phys. **118**, 444 (2003).

[272] S. Leibler and D. Andelman, *Ordered and curved meso-structures in membranes and amphiphilic films*, J. Phys. France **48**, 2013 (1987).

[273] H. Frielinghaus, private communication.

[274] H. R. Schwarz, *Numerische Mathematik*, chapter 4, pages 141–165, B. G. Teubner, Stuttgart, 4th edition, 1997.

[275] M. Frigo and S. G. Johnson, The fastest Fourier transform in the west, Technical Report MIT-LCS-TR-728, Massachusetts Institute of Technology, 1997.

[276] M. Frigo and S. G. Johnson, FFTW: An adaptive software architecture for the FFT, in *Proc. 1998 IEEE Intl. Conf. Acoustics Speech and Signal Processing*, volume 3, pages 1381–1384, Los Alamitos, CA, 1998, IEEE.

[277] M. Frigo, A fast Fourier transform compiler, in *Proc. 1999 ACM SIGPLAN Conf. on Programming Language Design and Implementation*, volume 34, pages 169–180, ACM, 1999.

[278] D. C. Morse, *Topological instabilities and phase behavior of fluid membranes*, Phys. Rev. E **50**, R2423 (1994).

[279] G. Gompper and M. Schick, *Self-Assembling Amphiphilic Systems*, volume 16 of *Phase Transitions and Critical Phenomena*, Academic Press, London, 1994.

Danksagung

Mein Dank gilt Professor Gompper, der mir viel Freiraum bei der Gestaltung meiner Arbeit gelassen hat, aber trotzdem wirklich jederzeit bei Fragen aller Art ansprechbar und diskussionsbereit war. Er hat mir den Besuch von Ferienkursen und Konferenzen ermöglicht und stetes Interesse an den Resultaten gezeigt.

Professor Eisenriegler war ein sehr guter Ansprechpartner für Fragen zu analytischen Rechnungen.

Helga Paffen war in allen organisatorischen Fragen die erste Adresse und hat mir vor allem bei der Reiseplanung viel Arbeit abgenommen.

Frau Henkel, Herr Wingerath, Frau Schätzler, Frau Funk-Kath, Herr Westphal und Herr Heinen managen das Computersystem des IFF, haben die Bilder für diese Arbeit gescannt und waren bei Problemen meist sofort zur Stelle. Sie haben großen Anteil daran, daß meine Nerven trotz der stark rechnerbasierten Arbeit noch immer in einem guten Zustand sind. Von Christian Mosch und Alexander Achenbach habe ich 'in Sachen Computer' kräftig profitiert.

Die gemeinsamen Treffen mit den Arbeitsgruppen von Professor Strey in Köln und Professor Richter in Jülich haben wesentlich zur Motivation beigetragen und einen engeren Kontakt zum Experiment ermöglicht. Hitoshi Endo, Britta Jakobs und Mihaela Mihailescu haben mir Exemplare ihrer Doktorarbeiten übergeben. Dmitry Byelov und Henrich Frielinghaus haben mich über ihre Ergebnissen auf dem Laufenden gehalten.

Durch ein Gespräch mit Professor Daniels über polymerstabilisierten Emulsionen und einen Besuch in der Arbeitsgruppe von Professor Artmann hat sich mein Horizont bei den Anwendungen von (Polymer-)Membran-Systemen zusätzlich erweitert.

Karl-Heinz Herrmann, S. V. M. Satyanarayana, Regina Eich und Manfred Niesert haben mir die Kapitel meiner Arbeit zum Korrekturlesen quasi aus der Hand gerissen. Maryam Khodaverdi kam daher gar nicht mehr zum Zug.

Die Liste der Kollegen, die zu einem wirklich guten Arbeitsklima im Institut beigetragen haben, ist viel zu lang um sie an dieser Stelle abzudrucken.

Ich versichere, daß ich die von mir vorgelegte Dissertation selbständig angefertigt, die benutzten Quellen und Hilfsmittel vollständig angegeben und die Stellen der Arbeit — einschließlich Tabellen, Karten und Abbildungen —, die anderen Werken im Wortlaut oder dem Sinn nach entnommen sind, in jedem Einzelfall als Entlehnung kenntlich gemacht habe; daß diese Dissertation noch keiner anderen Fakultät oder Universität zur Prüfung vorgelegen hat; daß sie — abgesehen unten angegebenen Teilpublikationen — noch nicht veröffentlicht worden ist sowie, daß ich eine solche Veröffentlichung vor Abschluß des Promotionsverfahrens nicht vornehmen werde. Die Bestimmungen der Promotionsordnung sind mir bekannt. Die von mir vorgelegte Dissertation ist von Professor Gompper betreut worden.

1. T. Auth, G. Gompper
   Self-avoiding linear and star polymers anchored to membranes
   Phys. Rev. E **68**, 051801 (2003)

Jülich, den 24. November 2004

Thorsten Auth

Adresse	Baltenweg 1
	61118 Bad Vilbel
Geburtsdatum	10. Oktober 1974
Geburtsort	Frankfurt am Main
Familienstand	ledig
Staatsangehörigkeit	deutsch

1981 − 1985	**Grundschule**
	Ernst-Reuter-Schule
	Bad Vilbel
1985 − 1994	**Gymnasium**
	Wöhlerschule
	Frankfurt am Main
1994 − 2000	**Physikstudium**
	Johann-Wolfgang-Goethe-Universität
	Frankfurt am Main
1996	Vordiplom
2000	Diplom
	Diplomarbeit mit dem Thema
	„Relativistische Spindichtefunktionaltheorie"
seit Januar 2001	**Doktorarbeit**
	Forschungszentrum Jülich
seit Oktober 2002	**Promotionsstudium**
	Universität zu Köln

Jülich, den 19. Dezember 2003